Coupled Dynamics and Economic Analysis of Floating Wind Turbine Systems

by

Elizabeth Wayman

B.S., Civil and Environmental Engineering
Massachusetts Institute of Technology, 2004

Submitted to the Department of Mechanical Engineering
in partial fulfillment of the requirements for the degree of

Master of Science in Mechanical Engineering

at the

Massachusetts Institute of Technology

June 2006

Author .....
Department of Mechanical Engineering
May 15 2006

Certified by .....
Paul D. Sclavounos
Professor of Mechanical Engineering
Thesis Supervisor

Accepted by .....
Lallit Anand
Chairman, Departmental Committee on Graduate Students
Department of Mechanical Engineering

Coupled Dynamics and Economic Analysis of Floating Wind Turbine Systems

by

Elizabeth Wayman

Submitted to the Department of Mechanical Engineering
on May 12, 2006, in partial fulfillment of the
requirements for the degree of
Master of Science in Mechanical Engineering

Abstract

Against the backdrop of rising oil prices and increasing uncertainty in the future of energy and the health of the environment, wind energy is distinguished as a leading technology that is both technologically and economically viable for large-scale non-petroleum and non-polluting energy generation. The deployment of wind energy technology on floating platforms in deep water offshore environments has emerged as a forward-thinking application of this technology.

This thesis takes some early steps toward the development of innovative and cost-effective floating platforms to support a 5-MW wind turbine for deployment in water depths of 30 – 300 meters. A tool for performing a coupled structural, hydrodynamic, and aerodynamic analysis of floating wind turbine systems in the frequency domain was developed and is presented. This analysis tool includes the effects of the gyroscopic loads of the wind turbine rotor on the tower and floater, the aerodynamic damping introduced by the wind turbine rotor, the hydrodynamic added mass and damping introduced by wave-body interactions, and the hydrodynamic forces caused by wave excitation.

This analysis tool was applied to several structures representing excerpts of the design space of structures capable of supporting large wind turbines. The structures were evaluated on their dynamic performance in several environmental conditions and on their installed cost. An economic analysis was also carried out to determine the cost of the floating platform for the wind turbine per kWh of electricity generated.

Thesis Supervisor: Paul Sclavounos
Title: Professor of Mechanical Engineering

Acknowledgments

I am sincerely grateful to my thesis advisor and professor, Professor Paul Sclavounos, for his role in my education at MIT. He began as my UROP advisor, and gave me the opportunity to work on a project that truly excited me, and shared with me his time and his knowledge.

As my thesis advisor and professor, he gave me the opportunity to continue to work on the project to which I had been introduced as an undergraduate, he shared with me a wealth of knowledge, and he provided guidance through the nebulous challenges of research. Professor Sclavounos has also worked to create and maintain relationships with other researchers in wind energy, which has not only enriched my experience, but has strengthened the wind energy research community in New England and worldwide.

I would also like to express my gratitude toward Mr. Jason Jonkman, Mr. Sandy Butterfield, Mr. Walter Musial, and Dr. Robert Thresher for their support of my research and for the contribution of their time and expertise. Their hospitality at the National Renewable Energy Laboratory in Boulder, CO., their active role in the project, and their thorough review and support of my work is very much appreciated.

Finally, I would like to thank Mr. Kwang Lee for his tireless patience and his endless willingness to address any question or contribute to this work in any way.

Funding for this study has been provided by the U.S. Department of Energy under NREL Subcontract No. RFP RAM-3-33200 (Offshore Floating Wind Turbine Concepts. Fully Coupled Dynamic Response Simulations).

Contents

List of Figures

List of Tables

Part 1

Background and Setup

1. Introduction and Motivation

Wind energy has been among the fastest-growing energy technologies in the United States, with recent growth rates of 30 – 43% per year [2]. Advancements in technology and economies of scale have lowered the cost of wind energy to around $0.04/kWh, making the technology competitive with natural gas [5].

The deployment of wind energy technology on land, however, faces some challenges. For instance, the richest on-land wind resource in the U.S. lies in North and South Dakota, thousands of miles from the large load centers of the East and West coasts. Another challenge is the lack of social acceptance of large wind farms in certain areas.

Five to fifty miles off the East coast of the United States lies another rich wind resource, with an estimated capacity near 1 TW [22]. This resource presents an opportunity for offshore wind energy projects that will be closer to the load centers, but far enough from shore to be out of sight of potentially objecting coastal residents.

The sites with the best resource and the least visibility from shore mostly lie in water depths of over 30 m. At these depths, the current practice of installing wind turbines on monopiles that are driven into the seabed becomes economically infeasible. The deployment of wind power technology on floating platforms offers a promising solution to the challenge of utilizing deepwater wind resources.

While the development of on-land, and potentially shallow-water, wind energy projects will continue to be prosperous and successful in the near future, the wind industry has begun to consider the deployment of wind energy technology in deeper waters on floating

platforms as a forward-thinking solution to some of the challenges facing on-land and shallow-water wind energy. Furthermore, in many European countries where land is much less available, the wind industry and the local governments have already made moves toward offshore wind energy development.

Previous simulation studies by J. E. Withee [21], K. H. Lee [9] and [10], and K. C. Tong [17] show promising results for the behavior of floating wind turbine systems. However, the full coupling between the wind turbine and the floating platform has been simulated only to a limited extent, and the optimal design concept for these systems remains unknown. Furthermore, the chore of installing a wind turbine onto a floating platform at sea may make the cost of this technology prohibitive.

This study, therefore, has four goals:

1.) To make a preliminary step toward coupling proven codes from the wind power industry with codes from the offshore oil and gas industry to create a tool for modeling and analyzing coupled wind turbine and floating platform systems.
2.) To understand the design space of platforms that achieve total system stability, and to identify the most cost-effective structures in that design space.
3.) To study and understand the behavior of these coupled systems in various wind and wave environments.
4.) To identify systems that avoid the need to install the wind turbine on the platform while at sea, and compare them to systems that require turbine installation at sea.

The approach taken to achieve these goals consists of two main phases; an initial design and steady-state analysis phase, and a design refinement and dynamic analysis phase. The initial design phase concludes with a preliminary cost assessment, which indicates the most viable candidates to be passed to the second phase. At the conclusion of the second phase, a more detailed cost assessment is carried out for the final structures, resulting in a cost of energy assessment. This process is outlined in the following section.

2. Overall Study Approach

To achieve the goals set forth, the study first examines the mechanisms that provide restoring to a structure to allow the structure to achieve acceptable steady-state performance. With this knowledge, the design space of structures that achieve adequate steady-state performance is mapped out. A static design process is carried out to evolve structures from this space that are of relatively low cost and promise to provide adequate restoring for the system to achieve an acceptable steady-state operating point once installed. These structures are passed to a static analysis phase where the steady-state operating points in various wind speeds are evaluated. Next, the systems and their steady-state operating conditions are passed to a dynamic analysis phase where their dynamic properties, including the systems' response amplitude operators (RAOs), natural frequencies, and the standard deviations of motions in various wind speeds and sea states, are calculated. Finally, an economic analysis is performed to determine the cost of each structure per MWh. This process is carried out for systems that achieve enough stability to be towed to the installation locations while fully assembled, and for systems that are only stable once moored and must be assembled at sea. This general process is outlined in **Figure 1**.

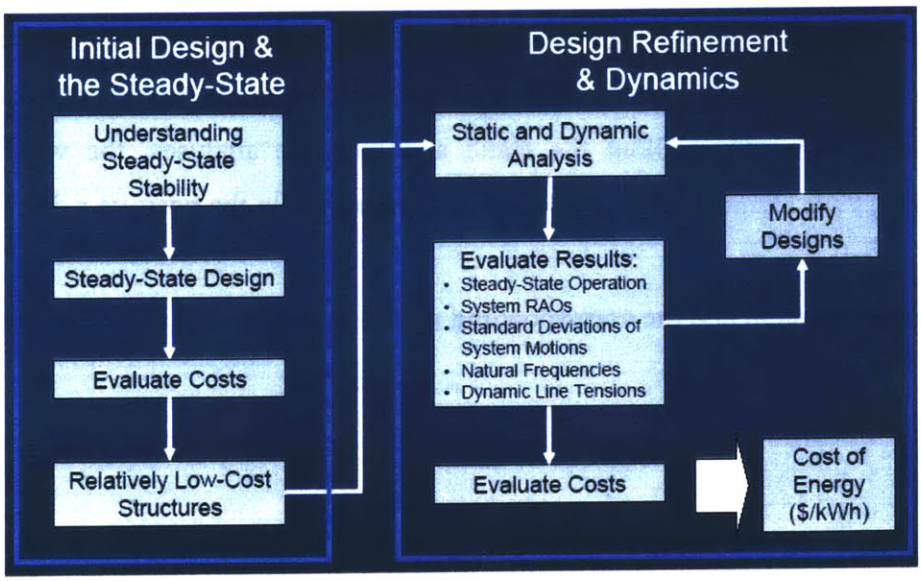

Figure 1: Overall Study Approach

3. Model Components and Assumptions

The physical models used in this study consist of 3 major components; the floating platform, the wind turbine, and the mooring system. These systems are analyzed separately, then considered together, as will be explained in Section 9. The model of the floating platform and mooring system change with each design concept, and will be explained in the relevant section. The sections below describe the assumptions about the motions of these systems, and also detail the wind turbine chosen for this study.

3.1 Coordinate System and Modes of System Motion

The combined wind turbine and floating platform system is assumed to undergo rigid body motions in the standard modes of motion that are considered in wave-body interaction theory, translational and rotational motions along the x, y, and z axes. Modes 1–3 are the translational modes of surge, sway, and heave, and represent translation along the x, y, and z axes, respectively. Modes 4–6 are the rotational modes of roll, pitch, and yaw, and represent rotation about the x, y, and z axes, respectively.

The origin of this coordinate system is taken as the x and y locations of the floating platform's center of gravity, on the calm water surface; the z = 0 plane coincides with the calm water surface. Throughout the static and dynamic analyses, the wind and the ambient waves are assumed to be aligned and to propagate in the positive *x* direction.

This coordinate system and the corresponding modes of motion are shown in **Figure 2.**

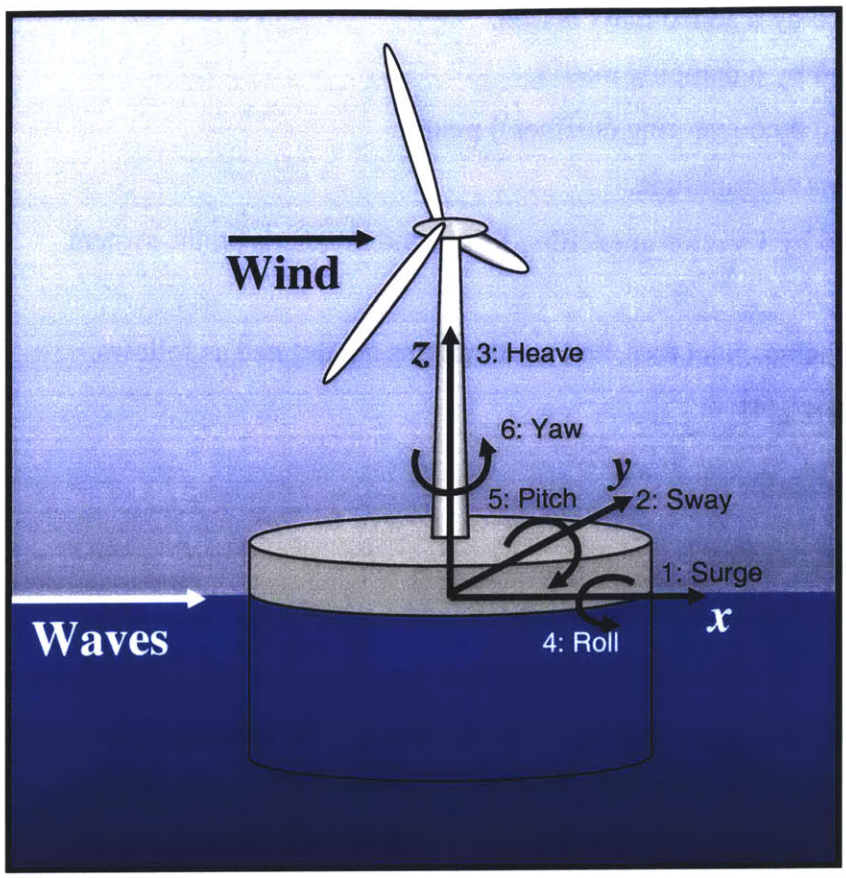

Figure 2. Coordinate System and Modes of System Motion

The equations of motion governing the rigid-body motions of a floating consist of standard Newtonian equations of motion, and are summarized in matrix form below, describing the 6 modes of motion.

$$(M + A)\ddot{\xi}(t) + B\dot{\xi}(t) + C\xi(t) = aXe^{iwt}$$

The symbols in this equation have the following meaning:

ξ = The 6 by 1 vector describing the system's displacement in the 6 modes of motion.

$\dot{\xi}$ = The 6 by 1 vector describing the system's velocities.

$\ddot{\xi}$ = The 6 by 1 vector describing the system's accelerations.

ω = Wave frequency.

M = The 6 by 6 mass matrix.

A = The 6 by 6 added mass matrix.

B = The 6 by 6 damping matrix.

C = The 6 by 6 restoring (stiffness) matrix.

a = The wave amplitude.

X = The 6 by 1 vector of exciting forces and moments on the system.

The displacements, velocities, and accelerations are defined as follows.

$$\xi(t) = \mathrm{Re}\{\Xi e^{i\omega t}\}$$

$$\xi'(t) = \mathrm{Re}\{i\omega \Xi e^{i\omega t}\}$$

$$\ddot{\xi}(t) = \mathrm{Re}\{-\omega^2 \Xi e^{i\omega t}\}$$

Substituting these expressions into the first equation, and taking the wave amplitude as unity, the equations of motion can be summarized in the frequency domain as below.

$$\left[-\omega^2\left(M + A(\omega)\right) + i\omega B(\omega) + C\right]\Xi(\omega) = X(\omega)$$

These equations of motion describe the system's rigid-body response to regular, plane progressive waves within linear theory. As explained in forthcoming sections, properties of the wind turbine, floating platform, and mooring system define the mass, added mass, damping, restoring matrices, and exciting forces, and compose the model of the combined wind turbine floating platform system. These equations of motion are evaluated to give the combined system motions in various conditions.

3.2 5-MegaWatt Wind Turbine

A wind turbine with a power rating of 5 MW was chosen as the wind turbine for the design of the floating structures in this study because it is speculated that 5 MW is the minimum power rating at which deepwater offshore wind energy can be cost effective.

At the time of the undertaking of this study, wind turbines with a power rating of 5 MW had not yet been developed. Therefore, the wind turbine model used in this study is the NREL 5-MW Offshore Baseline Wind Turbine model. This model does not correspond to an existing wind turbine, but its properties are drawn and extrapolated from operating machines and conceptual studies to create a realistic representation of a three-bladed upwind 5-MW wind turbine. Its general properties are described in **Table 1**. The details and rationale for this model are given by NREL in [6].

Table 1. Gross Properties of the NREL 5-MW Offshore Wind Turbine

Rotor Orientation	Upwind	
Control	Variable Speed, Collective Pitch	
Rotor Diameter/Hub Diameter	126 m/3 m	
Hub Height	90 m	
Max Rotor/Generator Speed	12.1 rpm/1,173.7 rpm	
Maximum Tip Speed	80 m/s	
Overhang/Shaft Tilt/Precone	5 m/ 5°/ -2.5°	
Rotor Mass	110,000 kg	Overall c.g. location: $(x,y,z)_t$ = (-.2,0,64)m
Nacelle Mass	240,000 kg	
Tower Mass	347,460 kg	

This model was analyzed by NREL using the wind turbine code FAST (Fatigue, Aerodynamics, Structures, and Turbulence) [5] to obtain various operational characteristics. The operational characteristics over the machine's operational wind speeds that are relevant to this study are summarized in **Table 2** and **Figure 3** [6].

The power curve, shown in green in **Figure 3**, is often used to characterize a wind turbine and wind speeds. The power curve has 3 main regions. Region 1 refers to wind speeds between zero and the cut-in wind speed that are too low for the wind turbine to operate, and is not depicted in **Figure 3**. The cut-in wind speed is the wind speed at which the turbine begins to operate. Region 2 begins at the cut-in wind speed, and refers to the wind speeds where the turbine's power increases with the wind speed. The highest wind speed in region 2 is the rated wind speed, or the wind speed at which the turbine generates the power for which the wind turbine is rated. In region 3, the wind turbine maintains constant power production as the wind increases by adjusting the pitch angle of the blades to allow for power to pass by. The highest wind speed of region 3 represents

the cut-out wind speed, or the speed beyond which the wind turbine completely feathers its blades, as to not capture any power. This is done to protect the wind turbine during extreme winds. Region 2.5 shown on **Figure 3** is the region of wind speeds preceding the rated wind speed, where the system begins to adjust for region 3.

Table 2. Description of Variables Characterizing the NREL 5-MW Offshore Baseline Wind Turbine

GenSpeed	Angular Speed of the High-Speed Shaft and Generator
RotPwr	Mechanical Rotor Power
GenPwr	Electrical Generator Power
RotThrust	Rotor Thrust

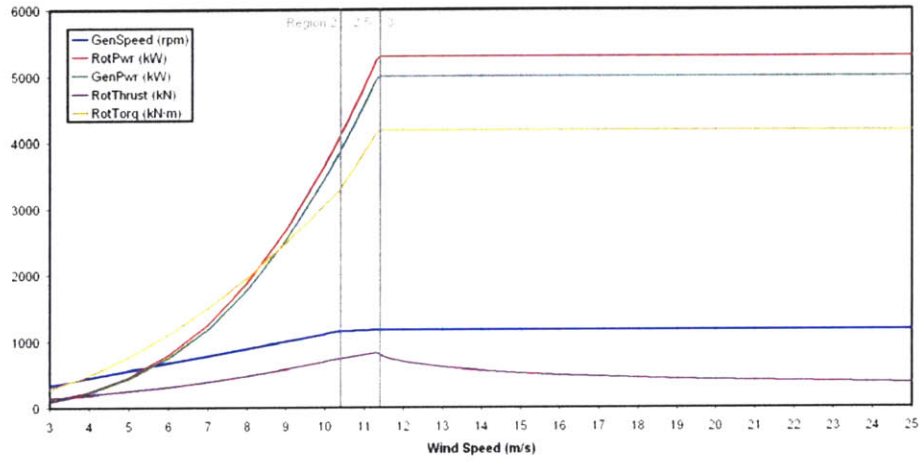

Figure 3. Wind Speed Relationship Curves Characterizing the NREL Offshore Baseline 5-MW Wind Turbine

To capture the performance of the coupled systems throughout the operational spectrum of the wind turbine, the systems were analyzed at four wind speeds, 9, 11.2, 15, and 25 m/s, which are drawn from each region of the power curve. The wind speed of 9 m/s represents region 2 of the power curve, and the wind speed at which the turbine is operating at roughly half of the system's rated power. The wind speed of 11.2 m/s represents the turbine's rated wind speed, the speed where the turbine first reaches its rated power. The wind speed of 15 m/s represents region 3 of the power curve, where the wind turbine feathers its blades to maintain rated power, and the speed of 25 m/s represents the cut-out wind speed, the highest wind speed where the turbine is in operation.

Part 2

Initial Design and the Steady-State

4. Design for Steady-State Performance

The rigid body motions of a floating system that are developed above are reproduced here.

$$\left[-\omega^2\left(M + A(\omega)\right) + i\omega B(\omega) + C\right]\Xi(\omega) = X(\omega)$$

The motions described by this system of equations are used to evaluate the system performance in steady wind and regular waves.

The first criteria, however, that drives the design of the platforms is the steady-state static performance of the combined wind turbine floating platform system. The combined system is designed to demonstrate favorable steady-state static performance in its installed state, about which the system oscillates in response to random waves. Therefore, before a system can be considered for dynamic motion, it must first demonstrate acceptable steady-state performance.

In steady-state, velocities and accelerations are zero, and the dynamic exciting forces and moments are replaced by steady-state forces and moments. The equations of motion then reduce to the equation of static equilibrium given below.

$$C\xi(\omega) = F_{\substack{Steady \\ State}}$$

The critical steady-state offset for floating wind turbine systems is the offset in pitch. The offset of the system in pitch not only brings the structure closer to capsizing, but also

compromises the efficiency of the wind turbine and introduces complicated loading to the wind turbine by causing the rotor to be at an angle relative to the inflow. For platforms with stiff mooring systems that do not allow pitch, the critical offset becomes the offset in surge, which will be described in later sections.

The system's steady-state pitch, ξ_5, is determined by the steady-state moment exerted on the system in pitch, F_5, and the system's restoring properties in pitch, C_{55}, as given in the equation below.

$$\xi_5 = \frac{F_5}{C_{55}}$$

F_5 is the moment that the thrust force, F_{Thrust}, makes about the origin by exerting a force at the location of the hub, Z_{Hub}. This is given in the equation below.

$$F_5 = F_{Thrust} Z_{Hub}$$

By limiting the structure's steady-state pitch to a certain threshold, a minimum value of restoring in pitch can be calculated that will serve as a design parameter. It is speculated that beyond a pitch angle of 10 degrees, the wind turbine will lose substantial efficiency. Therefore, the threshold pitch value in this study was taken as 10 degrees. The maximum wind loading was taken as 800,000 N, which is the steady state thrust at a wind speed of 11.2 m/s and acts on the wind turbine hub, at Z_{Hub}, which equals 90 m. The necessary restoring coefficient is found by solving for the restoring coefficient needed to limit the pitch to 10 degrees, as shown here.

$$C_{55} = \frac{F_5}{\xi_5} = \frac{F_{Thrust} \times Z_{Hub}}{\xi_{5,Limit}} = \frac{800,000 \times 90}{.1745} \frac{[N-m]}{[-]} = 4.126E+08 \text{ [N-m]}$$

The value of restoring in pitch calculated through the method above serves as the preliminary design parameter for candidate structures to support the 5-MW wind turbine.

5. Understanding Steady-State Restoring in Pitch

To understand the design space of structures that could achieve acceptable steady-state performance in pitch, it was necessary to understand the methods through which structures achieve steady-sate restoring. Restoring in pitch is achieved through three general mechanisms: waterplane area, ballast, and the mooring system. These mechanisms are described below, and can serve as a classification of floating structures, as developed Butterfield et al. in [1].

5.1 Restoring from Waterplane Area

Restoring from a structure's waterplane area is provided by the moment that the structure's waterplane area makes about the structure's center of rotation, which is assumed to coincide with the structure's coordinate system origin as described in **Figure 2**. Waterplane area moment about the x and y axes are given by the equations below, and the effect of waterplane area moment on a structure's restoring is shown in **Figure 4**.

$$M_{WP,x} = \iint x^2 dS$$

$$M_{WP,y} = \iint y^2 dS$$

S in this integral represents the waterplane area surface, when the structure is not offset in pitch or roll.

The dotted line on the structure in **Figure 4** represents the structure's waterplane. For small angles of deflection in pitch, the shape of the waterplane is relatively constant.

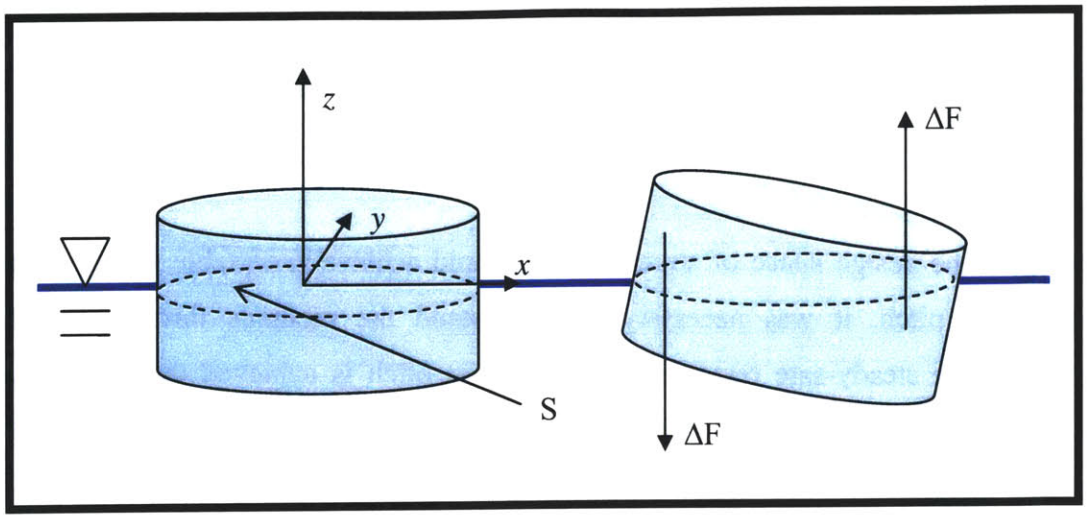

Figure 4. Restoring Through Waterplane Area

When the structure is perturbed in pitch, one side of the structure is submerged, and the other side is elevated from the water. The submerged side experiences an increase in buoyant mass, as a larger volume of water is displaced on that side. The other side experiences a decrease in buoyant mass, as a smaller volume of water is displaced on that side, equal to the increase on the other side. These increases and decreases in buoyant mass result in increases and decreases in buoyant force, ΔF. The moment the waterplane area makes about the y axis determines the moment that results from these ΔF forces. This moment opposes the moment exerted on the body to displace it in pitch, and results in a restoring moment. This restoring moment is given by the following equation.

$$M_{Restoring,WP,x} = \left(\rho g \iint x^2 dS\right) \sin \xi_5$$

$$M_{Restoring,WP,y} = \left(\rho g \iint y^2 dS\right) \sin \xi_4$$

Employing the small angle approximation, these equations reduce to the following expressions.

$$M_{Restoring,WP,x} = \left(\rho g \iint x^2 dS\right) \xi_5$$

$$M_{Restoring,WP,y} = \left(\rho g \iint y^2 dS\right) \xi_4$$

For a cylinder as shown in **Figure 4**, or other axisymetric bodies, restoring in pitch is equal to restoring in roll. This is because the waterplane area is symmetric about the x and y axes and thus creates an equal moment about both axes.

The effect of waterplane area symmetry on a structure's restoring can be illustrated by a canoe shown in **Figure 5**. Due to the long, slender shape of the canoe, the waterplane area moment about the x axis is significantly lower than the waterplane area moment about the y axis. As a result, the canoe is strongly restored about the y axis, but weakly restored about the x axis.

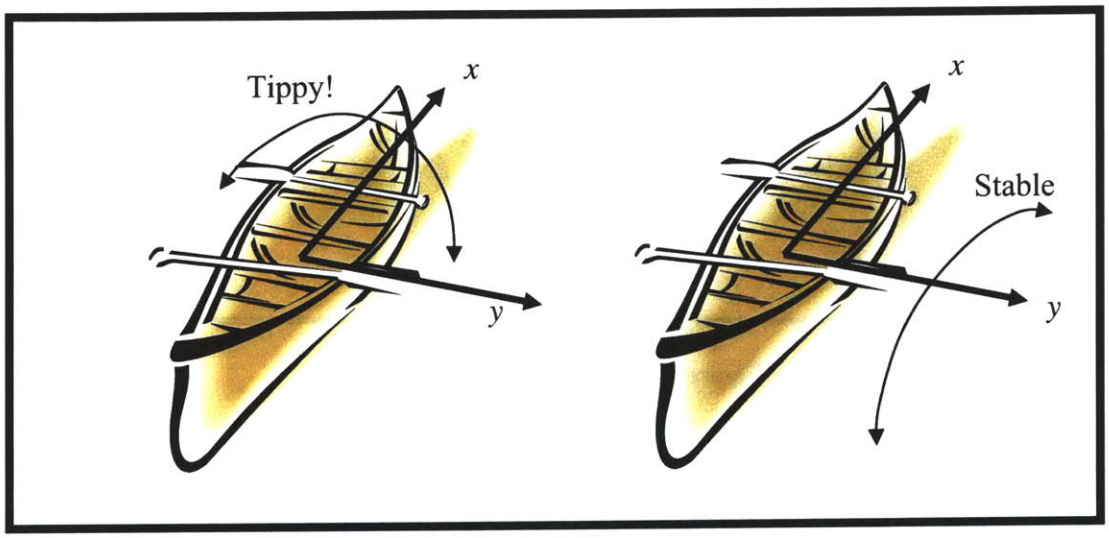

Figure 5. Restoring from Waterplane Area Moment of a Canoe

5.2 Restoring from Ballast

Restoring by ballast is achieved when enough ballast is added to the structure to lower the center of gravity to a location below the center of buoyancy. Restoring is then provided by the vertical separation between the structure's center of gravity and the structure's center of buoyancy. The restoring effect due to ballast then combines with the

restoring effect of waterplane area to form hydrostatic and inertial restoring. Hydrostatic and inertial restoring is illustrated in **Figure 6**.

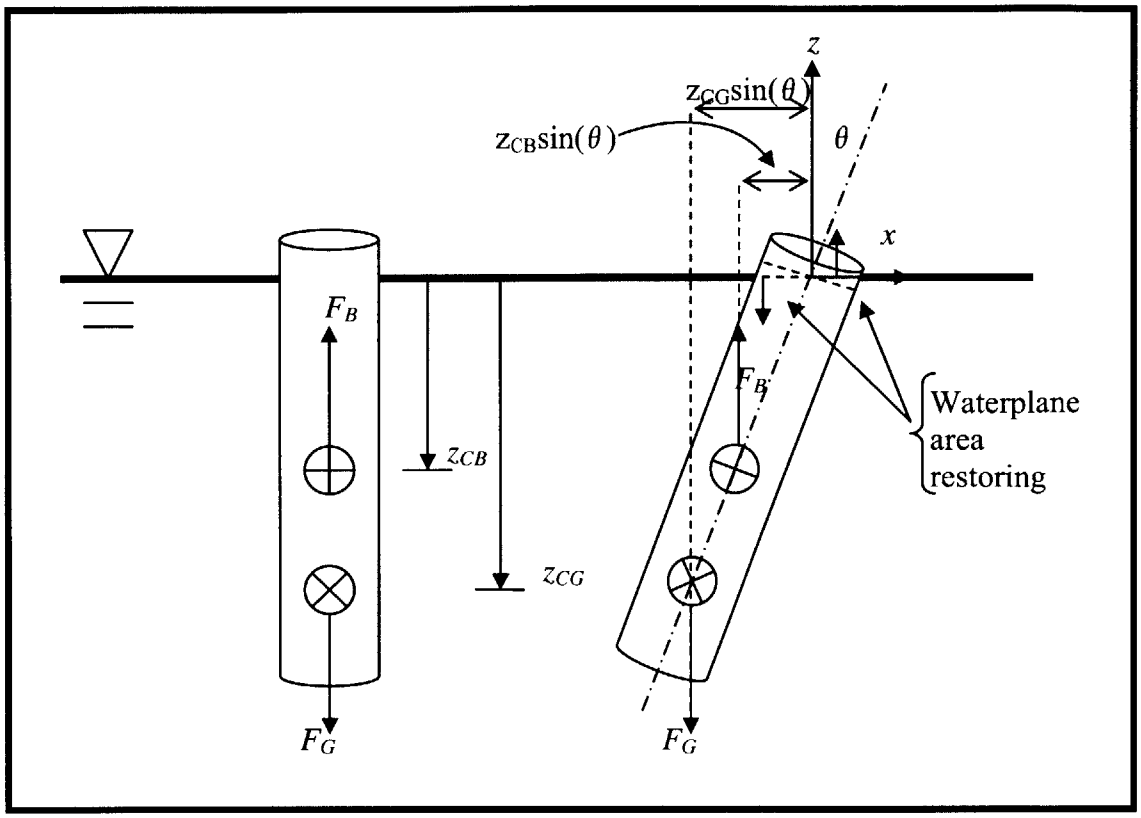

Figure 6. Restoring by Ballasting

As shown in **Figure 6**, when the system is offset in pitch, the buoyant force acting on the center of buoyancy creates a moment about the origin, and the gravitational force acting on the center of gravity creates a moment in the opposite direction about the origin. For a freely floating structure, the gravitational force is equal to the buoyant force, and the vertical distance between the center buoyancy and the center of gravity results in a net moment that has the tendency to restore the system to its vertical position when the system is offset in pitch.

When the system is offset in pitch, the waterplane area causes the center of buoyancy to shift toward the side of the structure that is submerged. This effect is captured by the

waterplane area component of restoring discussed in the previous section. The combined hydrostatic and inertial restoring moment is given by the equation below.

$$M_{Restoring,Ballast,x} = M_B g Z_{CB} \sin\xi_5 - M_G g Z_{CG} \sin\xi_5 + \left(\rho g \iint x^2 dS\right)\sin\xi_5$$

where M_G, M_B, Z_{CG}, Z_{CB} represent the gravitational and buoyant masses, and the centers of gravity and buoyancy respectively. Employing small angle approximations, this moment reduces to the following equation.

$$M_{Restoring,Ballast,x} = \left(M_B g Z_{CB} - M_G g Z_{CG} + \rho g \iint x^2 dS\right)\xi_5$$

5.3 Restoring from Mooring Lines

Restoring by mooring lines is provided by the moment that the mooring lines exert on the structure due to a displacement in pitch. The effect that the mooring lines have on the restoring properties of the structure is dependent on the mooring line configuration.

For slack mooring systems with catenary mooring lines, the restoring in pitch can be crudely modeled as the product of weight of the lines in water and the draft of the fairleads. The levels of restoring in pitch provided by catenary mooring systems are negligible compared to the amount of restoring required for structures capable of supporting large wind turbines. The restoring in pitch from catenary mooring lines is therefore taken as zero, and the structure itself is required to provide adequate restoring.

For tension leg mooring systems, as developed by Newman [13] and Faltinsen [3], the magnitude of restoring provided is dependent on the stiffness of the mooring system and the radial location of the fairleads where the mooring lines attach to the structure. The restoring coefficient in pitch provided by a tension leg mooring system is given below.

$$C_{55,Lines,TensionLeg} = 2\frac{(EA)_{Tethers}}{L_{Tethers}}\left(R + L_{Leg}\right)^2 + F_{Tethers}T$$

In this equation, $(EA)_{Tethers}$ is the product of the elastic modulus and the cross sectional area of the tethers, $L_{Tethers}$ is the unstretched length of the tethers, R is the cylinder radius, L_{Leg} is the length of the leg to which the line is attached, $F_{Tethers}$ is the total force exerted by the tethers, and T is the cylinder draft (or the vertical distance to the tether fairlead).

The equation above for restoring provided by a tension leg mooring system shows that the restoring coefficient in pitch is dependent upon the elastic properties of the mooring system. The scope of this study, however, includes only the rigid body motions of the system, and does not include elastic effects. Therefore, the mooring lines of a tension leg mooring system are taken to be infinitely stiff, with an infinite elastic modulus.

The infinite stiffness of the mooring lines prevents any significant motion in pitch, roll, and heave, and the platform's motions are therefore limited to surge, sway, and yaw. The mooring system must then be designed to adequately limit motions in these modes.

5.4 Total Restoring and the Restoring Coefficient in Pitch

Contributions to restoring from waterplane area, ballast, and mooring lines combine to result in the total restoring properties of a floating platform. The restoring coefficient is defined to characterize the total restoring properties due to the system's offset in pitch. As developed in the previous sections, the restoring moment that the structure experiences due to its geometry and its offset in pitch is summarized below.

$$M_{Restoring} = \left(M_B g Z_{CB} - M_G g Z_{CG} + \rho g \iint x^2 dS\right)\xi_5 + M_{Restoring,Lines}$$

This equation shows that the restoring moment that the structure experiences is proportional to the offset in pitch. The restoring coefficient is that coefficient of proportionality, and is given below.

$$C_{55} = \left(M_B g Z_{CB} - M_G g Z_{CG} + \rho g \iint x^2 dS \right) + C_{55,Lines}$$

$C_{55,Lines}$ describes the restoring provided by just the mooring lines, and is taken as zero for catenary systems and is assumed to be infinite for tension leg systems.

Conceptually, these three restoring mechanisms can be epitomized by three extreme structures: a shallow drafted barge representing restoring by waterplane area moment, a ballasted deep-drafted spar representing restoring by ballasting, and a Tension Leg Platform (TLP) that represents restoring by the mooring system. These restoring methods and their representative structures are shown in gray in **Figure 7**.

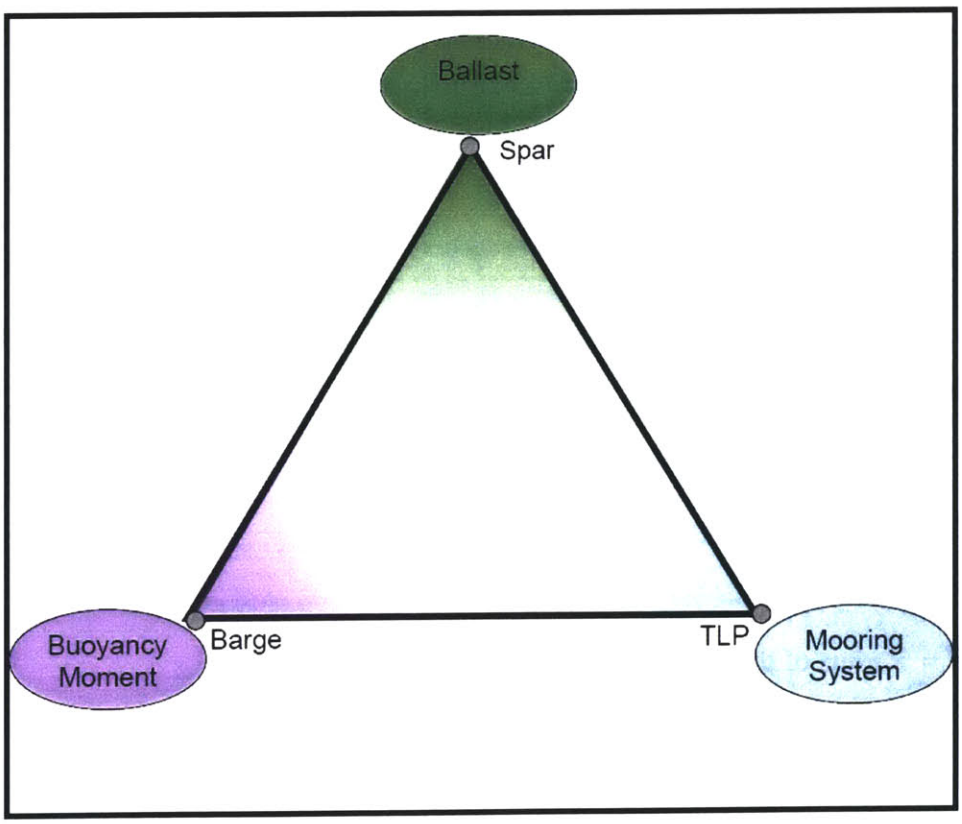

Figure 7. Restoring Mechanisms and Representative Structures

In reality, no structure can perfectly isolate a single restoring mechanism. Instead, structures achieve their restoring through a combination of these mechanisms. In the steady-state optimization phase, this study considers the entire design space spanned by the triangle in **Figure 7** to determine the lowest-cost structures that meet the steady state performance criteria. The lowest-cost structures are then passed to subsequent analysis phases where the structures are further evaluated.

The following sections outline the steady-state optimization process and the resulting structures.

5.5 Restoring Properties in Pitch of a Surface-Piercing Cylinder

The methods of restoring mentioned above can be expressed mathematically for any structure. For a surface-piercing cylinder, restoring in pitch is given by the following equation.

$$C_{55} = \left(M_B g Z_{CB} - M_G g Z_{CG} + \rho g \iint x^2 dS \right) + C_{55,Lines}$$

For a surface-piercing cylinder, the equation above is evaluated to give the following expression.

$$C_{55} = M_B Z_{CB} - M_G g Z_{CG} + \rho g \pi \frac{R^4}{4} + C_{55,Lines}$$

Where R = Radius of the cylinder.

6. Steady-State Design and Optimization

The goal of this phase was to identify the types of structures that demonstrate acceptable steady state performance in their installed state by achieving the required restoring in pitch at the lowest cost. To accomplish this, a selection of structure types was chosen such that the design space depicted in **Figure 7** was well represented. Within each structure type, a basic optimization was performed to identify the lowest cost structure representative of that type. A first order cost analysis was then performed on each structure considering materials, construction, and installation required for each structure to identify which structures were most promising on a cost-basis. These structures were then passed to the dynamic analysis phase for further evaluation.

The structures chosen to span the design space were the spar, the barge, the tri-floater, the TLP, and the concrete-ballasted cylinder (CBC). These structures are indicated on **Figure 8** and are defined below.

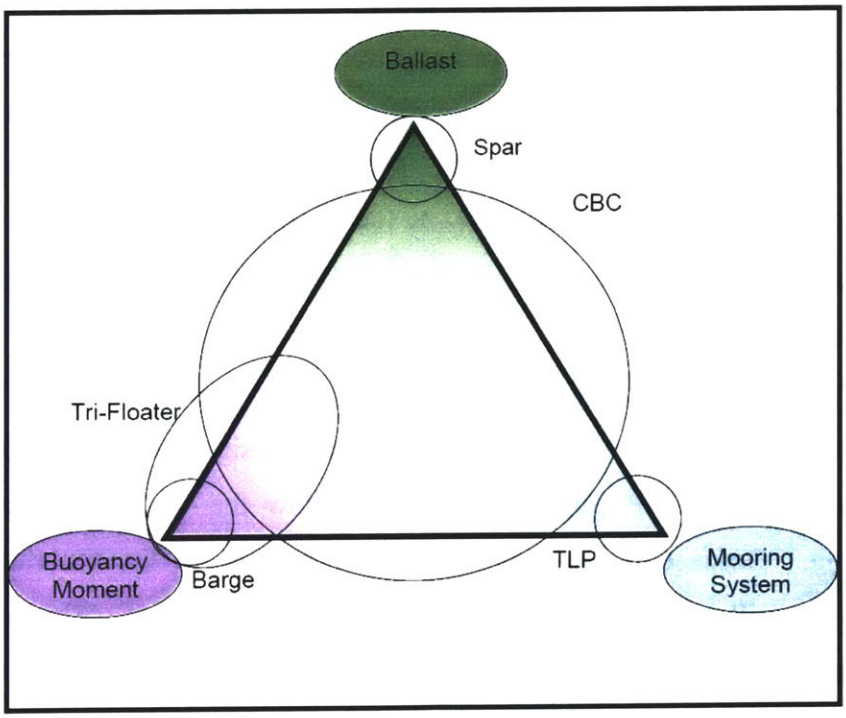

Figure 8. Structure Types that Span the Steady-State Stability Design Space

- **Spar**: Long slender ballasted cylinder that has enough ballast to lower the center of gravity below the center of buoyancy. Mooring lines provide station-keeping only. Hence, the gravitational and buoyant forces are approximately equal and restoring is provided by vertical separation between the structure's center of gravity and center of buoyancy. Because the mooring lines play a minimal role in providing steady-state restoring, the wind turbine can be installed to the platform in the shipyard, and the system can be towed to its operational location already assembled.
- **Barge**: Shallow-drafted cylinder with a very large waterplane area. Mooring lines provide station keeping only. Restoring is provided by the structure's large waterplane area. Because the system achieves adequate restoring without its mooring lines, the system can be towed to its operational location with the wind turbine already installed. The platform may include some ballasting to achieve the desired draft.
- **Tri-Floater**: Three surface-piercing cylinders that are joined in a triangle formation, with the cylinders spread out from the center. Mooring lines provide station-keeping only. Restoring is provided by the moment that the waterplane area makes about the system's center of rotation, created by a combination of the total waterplane area and the radial distance between the waterplane area of the cylinders and the center of rotation. The system can be towed to its operational location with the wind turbine already installed. The cylinders my include some ballasting to achieve the desired draft, and to limit the radial separation of the cylinders.
- **TLP**: A buoyant cylinder that is held at its draft by its tension leg mooring system. The tension leg mooring system provides significant downward force and restoring. The TLP can be submerged below the waterline to reduce wave loading. Because restoring is provided primarily by the mooring lines, this structure will not support a wind turbine without its lines. This structure will require the turbine to be installed to the platform while at sea, after the platform has been deployed and secured to its mooring lines.

- **CBC**: A surface-piercing cylinder that achieves adequate restoring through a mix between ballast, waterplane area, and mooring lines. Depending on this mix, the system may or may not be capable of being towed to its operational location with the turbine already installed to the platform.

An optimization of each structure was performed by solving for the platform geometry that achieves the required restoring to ensure acceptable steady-state performance of the system in operation. Because the groups of structures considered utilize different mechanisms of restoring as their primary restoring mechanism, the method used to optimize the structure within each structure group varied from group to group. Each distinct method and considerations are explained below.

6.1 Optimization of the Spar and Barge

The spar and the barge structures are intended to achieve adequate restoring without contributions from the mooring lines. Because mooring lines provide station-keeping functions only, these systems are designed to achieve restoring through ballasting and waterplane area only, respectively. Due to the lack of contribution from the mooring lines, the spar and the barge structure types are actually extreme examples of the concrete-ballasted cylinder with no mooring lines. For this reason, they may be optimized with the same method and considerations.

As developed above, by restricting the steady-state offset in pitch at the maximum thrust, a minimum value required for C55 can be obtained.

$$C_{55} = \frac{F_5}{\xi_5} = \frac{F_{Thrust} \times Z_{Hub}}{\xi_{5,Limit}} = \frac{800,000 \times 90}{.1745} \frac{[N-m]}{[-]} = 4.126E+08$$

The restoring in pitch of a surface-piercing cylinder, in the absence of mooring lines is given by the following equation.

$$C_{55,H\&I} = F_B Z_{CB} - M_G g Z_{CG} + \rho g \pi \frac{R^4}{4}$$

The optimal size and shape are determined by solving for the platform geometry that causes the platform to achieve the desired value of a restoring coefficient. For a concrete-ballasted surface-piercing cylinder, the geometry consists of defining the radius, R, the height of the cylinder, H, and the height of the internal concrete ballast, h, which are imbedded in the equation above in the Z_{CB}, F_B, M_G, and Z_{CG} terms.

Although the spar and the barge structures are intended to isolate the ballasting and waterplane area restoring methods, respectively, it is not physically possible for a structure completely isolate these methods. The spar buoy must pierce the surface of the water, and therefore can not avoid a small contribution of waterplane area to its total restoring. Likewise, the barge must achieve a realistic draft, and therefore must contain some ballast, which also contributes to its total restoring.

With this in mind, a range of geometries that satisfy the requirement for restoring were found. This was accomplished by setting the draft to a range of realistic values, and solving for the radius and the height of the concrete ballast required to achieve the target restoring, and to satisfy the balance between buoyant and gravitational forces. To arrive at the lowest cost structure, the cost associated with each geometry were then evaluated by assuming a cost per kilogram for steel and concrete, then calculating the mass of steel and concrete in each geometry, and calculating the total cost. The costs of steel and concrete were assumed to be $700/ton and $100/ton respectively.

The total material costs of these geometries found at each depth are summarized in **Figure 9**.

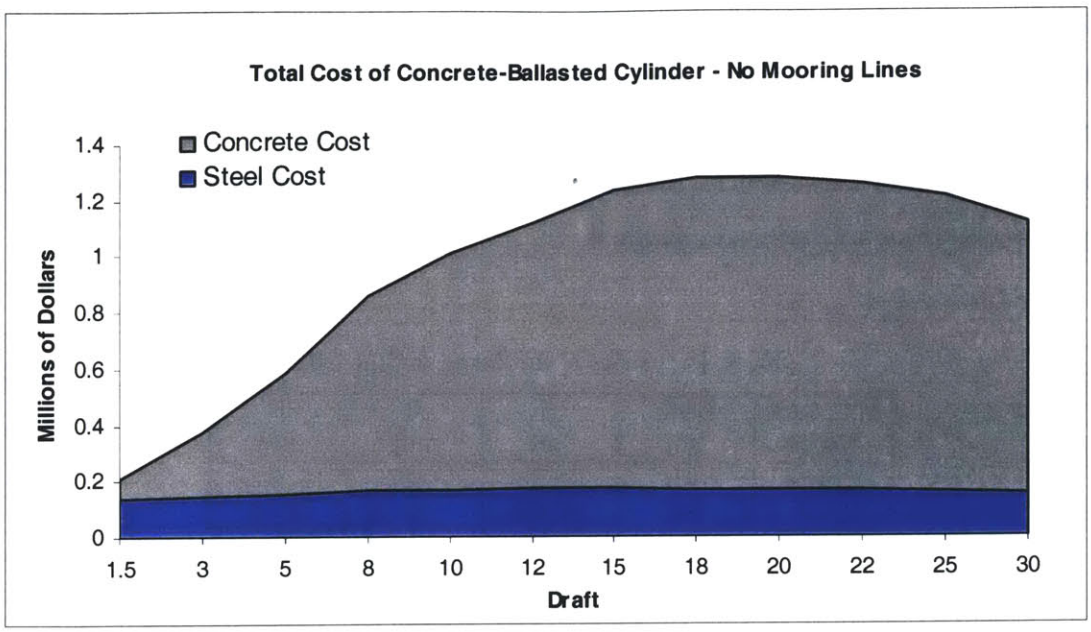

Figure 9. Total Cost of Concret-Ballasted Cylinders that Achieve Required Restoring in Pitch with No Mooring Lines

The cost curve in **Figure 9** shows that cost is minimized at very high and very low drafts. Practical considerations, however, put limits on the realistic draft of a structure; a structure with a draft beyond 30 meters could not be accommodated by any realistic shipyards or channels, and a structure with a draft below 1.5 meters will run the risk of slamming over the waves, as the troughs of the waves fall below its lower surface. Within these practical limits, the extreme drafts of 1.5 and 30 meters were chosen to represent realistic structures that minimize cost. The geometries corresponding to structures with these drafts are summarized in Table 3.

Table 3. Extreme Structures of the Concrete Ballasted Cylinder

Draft	R	h	H
[m]	[m]	[m]	[m]
1.5	18.34	0.27	3.00
30	10.465	10.985	31.50

As shown in **Table 3**, the deepest-drafted geometry has a radius of roughly 10.5 meters, and a draft of 30 meters. This geometry does not resemble a slender cylinder characteristic of a spar buoy. These results indicate that achieving the required restoring

in pitch by a spar buoy would necessitate a structure with an extremely deep draft that would not be feasibly accommodated in any shipyard or port. This conclusion led to the elimination of the spar buoy from candidate structures. The two extreme structures in **Table 3** were then classified as the barge and the concrete-ballasted cylinder (CBC). These structures are re-defined in **Table 4**.

Table 4. Properties of the Barge and the CBC

Stucture Name	Draft [m]	R [m]	h [m]	H [m]
Barge	1.5	18.34	0.27	3
CBC	30	10.465	10.985	31.5

6.2 Optimization of the Tri-Floater

The design of the Tri-floater was based on the design laid out in [16], and summarized in [12], but was adjusted to achieve the level of restoring required. This platform structure consists of 3 cylinders, joined in a triangle. The wind turbine tower is attached to the center of the triangle, and is supported by cross-bracing.

The cylinders and their radial spread were designed to achieve the required restoring properties with a reasonable draft and a reasonable radial spread. An extremely large radial spread presents challenges for transportation of the platform to the installation site, while a very small radial spread creates a structure that converges to a single cylinder.

Taking these issues into consideration, it was found that a smaller structure than that presented in [16] was able to achieve the required restoring. This structure is summarized in **Table 5**.

Table 5. Properties of the Tri-Floater

Number of Cylinders	3	[--]
Draft	9.35	[m]
R	7	[m]
h	3	[m]
H	11	[m]
$R_{origin\text{-}to\text{-}cylinder}$	25	[m]

6.3 Optimization of the TLP

The TLP is a structure that is intended to achieve adequate restoring primarily through the mooring system. The platform structure, therefore, is only intended to provide enough buoyancy to tension the mooring lines to the desired tension. The TLP is also intended to reduce wave loading by submerging the structure to a depth below significant wave action. These three intentions give rise to three optimization problems; to find the optimal shape of the submerged platform with respect to cost, to find the optimal depth to which the platform should be submerged with respect to wave loading, and to find the necessary tether tension.

6.3.1 Platform Shape

The first optimization problem is the simple algebraic exercise of minimizing the surface area of a cylinder with a given volume. Minimizing the surface are of the cylinder minimizes the steel used to create the cylinder, which minimizes the cost. This exercise shows that the optimal shape for the submerged cylinder is a cylinder with a diameter and height of the same length.

6.3.2 Platform Submersion Depth

The consideration of the variation of fluid particle velocity with depth due to a plane progressive wave gives insight into the second optimization problem. The horizontal and vertical velocities of a fluid particle due to plane progressive waves are shown by Newman in [13] to attenuate exponentially with depth. This would suggest that submerging the structure below the calm water surface would decrease wave loading on the structure, and would result in reduced motions of the coupled system. The result of submerging a structure below the surface, however, entails other effects that rise from

submerging the structure, including reduced added mass and hydrodynamic damping, and an increased submerged surface area of the structure. An increase in submerged surface area results in a larger area over which the hydrodynamic pressure acts, and could result in larger forces even if the pressures are reduced. In addition, dynamic analyses show that hydrodynamic damping is extremely significant to the total system motions. These additional effects make the outcome of submerging the platform below the surface unclear. For this reason, this study will compare the results of a TLP that floats on the surface with a TLP that is submerged.

6.3.3 Tether Tension

The final consideration for fully defining the properties of the TLP is the mooring line tension. A static design process along the lines developed by Withee in [21] and utilizing the theory developed by Faltinsen in [3] and Newman in [13] is carried out to determine the tether tension and dimensions of the TLP.

As developed in **Section 5.3**, the restoring coefficient in pitch provided by the tethers of a tension leg mooring system is shown below, but is assumed to be infinite.

$$C_{55,Lines,TensionLeg} = 2\frac{(EA)_{Tethers}}{L_{Tethers}}\left(R + L_{Leg}\right)^2 + F_{Tethers}T$$

$$(EA)_{Tethers} \to \infty$$

$$\Rightarrow C_{55,Lines,TensionLeg} \to \infty$$

This infinite stiffness prevents any significant motion in pitch, roll, and heave, but the mooring system must limit the motions to reasonable values in surge, sway, and yaw.

A tension leg mooring system must also maintain reasonable tension in all of its tethers. With the steady-state wind force acting in the positive x direction, the tension in upwind tether increases and the tension in downwind tether decreases to provide a balance of

forces and moments. This operational scenario is shown in **Figure 10**, where $F_{T,i}$ stands for the tension force in tether i, where tethers are numbered counter clockwise starting at the leg that corresponds with the positive x axis.

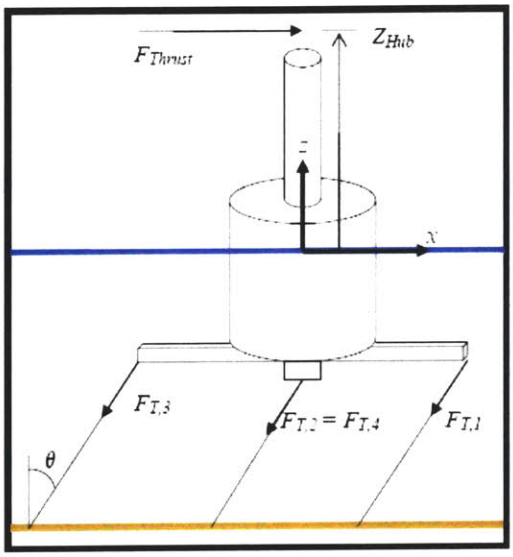

Figure 10. Steady-State Operational Configuration of the TLP

The initial tether tension must be chosen to ensure that the tension in the upwind tether does not exceed the maximum allowable tension and the tension in the downwind tether does not drop below the minimum allowable tension.

To summarize, the tether tension for this system must therefore fulfill two requirements: (1) the tethers must provide sufficient restoring in surge to adequately limit the steady-state offset in surge; and (2) the tension of the windward tether must never exceed the maximum allowable tension, and the leeward tether must never go slack or fall below the minimum allowable tension at any point during operation.

Under steady-state conditions, the platform will achieve its steady-state displacement in surge. At this displacement, the tethers will form an angle with the vertical, shown as θ in **Figure 10**. The tethers must be of sufficient tension to provide adequate restoring to limit this angle to about 5 degrees to prevent the system from experiencing highly nonlinear restoring and displacement.

Restoring in surge caused by the tethers is related to the tether tension and length through the following equation.

$$C_{11} = \frac{F_{Tethers}}{L_{Tethers}}$$

Restoring results in steady-state displacement through the following relation.

$$\xi_1 = \frac{F_1}{C_{11}} = \frac{F_{Thrust}}{C_{11}}$$

An initial limit for the tether tension is reached by limiting the system's steady-state displacement.

This tension must also satisfy the second requirement for the operational line tension. In operating conditions, the tension in each line is found by solving a balance of forces and moments for the tensions. As indicated in **Figure 10**, the tethers are numbered 1 through 4, where at rest the fairlead and anchor of tether 1 align with the positive x axis, tether 2, the positive y axis, tether 3, the negative x axis, and tether 4, the negative y axis. Assuming that the wind always propagates in the positive x direction, tether 3 is always the upwind tether and tether 1 is always the downwind tether.

A balance of forces in the vertical direction requires the buoyancy force plus the additional buoyancy gained by the setdown of the structure as shown in **Figure 10.** The system weight must equal the downward component of the sum of the tether tensions. This balance of forces is shown in the following equation, where θ represents the angle that the tethers make with the vertical.

$$F_B + \rho g \pi R^2 \left(L_{Tether} - L_{Tether} \cos\theta \right) - M_G g = \cos\theta \sum F_{T,i}$$

Employing the small angle approximation that cos θ is about equal to 1 and that sin θ is about equal to θ, this equation simplifies to

$$F_B - M_{11}g = \sum F_{T,i}$$

With four tethers spaced at 90-degree intervals around the structure, $F_{T,ave}$, the average tether tension is found by dividing the total tension force by four. Because tethers 2 and 4 are not affected by the moment exerted on the structure, they are assumed to have tensions equal to the average tension.

$$F_{T,2} = F_{T,4} = F_{T,ave} = \frac{F_B + \rho g \pi R^2 \left(L_{Tether} - L_{Tether}\cos\theta\right) - M_{11}g}{4\cos\theta}$$

Again invoking the small angle approximation, the tension in tethers 2 and 4 is given by

$$F_{T,2} = F_{T,4} = F_{T,ave} = \frac{F_B - M_{11}g}{4}$$

The tethers of concern are tethers 1 and 3, which are at risk of going slack or exceeding the maximum allowable tension, respectively. To balance the moment exerted on the system, tether 3 has a tension of $F_{T,ave}$ plus an additional tension, ΔF. To maintain the balance of forces in the vertical direction, tether 1 must then have a tension of $F_{T,ave}$ minus ΔF. This balance of moments is given by the following equation.

$$F_5 = F_{T,3}\left(R + L_{Leg}\right)\cos\theta - F_{T,1}\left(R + L_{Leg}\right)\cos\theta = \left(F_{T,ave} + \Delta F\right)\left(R + L_{Leg}\right)\cos\theta - \left(F_{T,ave} - \Delta F\right)\left(R + L_{Leg}\right)\cos\theta$$

Employing the small angle approximation, this equation simplifies to the following equation.

$$F_5 = F_{T,3}\left(R + L_{Leg}\right) - F_{T,1}\left(R + L_{Leg}\right) = \left(F_{T,ave} + \Delta F\right)\left(R + L_{Leg}\right) - \left(F_{T,ave} - \Delta F\right)\left(R + L_{Leg}\right)$$

The initial line tension must be chosen to prevent the tensions in the individual tethers from going to zero or exceeding the maximum allowable tension.

The requirements outlined above are considered together to arrive at the TLP's size, shape, and tether tension. The system properties that result from this iterative static design process are summarized in **Table 6**.

The final consideration for fully defining the TLP properties is the amount of buoyancy desired in the platform to tension the mooring lines to the desired value. Although mooring line tension does affect the steady-state properties, it has more implications to the dynamic properties. Therefore, for the steady-state design and optimization phase, a reserve buoyancy of about 5 is assumed. Reserve buoyancy is defined as the ratio of excess buoyancy to the total system mass, or

$$B_R = \frac{M_B - M_G}{M_G},$$

where M_B and M_G are the buoyant and gravitational masses, respectively. The TLP properties are summarized in **Table 6**.

Table 6. Properties of the TLP

Structure Name	R [m]	H [m]	h [m]	Z_{tower} [m]	$F_{Tethers}$ [kN]
TLP	9.5	19	0	-10	

7. Final Designs and First Order Cost Comparison

The final designs that resulted from this steady-state optimization process are summarized in **Table 7**.

Table 7. Summary of Structures

Structure Name	R [m]	H [m]	h [m]	L_{Leg} [m]	$R_{origin\ to\ cylinder}$ [m]	Z_{tower} [m]
TLP	9.5	19	0	0	0	-10
CBC	9.39	31.5	10.77	0	0	1.5
Barge	18.345	3	0.27	0	0	1.5
Tri-Floater	7	11	3	0	25	1.5

A cost analysis was performed on the structures in **Table 7** to estimate the total cost of the floating structure, mooring systems, and installation processes associated with each design. The costs estimated here do not include the wind turbine, power electronics, or transmission system.

Several assumptions were made about the construction and installation process, and the costs of labor, materials, and equipment. These assumptions were based on quotes from manufacturers, consultants, and contractors in the marine industry, and are detailed in **Table 8**, and explained below.

Floating wind turbine systems are intended for deployment in a wind farm setting, consisting of many individual units. This application has motivated an assumption that the structures may be fabricated and assembled in an assembly-line fashion. Therefore, the platforms will first be fabricated in the shipyard. Next, for all structures except the TLP, the turbines will be installed to the platform using a crane at the shipyard. The mooring system will then be installed at the final installation site, and the floating wind turbine units will then be towed to their installation sites and attached to their mooring lines. For the TLP, the floating platform and the wind turbine will be transported to the installation site not yet assembled. The platform will then be secured to its mooring lines, and the wind turbine will be installed onto the platform at sea.

It is also assumed that these structures are intended for deployment in U.S. coastal waters, and are therefore manufactured and commissioned in the United States.

The cost of steel and concrete were estimated by considering quotes from manufacturers, and were taken to reflect unfinished steel and batch concrete produced in the United States.

The cost of mounting the wind turbine to the floating platform was estimated for mounting the wind turbine at the shipyard and at sea. For the option of mounting the wind turbine at sea, a costly crane would be required, and with a full crew manning the process 24 hours a day, it was estimated that 2 installations could be accomplished in 24 hours. This option is subject to unpredictable weather patterns and requires a large crew to be stationed at sea during the entire installation process. For the option of mounting the wind turbine at the shipyard, it is assumed that a crane would be on site that would charge a lifting fee per wind turbine. Once the platforms are manufactured, mounting the wind turbine at the shipyard would then be an assembly line process utilizing the crane on site. Due to the assembly line style of this process, mounting wind turbines to platforms in a shipyard is estimated to be even less expensive and time consuming than mounting a wind turbine onto a foundation on land.

Anchor and mooring line costs were taken from quotes from experts in the offshore industry and from product manuals. Two alternative anchoring technologies were considered, the drag embedment vertical load anchor (VLA) and the suction pile. The VLA is a patented, proprietary technology, and is installed either by 1 or 2 anchor handling vehicles (AHVs) that drag the anchor into the sea bed. Once the AHV loads the anchor to its installation load, the anchor snaps into its vertical load-bearing orientation, and installation is complete. This installation technique avoids the need for subsea equipment, but can result in inaccurate anchor placement, and necessitates thorough geotechnical investigation of a large footprint of the sea floor. Suction pile anchors are cylindrical caissons that become embedded into the sea floor through suction. The caissons are lowered to the sea floor, and suction is applied to a valve at the top of the caisson. A combination of the suction applied and the exterior hydrostatic pressure drive the pile into the sea floor. This installation process requires the use of subsea pumps, and sometimes divers. The caissons, however, are easily manufactured, and avoid the retail

fees associated with the VLA. A cost of $25 and $15 per kN of vertical load, or a minimum anchor cost of $50,000 and $25,000 were estimated for the VLA and the suction pile, respectively.

Two methods of anchor installation were outlined as well. Installation Option 1 employs a barge and a tug, and Installation Option 2 requires an AHV. While Installation Option 1 has a lower cost on a daily rate, Installation Option 2 promises a lower cost per anchor. It is assumed that floating wind turbine systems will be installed in a wind farm array, and will require enough anchor installations to make Installation Option 2 more economical.

The cost of transporting the assembled system to its installation site, and installing it to its mooring lines was estimated assuming an installation site of 100 miles from the shipyard.

The tables and figures to follow detail these estimates and show the total cost breakdown for each system.

Table 8. Platform Cost Tables

Platform Construction and Materials

Steel Material Cost	**$700**	**/ton**
HSM Steel Structures (Aug 2005)	$1,100	/ton
US Steel Corp (July 2005)	$1,233	/ton finished steel
US Steel Corp (July 2005)	$633	/ton flat rolled
Baoshan, China: Predicted Cut	$560	/ton flat rolled
Concrete	**$100**	**/ton**
HSM Steel Structures (Aug 2005)	$80	/ton from mill
HSM Steel Structures (Aug 2005)	$1,100	/ton in place
Construction Labor	**$40**	**/hour**

Wind Turbine Installation In Shipyard

Hours per Installation	6	hours/turbine
Workers Per Installation	5	workers/turbine
Labor Rate	$40	/hour
Crane Fee per Tower	$6,250	/turbine
Inst. Cost Per Turbine:	**$7,450**	**/turbine**

Wind Turbine Installation at Sea

Installations per Day	2	/day
Labor	$16,800	/day
Crane	$500,000	/day
Barge	$10,000	/day
Tug	$30,000	/day
Inst. Cost Per Turbine	**$278,400**	**t**

Suction Pile Anchors

Synthetic Rope	$120	/meter
Anchor Cost per Load	$15	/kN vertical load
Minimum Anchor Cost	$25,000	/anchor
Installation Option 1		
Barge	$10,000	/day
Tug	$30,000	/day
Labor	$7,000	/day
Pumps + Divers	$7,000	/day
Anchors Installed	3	anchors/day
Installation per Anchor:	**$18,000.00**	**/anchor**
Installation Option 2		
AHV	$65,000	/day
Labor	$7,000	/day
Pumps + Divers	$7,000	/day
Anchors Installed	7	anchors/day
Installation per Anchor:	**$11,285.71**	**/anchor**

Platform Transportation and Installation

Mileage Fee	$200	/mile
Total Miles per Turbine	100	miles/turbine
Tug	$30,000	/day
Labor per day	$11,760	/day
Days for T&I	3	days/turbine
T&I Cost per Turbine	**$145,280**	**/turbine**

The total costs of the structures considered range from $1.5 to $2.25 million, and do not include the wind turbine, the power electronics, or the transmission systems. The general cost breakdown for each structure is shown in **Figure 11**. More detailed cost breakdowns of each general category are shown in **Figure 12, Figure 13,** and **Figure 14**.

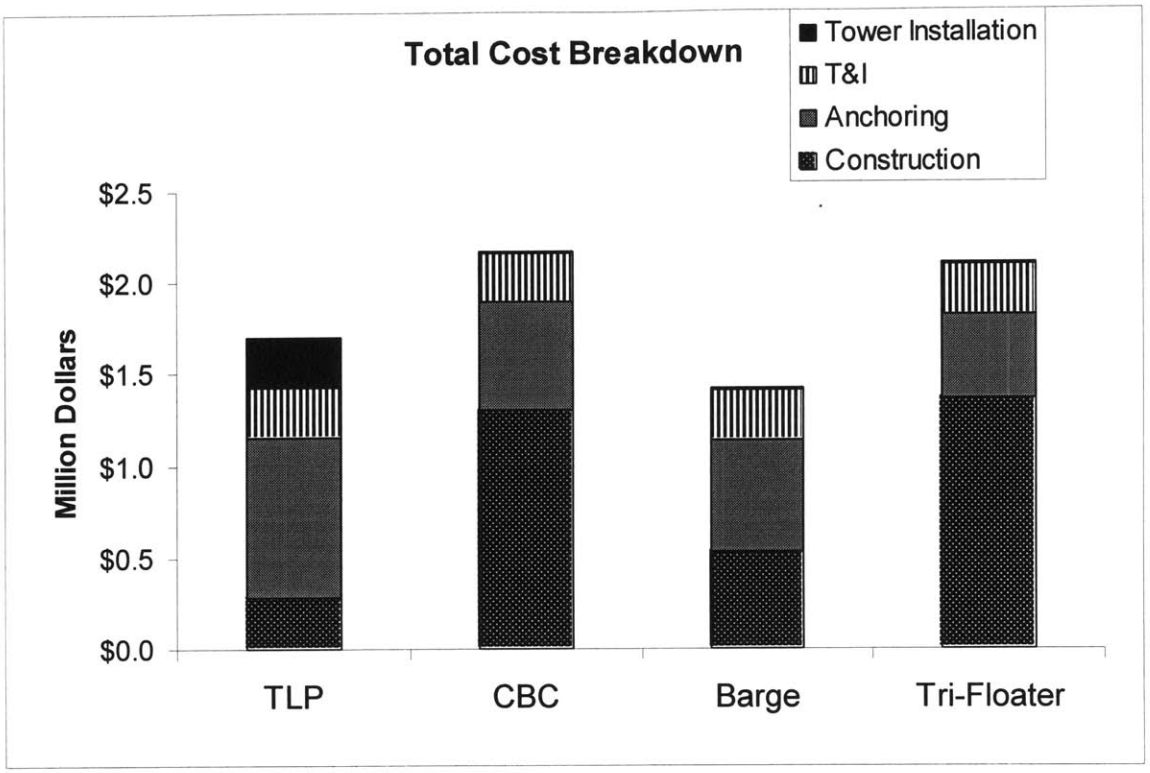

Figure 11. Total Cost Breakdown of Initial Structures

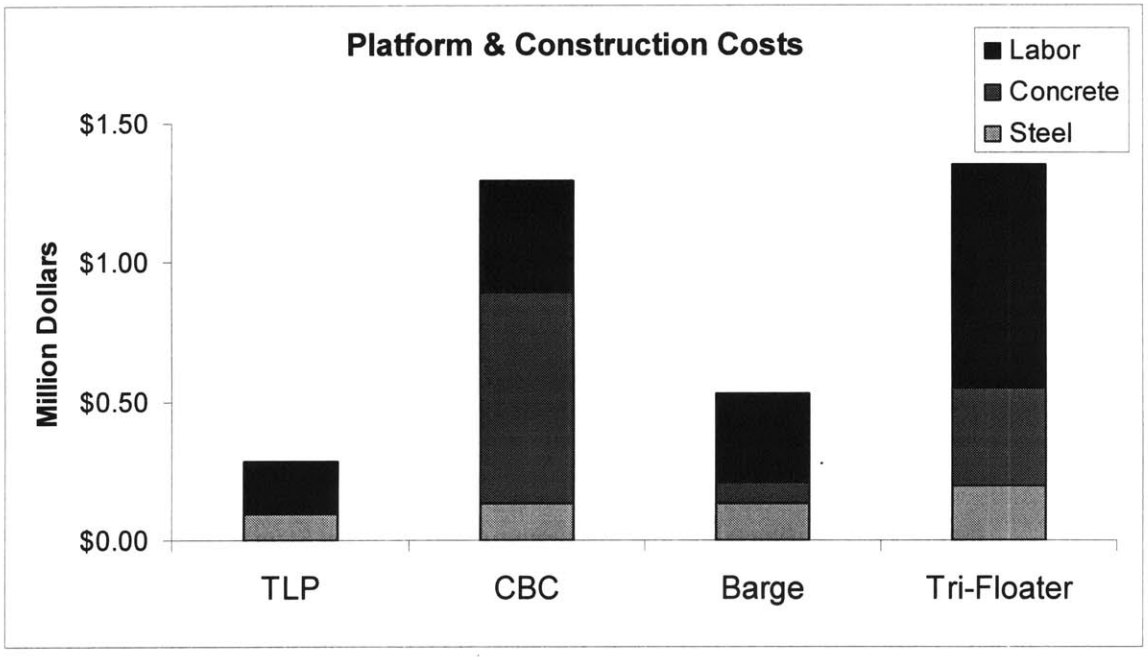

Figure 12. Cost of Construction for Initial Structures

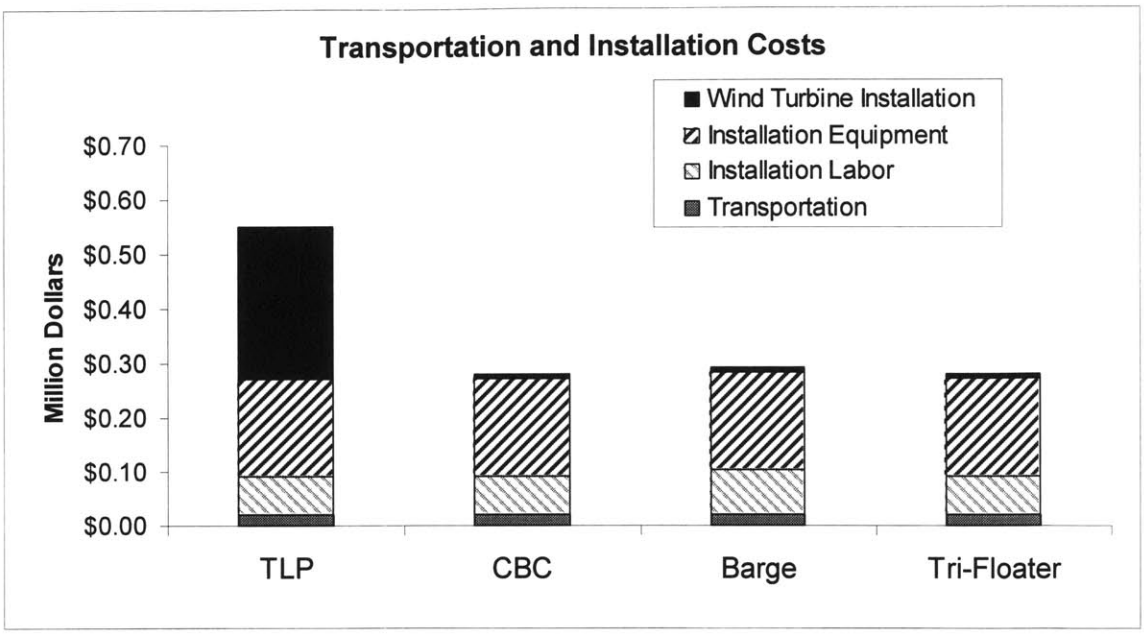

Figure 13. Mooring System and Mooring System Installation Costs for Initial Structures

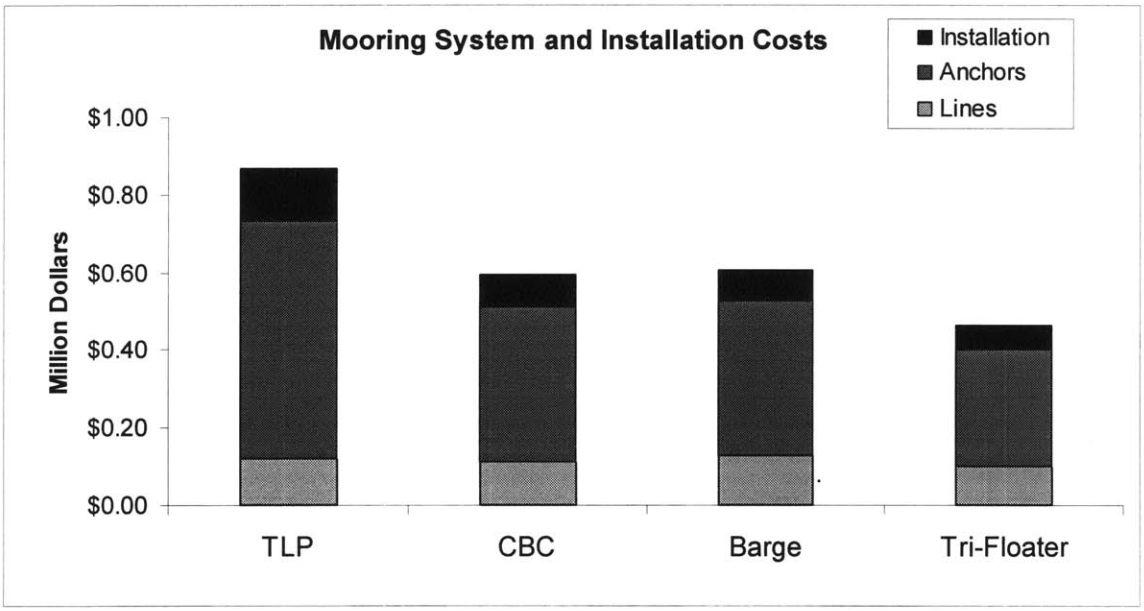

Figure 14. Transportation and Installation Costs of Initial Structures

Because the Barge and the TLP demonstrate the lowest costs, these designs are developed further, and are passed to the dynamic analysis phase.

Part 3

Design Refinement & Coupled Dynamic Analysis Methodology

8. Structures for Dynamic Analysis

The static design and analysis phase gave insight into the structures that would achieve acceptable steady-state performance. The most promising concepts from the cost perspective that met the steady-state performance criteria proved to be the barge and the TLP concepts. These concepts were then further refined and developed for dynamic analysis. This process and the resulting structures are described below for each structure-concept.

The systems are summarized in the coming sections in tabular form, with symbols described below.

$F_{Tethers,Total}$	=	Total downward force exerted on the body by the tethers
$F_{Tethers,each}$	=	Tension on each tether with no steady force acting on the system
ΔF	=	Change in tether tension due to a steady force on the system
$F_{T,3}$	=	Tension force in tether 3 with a steady force acting on the system
$F_{T,1}$	=	Tension force in tether 1 with a steady force acting on the system
$R_{G,4,O}$	=	Radius of Gyration in roll about the origin
$R_{G,5,O}$	=	Radius of Gyration in pitch about the origin
$R_{G,6,O}$	=	Radius of Gyration in yaw about the origin

8.1 MIT/NREL SDB

The structure estimated to have the lowest cost after the initial consideration was a structure of the barge concept. This concept was further developed into the

Massachusetts Institute of Technology (MIT) / National Renewable Energy Laboratory (NREL) Shallow Drafted Barge (SDB).

The initial barge concept was taken to be a lightly ballasted cylinder with a radius of 18.34 meters, a draft of 1.5 meters, and a cylinder height of 3 meters. Two concerns led to the modification of these properties. The first concern was that the extremely shallow draft would make the structure susceptible to slamming. Slamming occurs when the bottom surface of the structure becomes elevated above the water by a wave, then comes crashing down onto the water surface as the wave passes. The second concern was that the very shallow overall cylinder height would allow one side of the structure to be submerged as the wind turbine pitches and rolls, and would allow waves to crash on top of the structure. The submersion of any part of the structure below the water would cause the structure's waterplane area to be reduced. Because this structure derives most of its restoring from waterplane area, the structure would then lose its restoring properties, and the structure would immediately become unstable. Furthermore, slamming and waves crashing on the deck would induce highly nonlinear loading to the system.

For these reasons, the properties of the barge were altered to provide a structure with a deeper draft, and a larger total cylinder height. The modified structure, the MIT/NREL SDB has the properties listed in **Table 9**.

As stated in **Section 5.3**, catenary mooring lines are assumed to provide restoring only in surge and sway. To estimate a reasonable value of restoring in these modes, the program LINES [15] was used to model a catenary mooring system attached to a platform in its offset position. In this position, the upwind catenary mooring lines become taut, and the system behaves like a spread moored system. For a mooring system consisting of 8 mooring lines in a water depth of 200 m, with a diameter of .127 m, a radial spread of 200 m, and a tension of 1.56 MN, the restoring in surge and sway was estimated to be 4.16E+06 N/m. A value of 4E+06 N/m was then taken as the restoring coefficient in surge and sway for the catenary mooring system of the SDB.

Table 9. Properties of the MIT/NREL SDB

Radius	18.00	m
Cylinder Height	9.5	m
Concrete Ballast Height	1.595	m
Steel Thickness	0.015	m
Steel Mass	366	metric ton
Concrete Mass	4153	metric ton
Turbine Mass	698	metric ton
Total Mass	5217	metric.ton
$R_{G,4,0}$	10.07	m
$R_{G,5,0}$	10.07	m
$R_{G,6,0}$	12.89	m
Buoyant Mass	5217	metric ton
Reserve Buoyancy	0.00%	
Center of Gravity	4.39	m
Center of Buoyancy	-2.50	m
Installed Draft	5.00	m
Deck Clearance	4.50	m
Number of Lines	8	--
Number of Anchors	8	--
Radius of Anchors	200	m
Line Length	280	m
Line Diameter	0.156	m
Tension at Fairlead	1.76E+06	N
Tension at Anchor	1.66E+06	N
Maximum Breaking Load	2.38E+07	N

8.2 MIT/NREL TLP's

The TLP was another promising structure concept from the cost and steady-state performance perspectives. However, the need to mount the wind turbine at sea makes this concept vulnerable to dramatic increase in cost due to weather during the installation process. Because these structures are intended to be deployed in a wind farm setting, installation of the entire farm could span several months. During this time period, intervals of bad weather are guaranteed to occur, and to interfere with installation activities. Due to the costly daily rate of the equipment required for installing wind turbines to the platforms at sea, prolonged installation processes will result in dramatically increased project costs.

To avoid this vulnerability, the TLP was modified to a structure that could be ballasted with water to achieve adequate restoring to support the wind turbine during the installation processes, and deballasted at the site of installation once attached to the tethers to transfer the restoring role to the tethers. The wind turbine could then be mounted to the platform at the shipyard, and the entire system could be towed to its operation location already assembled.

During installation, the structure is filled with water to a certain level, and the platform becomes a surface-piercing ballasted cylinder. This structure then achieves restoring through waterplane area and ballasting. Once the system is in place, the tethers are connected to the structure, and the water ballast is pumped out of the structure. The use of water ballast during installation not only provides restoring during installation, but serves to pretension the mooring lines as well.

This design strategy introduces a new requirement of the mooring system to those considered in **Section 6.3**. The tether tension for this system must now fulfill three requirements: (1) the tethers must provide sufficient restoring in surge to adequately limit the steady-state offset in surge; (2) the tension of the windward tether must never exceed the maximum allowable tension, and the leeward tether must never go slack or fall below the minimum allowable tension at any point during operation; and (3) the total force exerted by the tethers must be comparable to the weight of the water required to ballast the system for stability during installation.

The additional requirement for the MIT/NREL TLP is that its tether tension must be comparable to the weight of the water used as ballast to provide adequate restoring to the system during towing and installation. The restoring criteria for the TLP during installation are presented below.

The maximum force that the system is expected to experience during towing is taken as the minimum thrust exhibited by the turbine during its operation, 250,000 N. The turbine

will clearly not be operating during towing and installation, so the wind loading on the structure will certainly be lower than any wind loading during operation. Therefore, the minimum operational thrust serves as a definite upper bound to the installation wind loading.

Again, the system is required to achieve adequate hydrostatic and inertial restoring to limit the steady-state pitch to less than 10 degrees during towing and installation. This limit was chosen to ensure that the system will remain almost vertical during installation processes, allowing the installers to tow the system with little stabilization required. To enforce this requirement, the minimum hydrostatic and inertial restoring coefficient required during towing can be found with the following equation.

$$C_{55,H\&I,\min} = \frac{F_5}{\xi_5} = \frac{250,000 \times 90}{.1745}\left[\frac{N-m}{rad}\right] = 1.28E+08[N-m]$$

This restoring is achieved by adjusting the cylinder height and radius and the level of concrete and water ballast, while requiring that the amount of water ballast must be comparable to the tether tension once installed.

This system was designed for two final configurations once installed: a surface-piercing cylinder, and a submerged cylinder. Because the mooring lines provide adequate restoring in pitch once installed, restoring from waterplane area is no longer necessary. Therefore, the cylinder could be submerged to reduce wave loading, as discussed in **Section 6.3**. The submerged configuration was considered and compared to the surface-piercing configuration. The structures in these configurations are summarized in **Table 10** and in **Table 11.**

Table 10. Platform Properties of the MIT/NREL TLPs

Property	Surface TLP	Submerged TLP	Units
Radius	11	11	m
Cylinder Height	26	24	m
Tower Draft	0	10	m
Concrete Ballast Height	4.5	4.5	m
Steel Thickness	0.015	0.015	m
Steel Mass	301.1	301.1	metric ton
Concrete Mass	4371.5	4371.5	metric ton
Turbine Mass	697.5	697.5	metric ton
Leg Length	0	0	m
Leg Width	0	0	m
Leg Height	0	0	m
Number of Legs	4	4	--
Lines per Leg	2	2	--
$R_{G,4,0}$	21.04	31.72	m
$R_{G,5,0}$	21.04	31.72	m
$R_{G,6,0}$	7.94	9.89	m

Table 11. Operational Properties of the MIT/NREL TLPs

Property	Surface TLP	Submerged TLP	Units
Number of Tethers	8	8	--
Tether Diameter	0.2	0.156	m
$F_{Tethers,Total}$	3.43E+07	4.90E+07	N
$F_{Tethers,each}$	4.29E+06	6.12E+06	N
ΔF	3.27E+06	3.27E+06	N
$F_{T,3}$	5.92E+06	7.76E+06	N
$F_{T,1}$	2.65E+06	4.49E+06	N
Installed Draft	22.75	36.00	m
Deck Clearance	3.25	-10.00	m
Total Mass	5370	5370	metric ton
Buoyant Mass	10131	10420	metric ton
Reserve Buoyancy	88.65%	94.04%	--
Center of Gravity	-12.01	-25.26	m

8.3 NREL TLP's

Because the MIT/NREL TLP relies on ballasting, and during installation, waterplane area to achieve restoring as well as the mooring system, the MIT/NREL TLP is really more of a hybrid between a TLP and a CBC than it is a traditional TLP. To illustrate the properties of a traditional TLP along the lines developed in **Section 6.3,** the NREL TLPs were developed and analyzed.

The NREL TLPs consist of a buoyant platform submerged to 10 meters below the calm water surface held in place by its tension leg mooring system.. The platform also has 4 legs, to which the mooring lines attach, that extend radially from its base. These legs lower the tension required to exert the required moment on the structure.

Reserve buoyancy of 2 and 6 are proposed to illustrate the effects of different tensions. These structures are summarized in **Table 12** and
Table 13.

Table 12. Platform Properties of the NREL TLPs

Property	RB = 2	RB = 6	Units
Radius	6.50	10	m
Cylinder Height	13	20	m
Tower Draft	10	10	m
Concrete Ballast Height	0	0	m
Steel Thickness	0.015	0.015	m
Steel Mass	169	297	metric ton
Concrete Mass	0	0	metric ton
Turbine Mass	698	698	metric ton
Leg Length	10	10	m
Leg Width	4	4	m
Leg Height	4	4	m
Number of Legs	4	4	--
Lines per Leg	2	2	--
$R_{G,4,0}$	17.67	22.61	m
$R_{G,5,0}$	17.67	22.61	m
$R_{G,6,0}$	8.04	10.19	m

Table 13. Operational Properties of the NREL TLPs

Property	RB = 2	RB = 6	Units
Number of Tethers	8	8	--
Line Diameter	0.102	0.156	m
$F_{Tethers,Total}$	2.06E+07	6.21E+07	N
$F_{Tethers,each}$	2.58E+06	7.77E+06	N
ΔF	2.12E+06	1.80E+06	N
$F_{T,3}$	3.63E+06	8.67E+06	N
$F_{T,1}$	1.52E+06	6.87E+06	N
Installed Draft	19.00	30	m
Deck Clearance	-5.00	-10	.m
Total Mass	882	995	metric ton
Buoyant Mass	3010	7386	metric ton
Reserve Buoyancy	241%	642%	--
Center of Gravity	31.88	16.55	m

9. Static and Dynamic Analysis Methodology

The combined wind turbine and floating platform systems were analyzed in the frequency domain by following the process outlined in **Figure 15**.

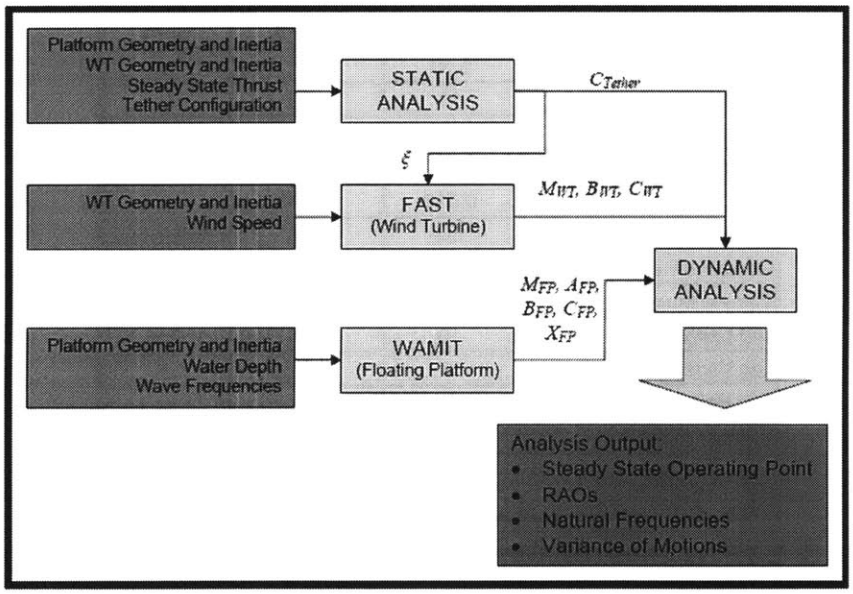

Figure 15. Static and Dynamic Analysis Process

Inputs to this analysis process are shown in blue in this figure, analysis modules are shown in yellow, quantities passed between the modules are shown along the arrows, and the final outputs are shown in green.

This process first takes the platform and wind turbine geometry and inertia, the steady-state thrust of the wind turbine, and the tether configuration into the STATIC ANALYSIS module. This module calculates the steady forces on the system and the system's restoring, and computes the steady-state operating point, summarized by the six element vector, ξ.

This steady-state operating point is passed to the FAST module that calculates the linearized properties of the wind turbine about the initial conditions. These properties include the wind turbine's mass, damping, and stiffness matrices that incorporate contributions from aerodynamics and gyroscopics, shown in **Figure 15** as M_{WT}, B_{WT}, C_{WT}, respectively. The platform geometry and inertia and the water depth are then passed to WAMIT, which calculates the platform's mass, added mass, damping and restoring (stiffness) matrices, and exciting forces M_{FP}, $A_{FP}(\omega)$, $B_{FP}(\omega)$, C_{FP}, and $X_{FP}(\omega)$ at each frequency.

The matrices for the wind turbine, the platform, and the mooring system are passed to the DYNAMIC ANALYSIS module, where they combined to represent the coupled system. This module then calculates the RAOs, natural frequencies, and standard deviations of motions for the combined system, and the maximum and minimum line tensions of the TLP tethers due to wind and wave loading.

The details of the calculations performed in each module are detailed in the following sections.

9.1 Steady-State Operating Point

A static analysis is first carried out to determine the steady-state operating configuration of the combined wind turbine-floating platform system in its moored condition. This configuration is governed by the static equilibrium equation, summarized in matrix form:

$$[C_{H\&I} + C_{Tethers}]\left(\xi_{\substack{Steady \\ State}}\right) = \left(F_{\substack{Steady \\ State}}\right)$$

where $C_{H\&I}$ and $C_{Tethers}$ represent the six-by-six restoring matrices from the hydrostatics and inertia from the tethers, respectively, $\xi_{Steady\ State}$ represents the six-element steady-state displacement vector, and $F_{Steady\ State}$ represents the six-element steady-state force and moment vector exerted on the system by the wind.

Assuming small rotations and displacements, the restoring coefficients are as follows. The hydrostatic and inertial restoring matrix for a surface-piercing cylinder contains all zeros except for the 33, 44, and 55 entries, which are defined here.

$$C_{33,H\&I} = \rho g \pi R^2$$

$$C_{44,H\&I} = F_b z_b - M_{11} g z_g + \frac{\rho g \pi R^4}{4}$$

$$C_{55,H\&I} = F_b z_b - M_{11} g z_g + \frac{\rho g \pi R^4}{4}$$

The restoring matrix for a tension leg mooring system contains all zeros except the following entries. As explained in Section 5, the tethers of the tension leg mooring system are modeled as infinitely stiff tethers to model purely rigid body motions. This drives $C_{33,Tethers}$, $C_{44,Tethers}$, and $C_{55,Tethers}$ toward infinity.

$$C_{11,Tethers} = \frac{F_{Tethers}}{L_{Tethers}}$$

$$C_{22,Tethers} = \frac{F_{Tethers}}{L_{Tethers}}$$

$$C_{33,Tethers} = \frac{E_{Tethers} A_{Tethers}}{L_{Tethers}} \to \infty$$

$$C_{44,Tethers} = 2\frac{E_T A_T}{L_T}\left(R_{Fairlead}\right)^2 + (F_B - M_{11}g)T \to \infty$$

$$C_{55,Tethers} = 2\frac{E_T A_T}{L_T}\left(R\right)^2 + (F_B - M_{11}g)T \to \infty$$

$$C_{66,Tethers} = \frac{\left(R_{Fairleed}\right)^2}{L_{Tethers}}\left(F_b - M_{11}g\right)$$

$$C_{51,Tethers} = C_{42,Tethers} = -\frac{F_{Tethers}}{L_{Tethers}}T$$

The MIT/NREL SDB is intended to represent a system that achieves stability through waterplane area. A mooring system is used with this design for station keeping only. Therefore, restoring is assumed to be provided only by the mooring lines in the mode of surge.

Steady-state static displacement is then calculated as follows.

$$\xi_{\substack{Steady \\ State}} = \left[C_{H\&I} + C_{Tethers}\right]^{-1}\left(F_{\substack{Steady \\ State}}\right)$$

9.2 Response Amplitude Operators

The RAOs are calculated in the DYNAMIC ANALYSIS module for the combined wind turbine and floating platform system.

The equations of motion that govern the linear dynamic motions of the system are summarized in matrix form:

$$\left[-\omega^2\left(M+A(\omega)\right)+i\omega B(\omega)+C\right]\Xi(\omega)=X(\omega)$$

where M, A(ω), B(ω), and C represent the 6 by 6 combined mass, added mass, damping, and restoring (stiffness) matrices, respectively, and X(ω), the 6 by 1 vector that contains the hydrodynamic exciting forces.

The mass matrix can be found easily, while the added mass matrix, the damping matrix, and exciting forces are evaluated by WAMIT and FAST. The restoring matrix represents the restoring from hydrostatics, inertia, and the mooring system, as developed in the previous section.

The symbol Ξ(ω) represents the system's dimensional response in each mode of motion at each frequency. The RAO is then reported as the dimensionless motion.

For the translational modes of motion, the RAO is given by

$$RAO_i(w)=\left|\frac{\Xi_i(w)}{A_{wave}}\right| \qquad i = 1,2,3$$

and for the rotational modes of motion, the RAO is given by

$$RAO_i(\omega)=\left|\frac{\Xi_i(\omega)}{A_{wave}/R}\right| \quad i = 4,5,6$$

where the subscript i denotes the mode of motion, A_{wave} represents the wave amplitude, and R is the cylinder radius.

Although the RAOs are independent of the sea state, the damping and stiffness properties of the wind turbine depend on wind speed, which causes the RAOs of the combined system to depend on wind speed.

9.3 Natural Frequencies

The natural frequencies of the combined wind turbine and floating platform system can be estimated by considering the system's restoring and inertial properties, as given in the equation below.

$$\omega_i^* = \sqrt{\frac{C_{ii}}{M_{ii} + A_{ii}(0)}},$$

where the subscript i indicates the mode of motion, and $A_{ii}(0)$ indicates the zero-frequency limit of the added mass in that mode.

In weakly restored modes of motion, the natural frequency will be calculated as zero. These modes of motion, however, pick up a natural frequency through cross coupling to other modes of motion. In this case, the natural frequencies can be determined graphically, by examining the frequency at which the peak of the RAO occurs.

9.4 Standard Deviation of System Motions

By virtue of linear system theory, once the RAOs of the system have been determined, the variance and standard deviation of the system motions in various sea states can be ascertained, as developed by Sclavounos in [14] and in [11]. An assumption of linear system theory is that given a Gaussian input signal, the output of the linear system will also be Gaussian with a variance determined by the Wiener-Khinchine theorem. The

variance is then calculated from the input signal and the RAO, as shown in the following equation for the translational modes:

$$\sigma_{\xi_i}^2 = \int S_\zeta(\omega)\left|RAO_i\right|^2 d\omega \qquad i = 1,2,3,$$

and by the equation below for the rotational modes,

$$\sigma_{\xi_i}^2 = \int S_\zeta(\omega)\frac{\left|RAO_i\right|^2}{R^2} d\omega \qquad i = 4,5,6$$

where $\sigma_{\xi_i}^2$ represents the variance of system motion in mode i, $S_\zeta(\omega)$, the spectral density of the ambient waves in the given sea state, ω , the wave frequency, and R, the radius that was used originally to make the *RAO* non-dimensional.

The spectral density for fully developed seas has been defined by the International Ship Structures Committee (ISSC) and the International Towing Tank Conference (ITTC) [14].

$$S_\zeta(\omega) = \left(H_s^2 T_m\right)\left(\frac{.11}{2\pi}\right)\left(\frac{\omega T_m}{2\pi}\right)^{-5} \exp\left\{.44\left(\frac{\omega T_m}{2\pi}\right)^{-4}\right\}$$

H_S and T_m represent significant wave height and mean period in the given sea state, respectively. The sea states considered in this study are summarized in **Table 14**, and their spectral densities are shown in **Figure 16**. The DYNAMIC ANALYSIS module performs this calculation to give the standard deviation of the system motion in the 5 sea states defined in **Table 14.**

Table 14. Sea State Definition

Sea State	H_s [m]	T_m [s]
1	0.09	2.0
2	0.67	4.8
3	2.44	8.1
4	5.49	11.3
5	10.00	13.6

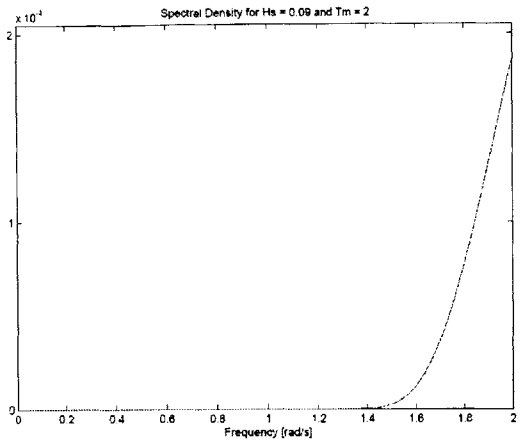

(a) Sea State 1

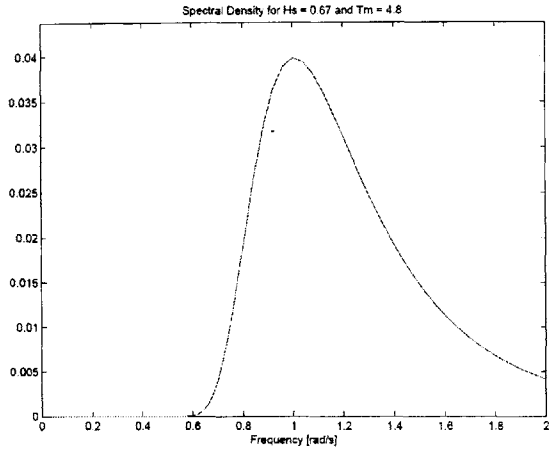

(b) Sea State 2

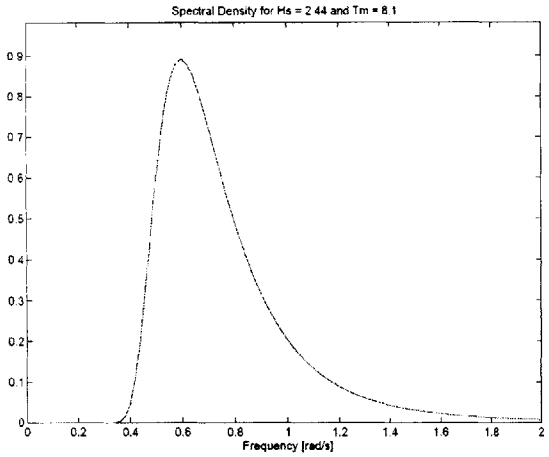

(c) Sea State 3

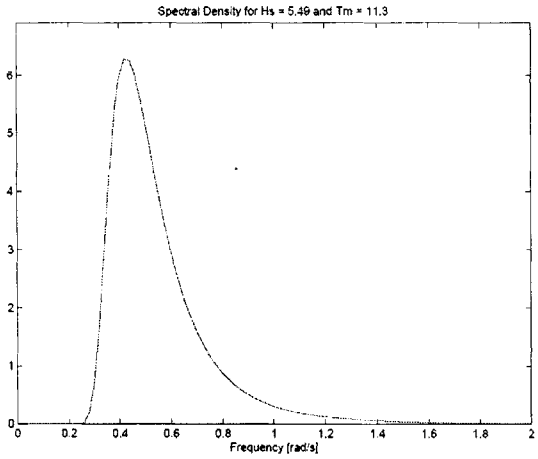

(d) Sea State 4

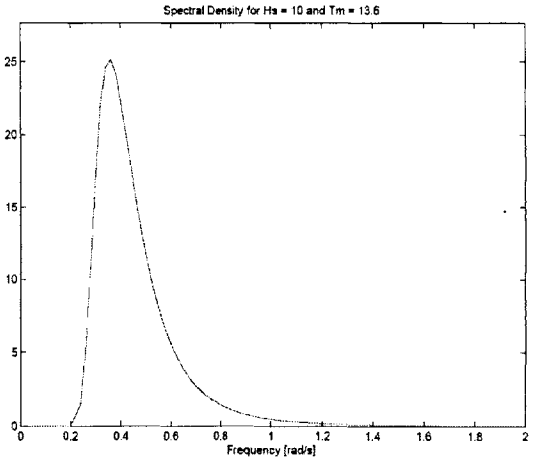

(e) Sea State 5

Figure 16 (a) – (e). Spectral Densities of the Sea States

9.5 Dynamic Line Tension

The line tensions of the upwind and downwind lines of the TLPs are solved for in a similar manner developed in **Section 6.3** for the static case. For the dynamic case, the exciting force in pitch is added to the steady-state force in pitch as shown in the following equation.

$$F_5 + X_5 = \left(F_{T,ave} + \Delta F\right)\left(R + L_{Leg}\right) - \left(F_{T,ave} - \Delta F\right)\left(R + L_{Leg}\right)$$

Using this equation, ΔF can be found, and the tensions of the upwind and downwind tethers are found subsequently.

9.6 Analysis Cases

Analyses were performed by following this entire process for the structures outlined in the sections above in various wind, wave, and water depth conditions, and with various values of viscous damping. Results are reported in the sections that follow to illustrate the effects of coupling the wind turbine with the floating platform, the effects of water depth, wind speed, and viscous damping.

9.6.1 Base Case

The base case chosen has a water depth of 200 m, and a wind speed of 11.2 m/s. The water depth of 200 m was chosen because it is the baseline water depth for NREL offshore wind energy studies, and would allow direct comparison between this study and other NREL studies. The wind speed of 11.2 m/s was chosen because it is the wind turbine's rated wind speed, and will therefore represent the likely operating conditions for the wind turbine.

9.6.2 Water Depth Effects

To illustrate the effects of water depth, the responses of the structures are presented in water depths up to 200 m for the SDB, and 300 m for all other structures. The MIT/NREL SDB is presented in water depths of 10, 30, 62.5, 100, and 200, while all other structures are presented in depths of 62.5, 100, 200, and 300 m. The SDB is analyzed in shallower water depths because it is thought that this type of structure is more appropriate for deployment closer to shore and in shallower water than the TLPs. An analysis of the SDB at 10 m was performed to examine this structure as a potential alternative to monopiles in shallow water. 30 m represents the depth where monopiles become technically and economically challenging to install, and the possible transition depth to the use of floating structures. The depth of 62.5 m was considered because this depth represents the former NREL baseline water depth, and allows this study to be compared to earlier studies. Finally the depths of 100 and 200 m were studied to illustrate the effects of increasing depth, and to comply with the current NREL baseline water depth of 200 m.

The TLPs were analyzed in slightly deeper waters, starting at 62.5 m, the former NREL baseline depth. Analyses in water depths of 100, 200, and 300 are presented to illustrate the effects of increasing water depth, surrounding the current NREL baseline depth of 200 m.

9.6.3 Wind Speed Effects

To illustrate the system performance in various wind speeds, results of the coupled systems are reported in wind speeds representative of different regions of the turbine power curve. The wind speed of 9 m/s represents Region 2 of the power curve, and is the wind speed where the turbine is producing roughly half its rated power. The wind speed of 11.2 m/s represents the turbine's rated wind speed, the speed at which the turbine first produces its maximum power. The wind speed of 15 m/s represents Region 3 of the power curve, while the speed of 25 m/s represents the cut-out wind speed.

9.6.4 Viscous Damping Effects

Finally, the effects of viscous damping on the platforms were considered. At low frequencies, hydrodynamic damping is close to zero. In practice, however, damping will occur at very low frequencies due to viscous effects [8]. Viscous damping can be achieved and tuned in the structure by, for example, adding damping plates or other drag elements. Although these physical mechanisms were not modeled here, viscous damping was added to the model to observe the effects on the system's response, which is defined by the viscous damping ratio, γ.

$$\gamma = \frac{B_{Viscous}}{2\omega^{*}(M+A)}$$

The viscous damping matrix was solved for, for different values of γ ranging from 0 to .1, and was added to the total damping matrix.

This consideration was only carried out for the TLPs because the natural frequencies of the SDB fell in zones with high hydrodynamic damping. Thus, viscous damping has negligible effect on its responses.

Part 4

Coupled Dynamic Analysis Results

10. The MIT/NREL SDB

10.1 Base Case – Coupled Effects

10.1.1 Results

Table 15. Steady State Pitch, MIT/NREL SDB, Base Case

Wind Speed [m/s]	Thrust [kN]	Restoring [N-m]	Pitch [deg]
11.2	800	4.76E+08	8.66

Table 16. Natural Frequencies, MIT/NREL SDB, Base Case

Mode	Natural Frequency	
Surge	0.7702	[rad/s]
Sway	0.7702	[rad/s]
Heave	0.7012	[rad/s]
Roll	0.4481	[rad/s]
Pitch	0.4502	[rad/s]
Yaw	0.0000	[rad/s]

Table 17. Standard Deviations of System Motions, MIT/NREL SDB, Base Case

Sea State		1	2	3	4	5
Hs	[m]	0.09	0.67	2.44	5.49	10
Tm	[s]	2	4.8	8.1	11.3	13.6
Surge	[m]	0.000	0.199	1.310	1.931	2.598
Sway	[m]	0.000	0.000	0.006	0.022	0.035
Heave	[m]	0.000	0.094	0.623	1.401	2.532
Roll	[deg]	0.000	0.000	0.017	0.068	0.109
Pitch	[deg]	0.000	0.014	0.204	0.567	0.927
Yaw	[deg]	0.000	0.001	0.026	0.093	0.156

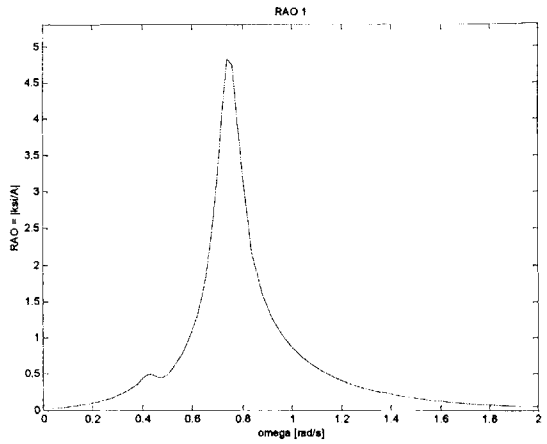

(a) RAO 1

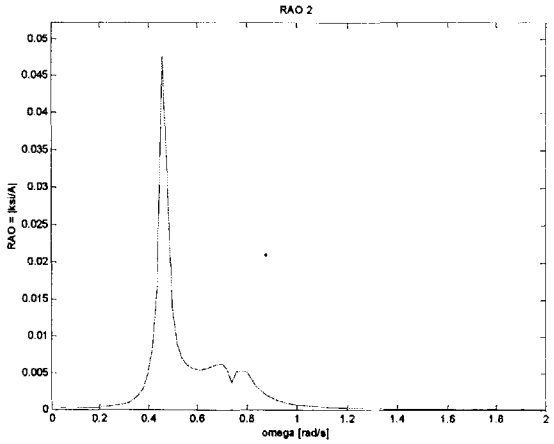

(b) RAO 2

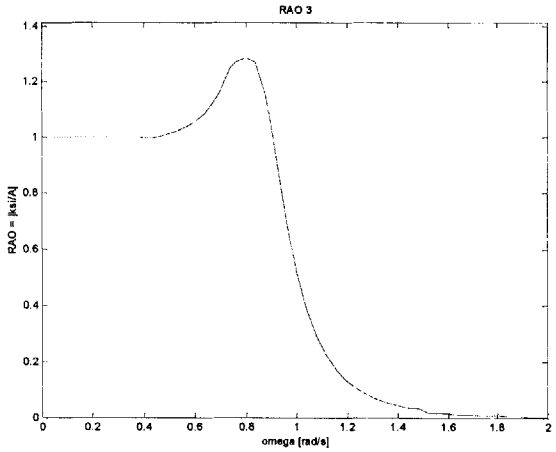

(c) RAO 3

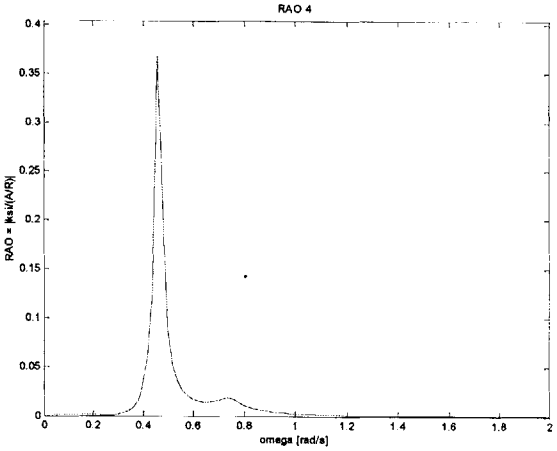

(d) RAO 4

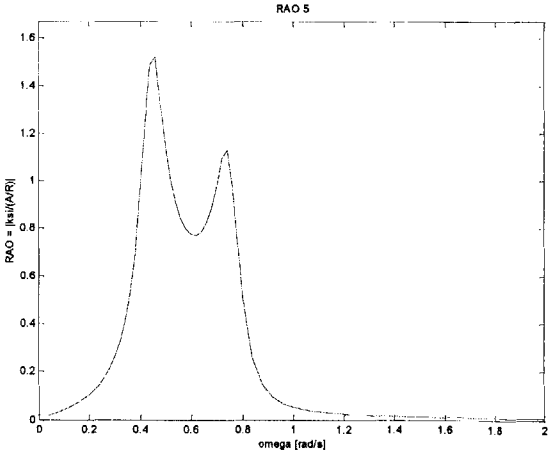

(e) RAO 5

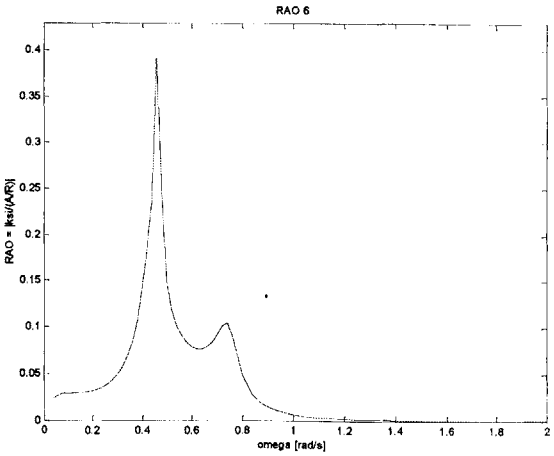

(f) RAO 6

Figure 17 (a) - (f). RAOs, MIT/NREL SDB, Base Case

10.1.2 Discussion

The RAOs of the combined wind turbine and floating platform are shown in **Figure 17**. Although the system is excited by wind and waves only in the modes of surge, heave, and pitch, it displays motion in the modes of sway, roll, and yaw as well. The system's response in these modes indicates the effects of the coupling mechanisms that result from combining the wind turbine with the floating platform.

The frequencies at which the ROAs show a peak also indicate effects of coupling between modes of motion. Although the system's natural frequency in sway is .77 rad/s, the RAO in sway only shows a small response at the frequency of .77 rad/s, and a large response at the frequency of .45 rad/s, the natural frequency of the system in pitch and roll. This indicates coupling between these modes of motion. Similarly, the RAOs in roll and pitch show small peaks at the frequency of .77 rad/s, again showing this cross coupling. The natural frequency in yaw is calculated to be zero, due to the lack of restoring in that mode, but the RAO shows resonant responses at frequencies of .45 and .77 rad/s, showing coupling to other modes.

Finally, the standard deviations of the system motions in 5 sea states are summarized in **Table 17**. For the MIT/NREL SDB, **Table 17** shows increasing standard deviations of system motions with increasing severity of sea state. This can be attributed to the shape of the RAOs and the shape of spectral densities describing different sea states. At lower sea states, the spectral density has a large spread, and is centered about relatively high frequencies. As the severity of the sea state increases, its spectral density becomes more narrow-banded, and centered about lower frequencies. The standard deviation of system motions increase with increasing sea state because the MIT/NREL SDB's natural frequencies are low compared to the frequencies where the peak of the spectral densities

occur. As the sea state increases, the peak of the spectral density approaches the natural frequency, which results in an increasing response with increasing sea state.

These results show the importance of considering the sea state properties of a site chosen for the installation of a floating structure. The structure must be tuned by adjusting the restoring properties to achieve RAOs whose peaks are not coincident with the peak of the spectral density describing the likely sea state at that site.

10.2 Wind Speed Effects

10.2.1 Results

Table 18. Steady-State Offset, MIT/NREL SDB, WInd Speed Effects

Wind Speed [m/s]	Thrust [kN]	Restoring [N-m]	Pitch [deg]
9	600	4.76E+08	6.50
11.2	800	4.76E+08	8.66
15	500	4.76E+08	5.41
25	400	4.76E+08	4.33

Table 19. Natural Frequencies, MIT/NREL SDB, Wind Speed Effects

Wind Speed	[m/s]	9	11.2	15	25
Surge	[rad/s]	0.770	0.770	0.770	0.770
Sway	[rad/s]	0.770	0.770	0.770	0.770
Heave	[rad/s]	0.701	0.701	0.701	0.701
Roll	[rad/s]	0.446	0.448	0.446	0.446
Pitch	[rad/s]	0.447	0.450	0.448	0.447
Yaw	[rad/s]	0.000	0.000	0.000	0.000

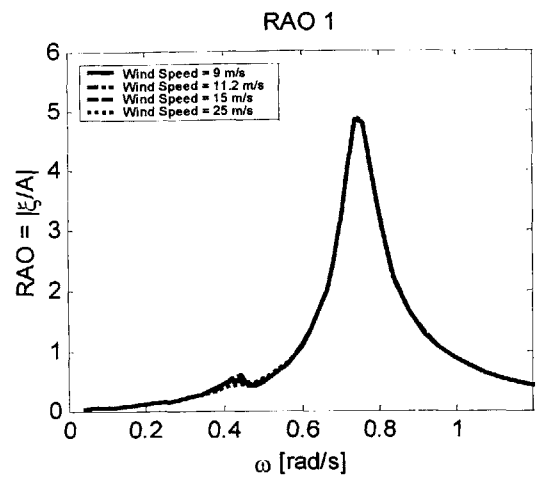

(a) RAO 1

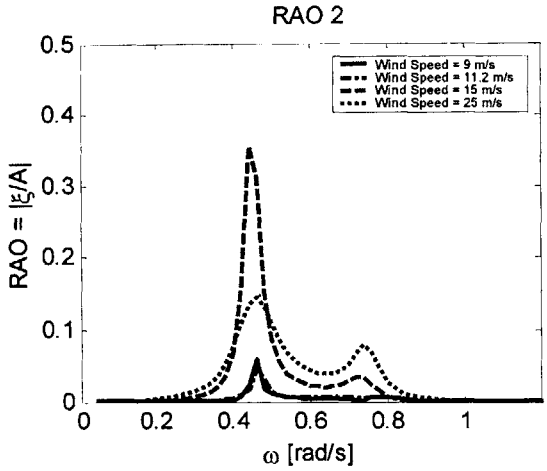

(b) RAO 2

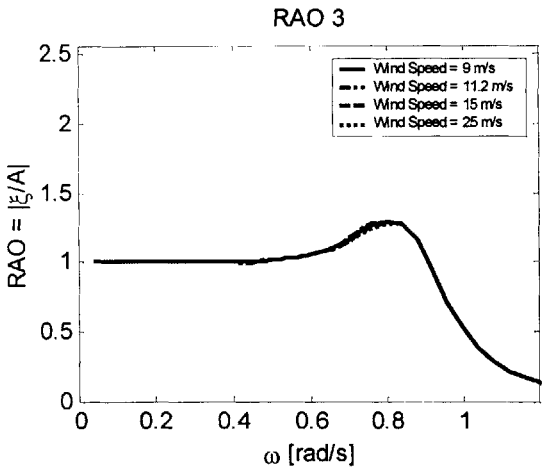

(c) RAO 3

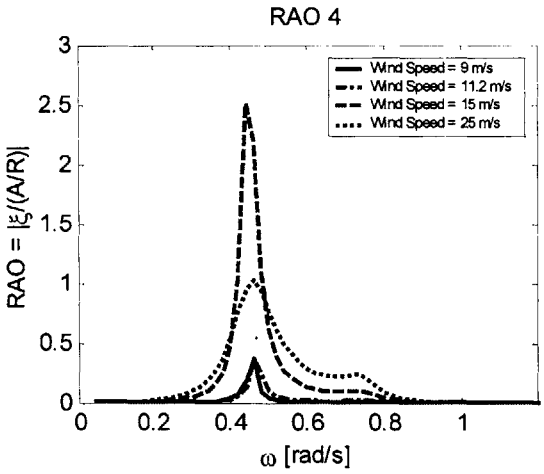

(d) RAO 4

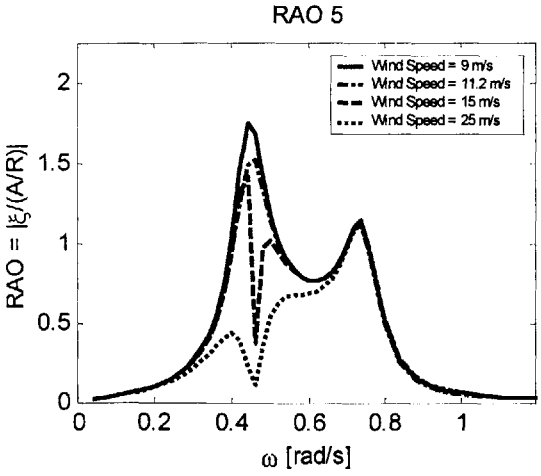

(e) RAO 5

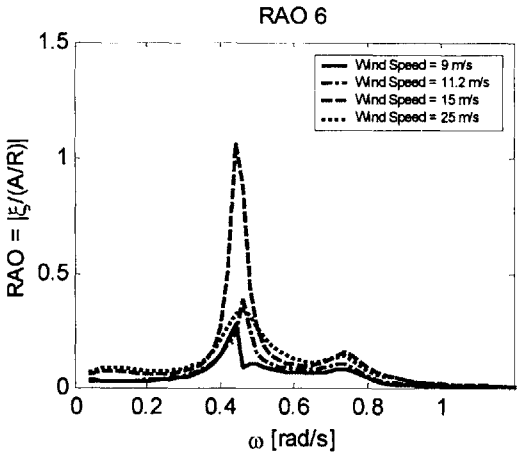

(f) RAO 6

Figure 18 (a) - (f). RAOs, MIT/NREL SDB, Wind Speed Effects

Table 20. Standard Deviations of System Motions, MIT/NREL SDB, Wind Speed Effects

Sea States	Hs [m]	0.09	0.67	2.44	5.49	10
	Tm [s]	2	4.8	8.1	11.3	13.6
Surge [m]	9 m/s	0.0004	0.1997	1.3126	1.9333	2.6012
	11.2 m/s	0.0004	0.1989	1.3103	1.9314	2.5981
	15 m/s	0.0004	0.2002	1.3129	1.9373	2.6100
	25 m/s	0.0004	0.2008	1.3192	1.9396	2.6006
Sway [m]	9 m/s	0.0000	0.0002	0.0059	0.0234	0.0375
	11.2 m/s	0.0000	0.0003	0.0060	0.0220	0.0350
	15 m/s	0.0000	0.0008	0.0412	0.1869	0.3098
	25 m/s	0.0000	0.0021	0.0356	0.1149	0.1884
Heave [m]	9 m/s	0.0000	0.0942	0.6215	1.4006	2.5316
	11.2 m/s	0.0000	0.0943	0.6231	1.4015	2.5319
	15 m/s	0.0000	0.0942	0.6202	1.4015	2.5344
	25 m/s	0.0000	0.0942	0.6195	1.4013	2.5345
Roll [deg]	9 m/s	0.0000	0.0002	0.0144	0.0638	0.1039
	11.2 m/s	0.0000	0.0003	0.0173	0.0685	0.1094
	15 m/s	0.0000	0.0012	0.1197	0.5528	0.9168
	25 m/s	0.0000	0.0028	0.0927	0.3312	0.5473
Pitch [deg]	9 m/s	0.0000	0.0147	0.2101	0.6152	1.0129
	11.2 m/s	0.0000	0.0144	0.2039	0.5675	0.9271
	15 m/s	0.0000	0.0149	0.1928	0.5031	0.8292
	25 m/s	0.0000	0.0147	0.1638	0.3090	0.4739
Yaw [deg]	9 m/s	0.0000	0.0011	0.0178	0.0678	0.1188
	11.2 m/s	0.0000	0.0014	0.0263	0.0933	0.1555
	15 m/s	0.0000	0.0023	0.0535	0.2360	0.3949
	25 m/s	0.0000	0.0021	0.0361	0.1186	0.2001

10.2.2 Discussion

The wind speed affects the system in 2 ways; by affecting the steady-state force on the system resulting in different steady-state offsets, and by affecting the wind turbine's dynamic properties resulting in different dynamic responses.

As the wind increases in Region 2 of the power curve, the thrust also increases, resulting in increased steady-state offsets in this region. In Region 3 of the power curve, the thrust reduces with wind speed, resulting in decreased steady-state offsets in this region.

The RAOs of the combined system in various wind speeds show that wind speed has negligible effects on the RAOs of surge and heave, but significant effects on the other RAOs. Wind speed affects the combined system dynamics primarily by introducing different levels of damping due to the wind turbine. The wind speed has little effect on

RAO 1 because wind turbine damping contributes very little to total damping. Changes in the wind turbine damping, therefore, has little effect on the system's performance in surge. RAO 3 is not affected because the wind turbine does not contribute at all to total system damping in this mode at any wind speed. Wind turbine damping contributes significantly to damping in pitch, however, and as a result, RAO 5 is highly affected by wind speed. RAOs 2, 4, and 6 demonstrate coupling mechanisms once again, as these modes are not directly excited by wind and waves.

The RAOs also demonstrate that the system response decreases from wind speeds 9 to 11.2 m/s, then increase to the maximum response at 15 m/s, then decrease slightly at wind speeds of 25 m/s. The decrease of response in Region 2 of the power curve (from 9 to 11.2 m/s) occurs because as the wind turbine increases power output with wind speed, the damping from the wind turbine also increases. The response then decreases in Region 3 (from 11.2 to 15 m/s), as the wind turbine feathers its blades to let some wind pass by without increasing its power output. As the blades begin to feather, they provide less damping, which results in increased motions. Finally, the slight decrease in response observed at the higher wind speeds of Region 3 of the power curve (from 15 to 25 m/s) can be explained by a slight increase in damping in this region. This increase in damping in this region is thought to occur because as the wind speed approaches cut-out wind speed, the airflow becomes very turbulent and fully separates from the blades.

The effects of wind speed on the system response are summarized by the standard deviations of system motions, which reflect the same behavior observed in the RAOs.

10.3 Water Depth Effects

10.3.1 Results

The water depth does not affect the restoring properties of the MIT/NREL SDB, and therefore does not affect the steady-state offset. Steady-state offset is summarized in the base case results section above.

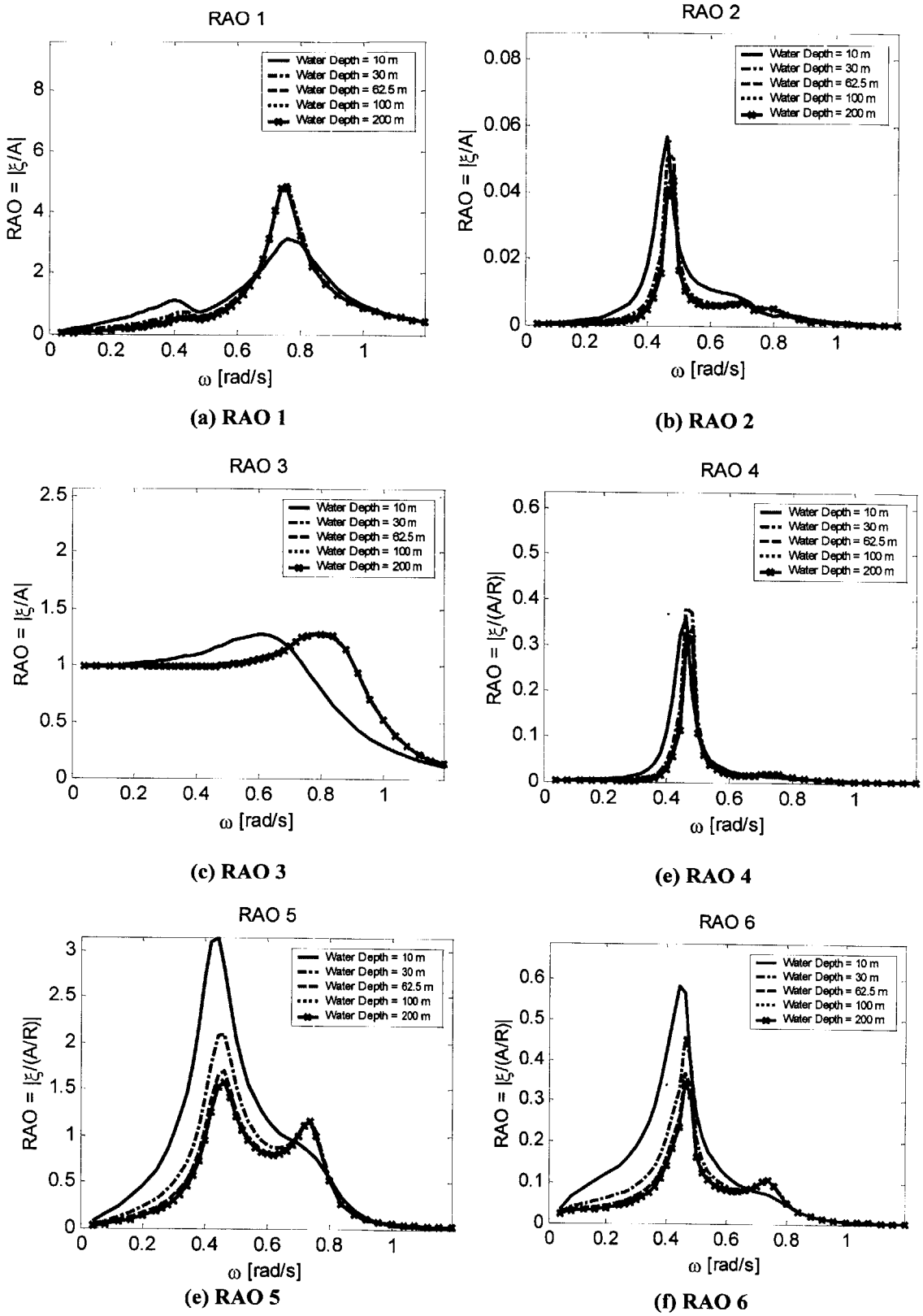

Figure 19. RAOs, MIT/NREL SDB, Water Depth Effects

Table 21. Natural Frequencies, MIT/NREL SDB, Water Depth Effects

Water Depth	[m]	10	30	62.5	100	200
Surge	[rad/s]	0.728	0.767	0.770	0.770	0.770
Sway	[rad/s]	0.728	0.767	0.770	0.770	0.770
Heave	[rad/s]	0.402	0.575	0.650	0.678	0.701
Roll	[rad/s]	0.437	0.451	0.452	0.452	0.448
Pitch	[rad/s]	0.439	0.453	0.454	0.454	0.450
Yaw	[rad/s]	0.000	0.000	0.000	0.000	0.000

Table 22. Standard Deviations of System Motions, MIT/NREL SDB, Water Dpeth Effects

Sea States	Hs [m]	0.09	0.67	2.44	5.49	10
	Tm [s]	2	4.8	8.1	11.3	13.6
Surge [m]	10 m	0.00038	0.186	1.101	1.859	2.870
	30 m	0.00039	0.205	1.340	2.024	2.803
	62.5 m	0.00039	0.199	1.312	1.948	2.647
	100 m	0.00039	0.199	1.306	1.928	2.604
	200 m	0.00039	0.199	1.310	1.931	2.598
Sway [m]	10 m	0.00000	0.000	0.009	0.034	0.056
	30 m	0.00000	0.000	0.008	0.028	0.044
	62.5 m	0.00000	0.000	0.007	0.024	0.037
	100 m	0.00000	0.000	0.006	0.023	0.035
	200 m	0.00000	0.000	0.006	0.022	0.035
Heave [m]	10 m	0.00004	0.056	0.613	1.526	2.760
	30 m	0.00004	0.094	0.626	1.411	2.547
	62.5 m	0.00004	0.094	0.624	1.403	2.534
	100 m	0.00004	0.094	0.623	1.402	2.532
	200 m	0.00004	0.094	0.623	1.401	2.532
Roll [deg]	10 m	0.00000	0.000	0.019	0.086	0.143
	30 m	0.00000	0.000	0.022	0.084	0.134
	62.5 m	0.00000	0.000	0.019	0.072	0.114
	100 m	0.00000	0.000	0.018	0.068	0.107
	200 m	0.00000	0.000	0.017	0.068	0.109
Pitch [deg]	10 m	0.00001	0.013	0.301	1.148	2.061
	30 m	0.00002	0.015	0.243	0.762	1.286
	62.5 m	0.00002	0.015	0.216	0.625	1.035
	100 m	0.00002	0.015	0.210	0.586	0.960
	200 m	0.00002	0.014	0.204	0.567	0.927
Yaw [deg]	10 m	0.00000	0.001	0.041	0.186	0.339
	30 m	0.00000	0.001	0.033	0.125	0.214
	62.5 m	0.00000	0.001	0.028	0.101	0.171
	100 m	0.00000	0.001	0.027	0.094	0.158
	200 m	0.00000	0.001	0.026	0.093	0.156

10.3.2 Discussion

The RAOs of the combined system show a decreasing response with increasing water depth, due to the effects of increasing water depth on hydrodynamic added mass and damping. These effects are also summarized by the standard deviation of system motions, which also decrease with increasing water depth. These results report a maximum standard deviation in pitch of only around 2 degrees. This shows that the SDB displays very acceptable motions, and is not limited to deployment in shallow waters.

11. MIT/NREL TLP Surface

11.1 Base Case – Coupled Effects

11.1.1 Results

Table 23. Steady-State Offset, MIT/NREL TLP Surface, Base Case

Wind Speed	9	m/s
Thrust	800000	N
Water Depth	200	m
Surge	4.13	m
Sway	0	m
Heave	0	m
Roll	0	deg
Pitch	0	deg
Yaw	0	deg

Table 24. Natural Frequencies, MIT/NREL TLP Surface, Base Case

Mode	Natural Frequency	
Surge	0.1271	[rad/s]
Sway	0.1271	[rad/s]
Yaw	0.2926	[rad/s]

Table 25. Standard Deviations of System Motions, MIT/NREL TLP Surface, Base Case

Sea State		1	2	3	4	5
Hs	[m]	0.09	0.67	2.44	5.49	10
Tm	[s]	2	4.8	8.1	11.3	13.6
Surge	[m]	0.00018	0.05512	0.45215	1.37497	2.91179
Sway	[m]	0.00000	0.00000	0.00001	0.00010	0.00035
Yaw	[deg]	0.00000	0.00001	0.00020	0.00115	0.00334

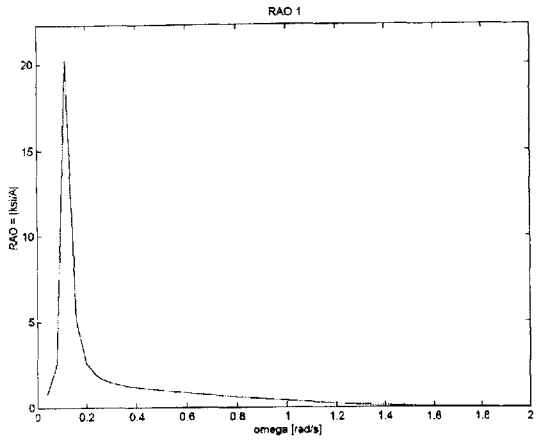

(a) RAO 1

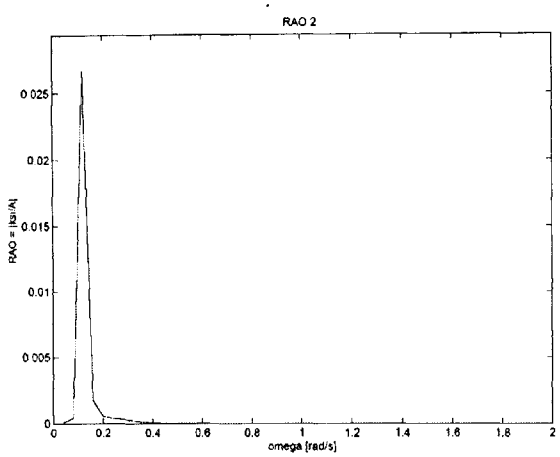

(b) RAO 2

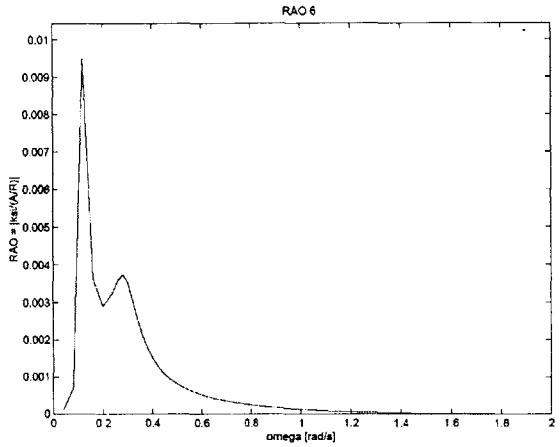

(c) RAO 6

Figure 20. RAOs, MIT/NREL TLP Surface, Base Case

Table 26. Dynamic Tether Tensions, MIT/NREL TLP Surface, Base Case

Max	1.39E+07	N
Min	3.35E+06	N

11.1.2 Discussion

The MIT/NREL TLP Surface has RAOs that show a strong response around the natural frequency, but demonstrates favorably small standard deviations of system motions in all sea states, and shows signs of cross coupling between modes of motion.

The RAOs show a strong resonance at the natural frequency that should be considered relative to the sea state spectrum. Because the natural frequencies of this system are low compared to the frequencies at which the peaks of the sea state occur, the system is not greatly excited by these sea states, and the standard deviations of motion remain low.

The significance of the value of the natural frequency becomes evident in the effects on the standard deviations of system motion due to increasing sea state. As the sea state grows in severity, the peak of the sea state spectrum approaches the system's natural frequency. As this occurs, the system's RAO curves have an increasing overlap with the spectra. This causes the standard deviation of motion to grow with increasing sea state.

As in the case of the MIT/NREL SDB, cross coupling between modes of motion are shown in the RAOs of the TLP Surface. Although motions are not directly excited in sway, the RAO in sway shows a response indicating cross coupling with surge. The RAO in yaw also shows cross coupling to the other modes as it shows a higher response at the frequency of .127 rad/s, which is the natural frequency in surge and sway, than it does at the frequency of .29 rad/s, which is the natural frequency in yaw.

11.2 Wind Speed Effects

11.2.1 Results

Table 27. Steady-State Offsets, MIT/NREL TLP Surface, Wind Speed Effects

Water Depth [m]		200
Wind Speed [m/s]	Thrust [N]	Surge [m]
9	600000	3.10
11.2	800000	4.13
15	500000	2.58
25	400000	2.07

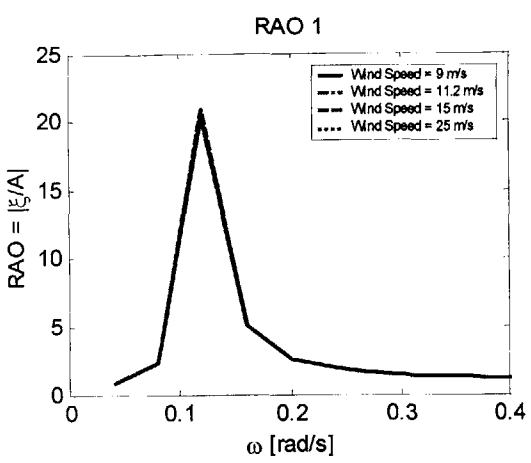

(a) RAO 1

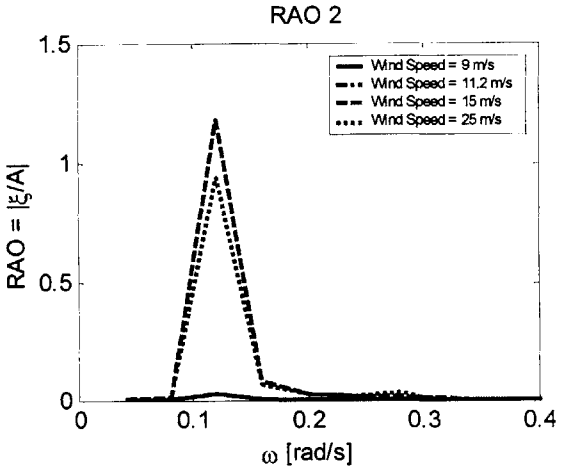

(b) RAO 2

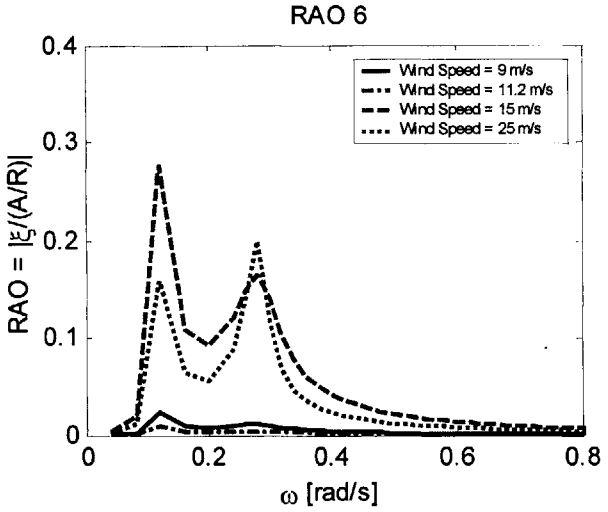

(c) RAO 5

Figure 21. RAOs, MIT/NREL TLP Surface, Wind Speed Effects

Table 28. Natural Frequencies, MIT/NREL TLP Surface, Wind Speed Effects

Wind Speed	[m/s]	9	11.2	15	25
Surge	[rad/s]	0.127	0.127	0.127	0.127
Sway	[rad/s]	0.127	0.127	0.127	0.127
Yaw	[rad/s]	0.287	0.293	0.283	0.279

Table 29. Standard Deviations of System Motions, MIT/NREL TLP Surface, Wind Speed Effects

Sea States	Hs [m]	0.09	0.67	2.44	5.49	10
	Tm [s]	2	4.8	8.1	11.3	13.6
Surge [m]	9 m/s	0.0002	0.0551	0.4522	1.3751	2.9120
	11.2 m/s	0.0002	0.0551	0.4521	1.3750	2.9118
	15 m/s	0.0002	0.0552	0.4524	1.3752	2.9121
	25 m/s	0.0002	0.0552	0.4523	1.3752	2.9120
Sway [m]	9 m/s	0.0000	0.0000	0.0000	0.0002	0.0006
	11.2 m/s	0.0000	0.0000	0.0000	0.0001	0.0004
	15 m/s	0.0000	0.0000	0.0002	0.0035	0.0168
	25 m/s	0.0000	0.0000	0.0002	0.0035	0.0208
Yaw [deg]	9 m/s	0.0000	0.0000	0.0005	0.0028	0.0088
	11.2 m/s	0.0000	0.0000	0.0002	0.0012	0.0033
	15 m/s	0.0000	0.0003	0.0053	0.0343	0.1167
	25 m/s	0.0000	0.0002	0.0030	0.0226	0.0988

Table 30. Dynamic Tether Tensions, MIT/NREL TLP Surface, Wind Speed Effects

Wind Speed	Max [N]	Min [N]
9 m/s	1.30E+07	4.18E+06
11.2 m/s	1.39E+07	3.35E+06
15 m/s	1.26E+07	4.60E+06
25 m/s	1.22E+07	5.02E+06

11.2.2 Discussion

Wind speed affects the steady state force on the system and the properties of the wind turbine. The different levels of steady state force on the system due to different wind speeds cause the system to achieve different levels of steady state offsets. As thrust increases in Region 2 of the power curve, the offsets also increase. In Region 3 of the power curve, the thrust reduces so the wind turbine maintains a level of power production at rated power, despite the increase in wind speed. This reduction in thrust in this region causes the system to achieve reduced levels of steady-state offsets at these wind speeds.

Wind speed also significantly affects the damping properties of the wind turbine. Damping from the wind turbine, however, makes a very small contribution to total damping in surge and sway of this system. This results in very little effect in the system's total response, visible in the RAOs and in the standard deviations of system

motion. The wind turbine contributes more to damping in yaw, which is reflected in the system's RAO in yaw.

11.3 Water Depth Effects

11.3.1 Results

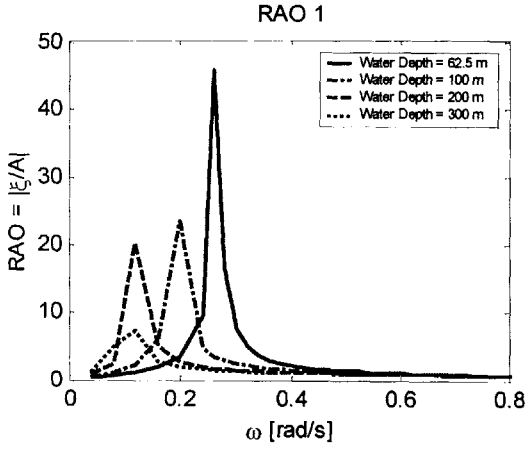

(a) RAO 1

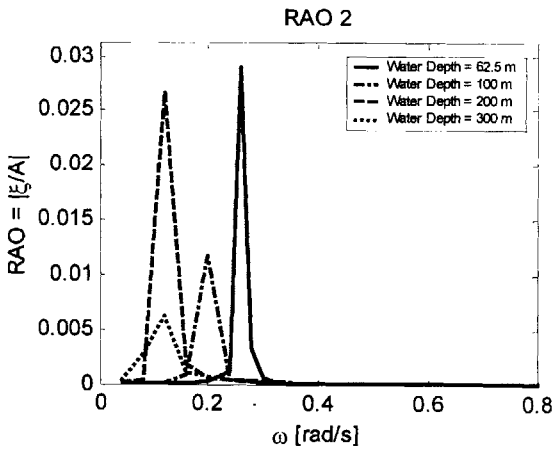

(b) RAO 2

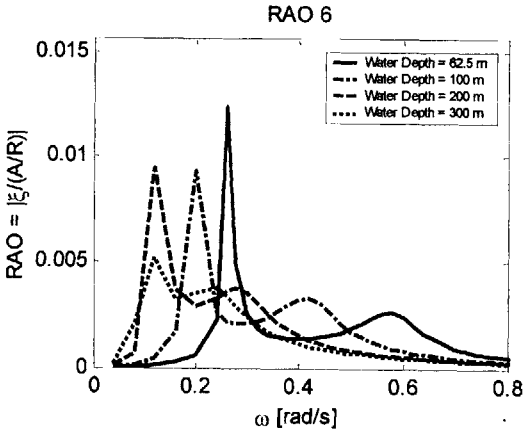

(c) RAO 6

Figure 22 (a) – (c). RAOs, MIT/NREL TLP Surface, Water Depth Effects

Table 31. Steady-State Offsets, MIT/NREL TLP Surface, Water Depth Effects

	Wind Speed [m/s]	11.2
	Thrust [N]	800000
Water Depth [m]	Restoring [N]	Surge [m]
62.5	8.63E+05	0.93
100	4.44E+05	1.80
200	1.93E+05	4.13
300	1.24E+05	6.47

Table 32. Natural Frequencies, MIT/NREL TLP Surface, Water Depth Effects

Water Depth	[m]	62.5	100	200	300
Surge	[rad/s]	0.268	0.192	0.127	0.102
Sway	[rad/s]	0.268	0.192	0.127	0.102
Yaw	[rad/s]	0.582	0.425	0.293	0.243

Table 33. Standard Deviations of System Motions, MIT/NREL TLP Surface, Water Depth Effects

Sea States	Hs [m]	0.09	0.67	2.44	5.49	10
	Tm [s]	2	4.8	8.1	11.3	13.6
Surge [m]	62.5 m	0.0002	0.0590	0.5618	3.0192	18.4060
	100 m	0.0002	0.0565	0.4828	1.6520	4.1133
	200 m	0.0002	0.0551	0.4521	1.3750	2.9118
	300 m	0.0002	0.0547	0.4452	1.3278	2.7340
Sway [m]	62.5 m	0.0000	0.0000	0.0000	0.0007	0.0095
	100 m	0.0000	0.0000	0.0000	0.0001	0.0003
	200 m	0.0000	0.0000	0.0000	0.0001	0.0004
	300 m	0.0000	0.0000	0.0000	0.0001	0.0003
Yaw [deg]	62.5 m	0.0000	0.0000	0.0006	0.0016	0.0043
	100 m	0.0000	0.0000	0.0004	0.0019	0.0039
	200 m	0.0000	0.0000	0.0002	0.0012	0.0033
	300 m	0.0000	0.0000	0.0002	0.0009	0.0025

Table 34. Dynamic Tether Tensions, MIT/NREL TLP Surface, Water Depth Effects

	Max [N]	Min [N]
62.5	1.39E+07	3.35E+06
100	1.39E+07	3.35E+06
200	1.39E+07	3.35E+06
300	1.39E+07	3.35E+06

11.3.2 Discussion

The primary effect of water depth is the effect on the restoring properties of the mooring system. Restoring in surge from the mooring lines is given as the total tension force divided by the length of the line. Therefore as the line tension is held constant for all

depths, the restoring properties of the mooring lines decrease with water depth, as the length of the mooring lines increase.

The decrease in restoring in surge provided by the mooring lines then in turn affects the natural frequency. A decrease in the restoring coefficient in surge results in a decrease in the natural frequencies with increasing water depth. This moves the peak of the system's response further away from the peak of the sea state spectra, resulting in a decreasing standard deviation of system motion with water depth.

This result implies that by adjusting the tether tension, the structure's response can be manipulated to achieve a desired resonant frequency.

11.4 Viscous Damping Effects

11.4.1 Results

Steady state offset, natural frequencies, dynamic tether tensions are not affected by viscous damping, and are summarized in the base case results section above.

Table 35. Standard Deviations of System Motions, MIT/NREL TLP Surface, Viscous Damping Effects

Sea States	Hs [m]	0.09	0.67	2.44	5.49	10
	Tm [s]	2	4.8	8.1	11.3	13.6
Surge [m]	g = 0	0.0002	0.0551	0.4521	1.3750	2.9118
	g = .05	0.0002	0.0548	0.4507	1.3721	2.9057
	g = .1	0.0002	0.0546	0.4490	1.3678	2.8946
Sway [m]	g = 0	0.0000	0.0000	0.0000	0.0001	0.0004
	g = .05	0.0000	0.0000	0.0000	0.0001	0.0004
	g = .1	0.0000	0.0000	0.0000	0.0001	0.0004
Yaw [deg]	g = 0	0.0000	0.0000	0.0002	0.0012	0.0033
	g = .05	0.0000	0.0000	0.0002	0.0011	0.0033
	g = .1	0.0000	0.0000	0.0002	0.0011	0.0033

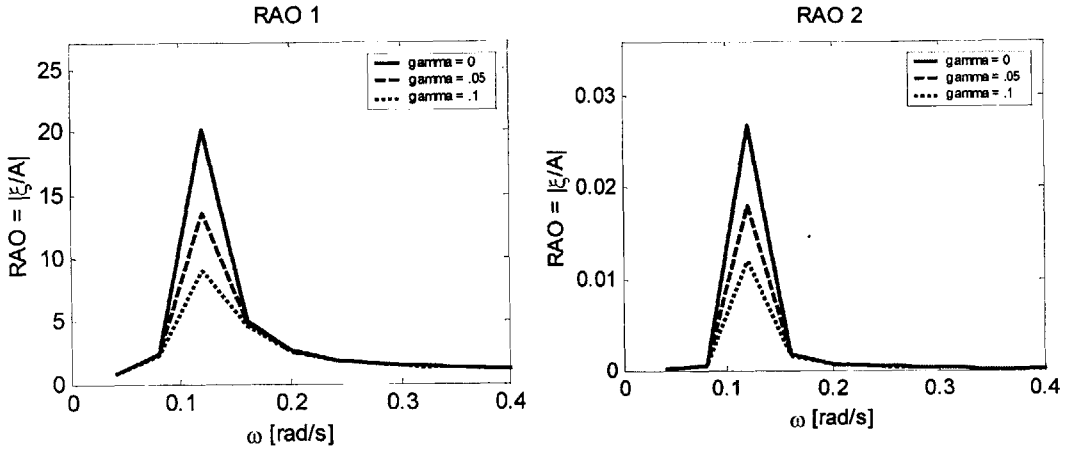

(a) RAO 1

(b) RAO 2

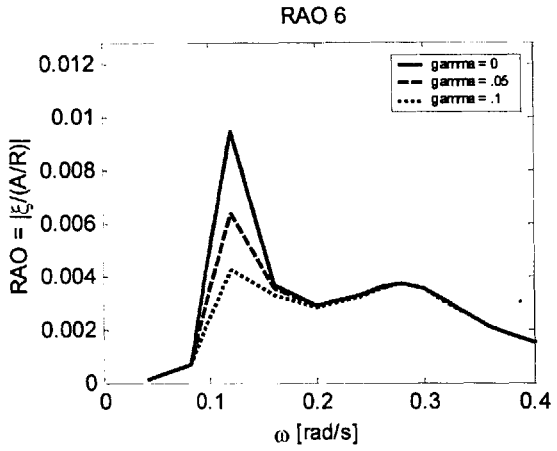

(c) RAO 6

Figure 23. RAOs, MIT/NREL TLP Surface, Viscous Damping Effects

11.4.2 Discussion

As expected, reasonable levels of viscous damping reduce the magnitude of the peaks of the RAOs. The natural frequencies of the system at a water depth of 200 m are so low, however, that the peaks of the RAOs lie outside of the peaks of the sea state spectra. This causes viscous damping to have very little effect on the values of the standard deviations of system motions.

12. MIT/NREL TLP Submerged

12.1 Base Case – Coupled Effects

12.1.1 Results

Table 36. Steady-State Offsets, MIT/NREL TLP Submerged, Base Case

Wind Speed	9	m/s
Thrust	800000	N
Water Depth	200	m
Surge	2.68	m
Sway	0	m
Heave	0	m
Roll	0	deg
Pitch	0	deg
Yaw	0	deg

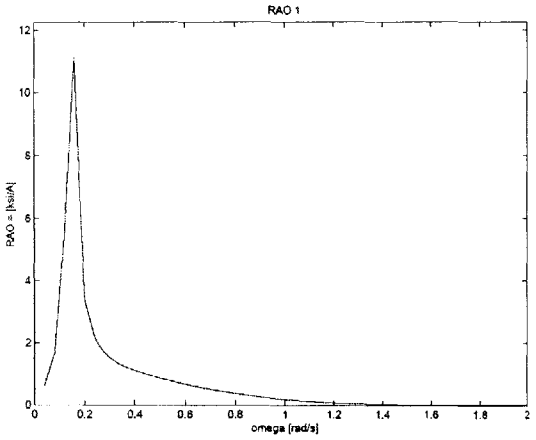

(a) RAO 1

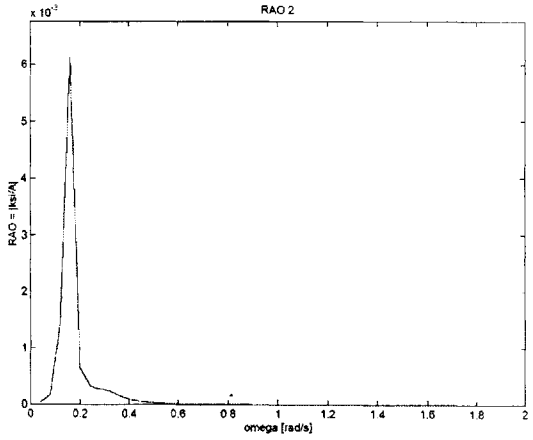

(b) RAO 2

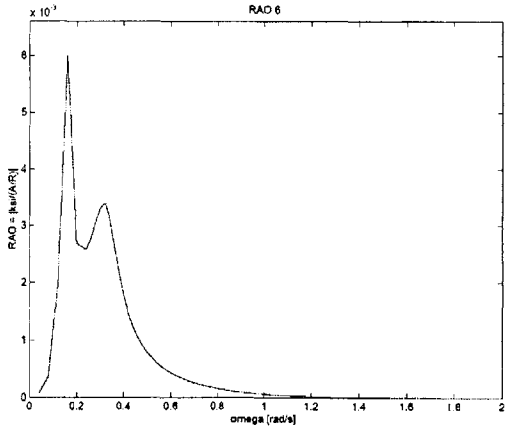

(c) RAO 6

Figure 24. RAOs, MIT/NREL Submerged, Base Case

Figure 25. Natural Frequencies, MIT/NREL TLP Submerged, Base Case

Mode	Natural Frequency	
Surge	0.1456	[rad/s]
Sway	0.1456	[rad/s]
Yaw	0.3277	[rad/s]

Table 37. Standard Deviations of System Motions, MIT/NREL TLP Submerged, Base Case

Sea State		1	2	3	4	5
Hs	[m]	0.09	0.67	2.44	5.49	10
Tm	[s]	2	4.8	8.1	11.3	13.6
Surge	[m]	0.000	0.029	0.347	1.227	2.798
Sway	[m]	0.00000	0.00000	0.00001	0.00011	0.00036
Yaw	[deg]	0.00000	0.00001	0.00019	0.00130	0.00355

Table 38. Dynamic Tether Tensions, MIT/NREL TLP Submerged, Base Case

Max	2.52E+07	N
Min	1.33E+07	N

12.1.2 Discussion

The MIT/NREL TLP Submerged has a favorably small response in all modes of motion. The RAOs show a strong resonance at the natural frequency. Although the response of the system is lower than that of the MIT/NREL TLP Surface, the natural frequency at where the response occurs is higher than the natural frequency of the surface structure. The higher natural frequencies of the submerged structure are closer to the frequencies of the peaks of the sea state spectra, but the reduction in RAOs compared to the surface structure, are significant enough to reduce the standard deviations of motion compared to the surface structure.

Similar to the other system, the RAOs of the MIT/NREL TLP Submerged illustrate coupling between modes of motion. This is most evident in the system's RAO in yaw. Although this mode of motion is not directly excited by wind and waves, it shows a small response. Furthermore, the system shows a higher response in yaw at the natural frequency of surge and sway than at the natural frequency in yaw.

12.2 Wind Speed Effects

12.2.1 Results

Table 39. Steady-State Offsets, MIT/NREL TLP Submerged, Wind Speed Effects

Water Depth [m]		200
Wind Speed [m/s]	Thrust [N]	Surge [m]
9	600000	2.01
11.2	800000	2.68
15	500000	1.67
25	400000	1.34

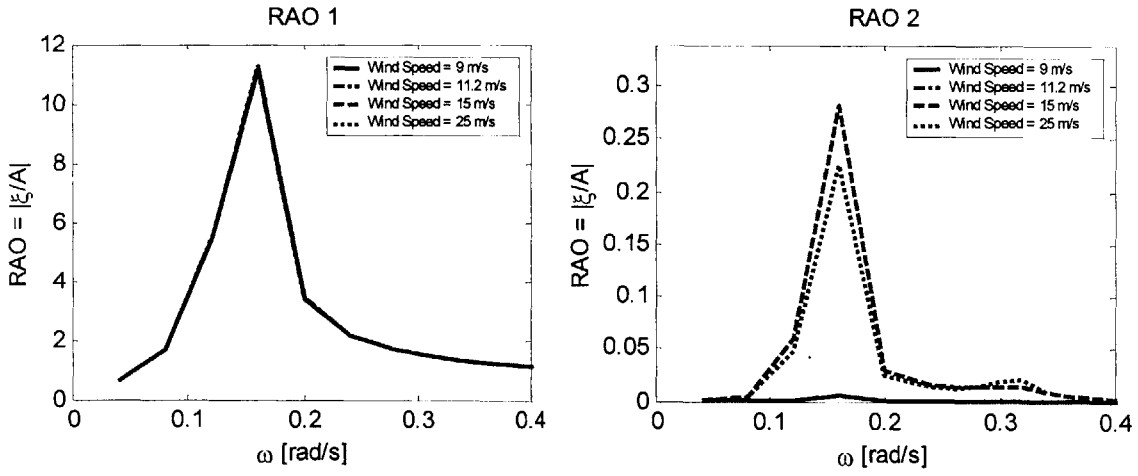

(a) RAO 1 **(b) RAO 2**

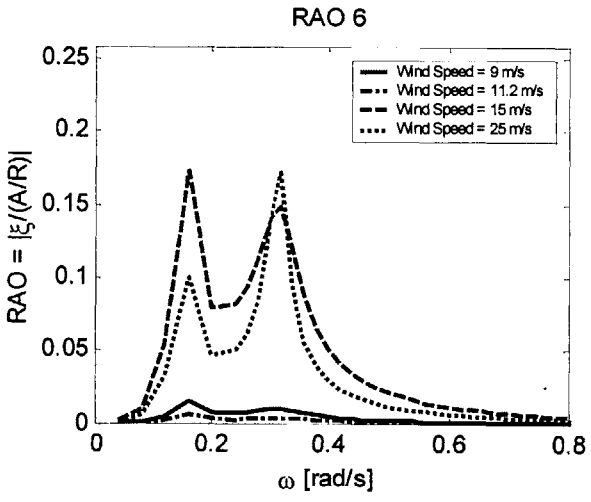

(c) RAO 6

Figure 26. RAOs, MIT/NREL TLP Submerged, Wind Speed Effects

Table 40. Natural Frequencies, MIT/NREL TLP Submerged, Wind Speed Effects

Wind Speed	[m/s]	9	11.2	15	25
Surge	[rad/s]	0.146	0.146	0.146	0.1456
Sway	[rad/s]	0.146	0.146	0.146	0.1456
Yaw	[rad/s]	0.323	0.328	0.319	0.3152

Table 41. Standard Deviations of System Motions, MIT/NREL TLP Submerged, Wind Speed Effects

Sea States	Hs [m]	0.09	0.67	2.44	5.49	10
	Tm [s]	2	4.8	8.1	11.3	13.6
Surge [m]	9 m/s	0.0001	0.0292	0.3468	1.2271	2.7982
	11.2 m/s	0.0001	0.0292	0.3468	1.2270	2.7981
	15 m/s	0.0001	0.0292	0.3469	1.2271	2.7985
	25 m/s	0.0001	0.0292	0.3468	1.2271	2.7984
Sway [m]	9 m/s	0.0000	0.0000	0.0000	0.0002	0.0006
	11.2 m/s	0.0000	0.0000	0.0000	0.0001	0.0004
	15 m/s	0.0000	0.0000	0.0003	0.0048	0.0180
	25 m/s	0.0000	0.0000	0.0002	0.0057	0.0222
Yaw [deg]	9 m/s	0.0000	0.0000	0.0004	0.0034	0.0096
	11.2 m/s	0.0000	0.0000	0.0002	0.0013	0.0035
	15 m/s	0.0000	0.0002	0.0050	0.0437	0.1316
	25 m/s	0.0000	0.0001	0.0028	0.0350	0.1183

Table 42. Dynamic Tether Tensions, MIT/NREL TLP Submerged, Wind Speed Effects

Wind Speed	Max [N]	Min [N]
9 m/s	2.44E+07	1.42E+07
11.2 m/s	2.52E+07	1.33E+07
15 m/s	2.40E+07	1.46E+07
25 m/s	2.36E+07	1.50E+07

12.2.2 Discussion

The primary effects of wind speed on this system are the effects on steady-state offset and the effects on the RAOs. The effects on the steady-state offset are directly related to the thrust at different wind speeds, while the effects on the RAOs are related to the effects of wind speed on the wind turbine properties.

Again, wind turbine damping has a small contribution to total system damping, but a distinct contribution, nonetheless. This effect on damping can be seen in the RAOs in

Figure 24 above. These RAOs show that wind speed has little effect on the RAO in surge, but a significant effect on the RAOs in sway and yaw. This is because damping in surge due to the wind turbine is very small compared to total damping, while the cross-coupling damping due to the wind turbine is larger comparable to total damping.

The RAOs in sway and yaw show that the system response decreases in Region 2 of the power curve, then increases to the maximum response at 15 m/s, then reduces again at 25 m/s. The decrease in response from 9 to 11.2 m/s occurs as the damping from the wind turbine increases in Region 2 of the power curve. The response then increases from 11.2 to 15 m/s because as the wind turbine feathers its blades to allow wind to pass by, the damping in this region decreases. The response then decreases again, but only slightly, at 25 m/s as the flow becomes more turbulent, and damping increases slightly.

12.3 Water Depth Effects

12.3.1 Results

Table 43. Steady-State Offsets, MIT/NREL TLP Submerged, Water Depth Effects

	Wind Speed [m/s]	11.2
	Thrust [N]	800000
Water Depth [m]	Restoring [N]	Surge [m]
62.5	1.85E+06	0.43
100	7.66E+05	1.05
200	2.99E+05	2.68
300	1.86E+05	4.31

Table 44. Natural Frequencies, MIT/NREL TLP Submerged, Water Depth Effects

Water Depth	[m]	62.5	100	200	300
Surge	[rad/s]	0.354	0.231	0.146	0.115
Sway	[rad/s]	0.354	0.231	0.146	0.115
Yaw	[rad/s]	0.758	0.501	0.328	0.268

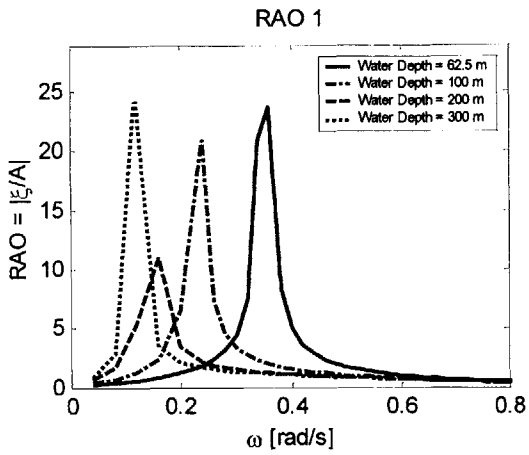

(a) RAO 1

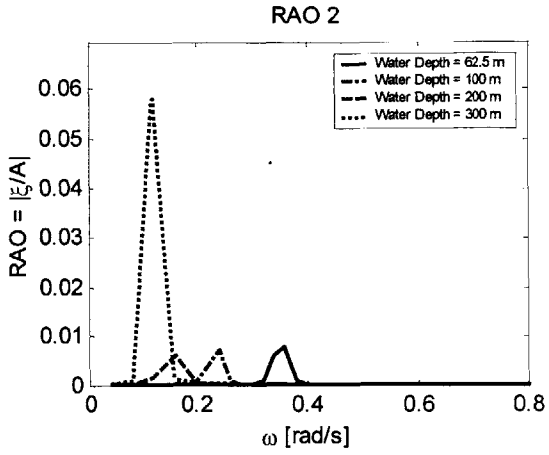

(b) RAO 2

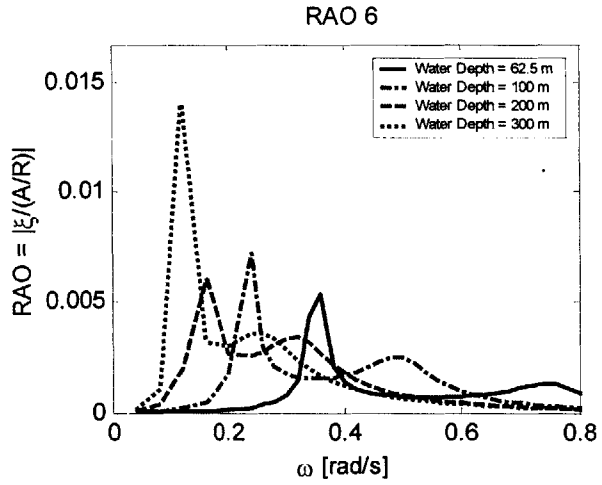

(c) RAO 6

Figure 27. RAOs, MIT/NREL TLP Submerged, Water Depth Effects

Table 45. Dynamic Tether Tensions, MIT/NREL TLP Submerged, Water Depth Effects

Water Depth [m]	Max [N]	Min [N]
62.5	2.53E+07	1.33E+07
100	2.52E+07	1.33E+07
200	2.52E+07	1.33E+07
300	2.52E+07	1.33E+07

Table 46. Standard Deviations of System Motions, MIT/NREL TLP Submerged, Water Depth Effects

Sea States	Hs [m]	0.09	0.67	2.44	5.49	10
	Tm [s]	2	4.8	8.1	11.3	13.6
Surge [m]	62.5 m	0.0001	0.0345	0.6671	9.6016	24.3467
	100 m	0.0001	0.0306	0.3942	1.7329	6.8614
	200 m	0.0001	0.0292	0.3468	1.2270	2.7981
	300 m	0.0001	0.0288	0.3378	1.1612	2.5434
Sway [m]	62.5 m	0.0000	0.0000	0.0001	0.0027	0.0070
	100 m	0.0000	0.0000	0.0000	0.0001	0.0016
	200 m	0.0000	0.0000	0.0000	0.0001	0.0004
	300 m	0.0000	0.0000	0.0000	0.0001	0.0003
Yaw [deg]	62.5 m	0.0000	0.0000	0.0003	0.0016	0.0038
	100 m	0.0000	0.0000	0.0005	0.0016	0.0032
	200 m	0.0000	0.0000	0.0002	0.0013	0.0035
	300 m	0.0000	0.0000	0.0002	0.0009	0.0027

12.3.2 Discussion

The effects of water depth can again be seen in the RAOs, the natural frequencies, and the standard deviations of the system motions. As discussed previously, the increasing water depth results in decreasing restoring. This results in a lower natural frequency, and in general a higher response of the system at that natural frequency with increasing water depth. Despite the increased response with increased water depth, the standard deviations of motions decrease with increasing water depth. This effect is due to the lower natural frequencies resulting from the lower values of restoring in surge at higher water depths.

12.4 Viscous Damping Effects

12.4.1 Results

Steady-state offsets, Natural frequencies, and dynamic tether tensions are not effected by viscous damping, and are summarized in the base case results section above.

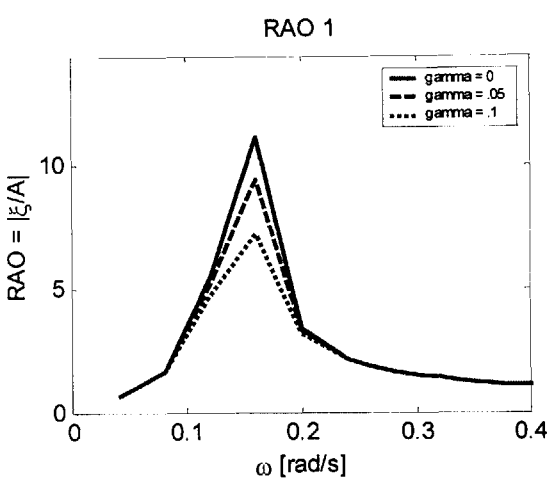

(a) RAO 1

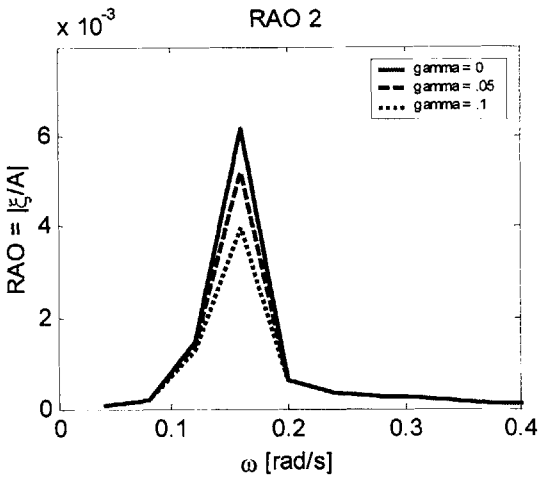

(b) RAO 2

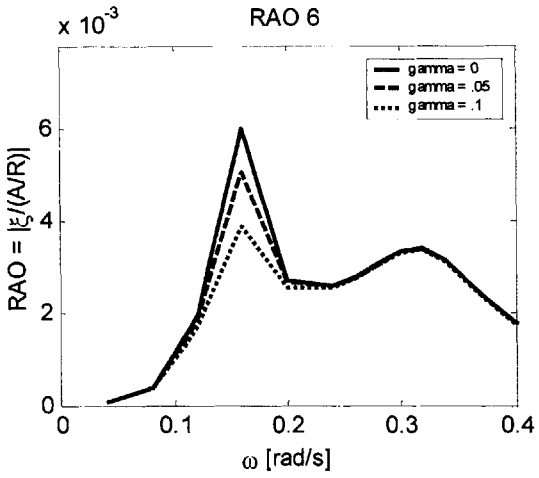

(c) RAO 6

Figure 28. RAOs, MIT/NREL TLP Submerged, Viscous Damping Effects

Table 47. Standard Deviations of System Motions, MIT/NREL TLP Submerged, Viscous Damping Effects

Sea States	Hs [m]	0.09	0.67	2.44	5.49	10
	Tm [s]	2	4.8	8.1	11.3	13.6
Surge [m]	g = 0	0.0001	0.0292	0.3468	1.2270	2.7981
	g = .05	0.0001	0.0291	0.3461	1.2245	2.7905
	g = .1	0.0001	0.0290	0.3451	1.2199	2.7752
Sway [m]	g = 0	0.0000	0.0000	0.0000	0.0001	0.0004
	g = .05	0.0000	0.0000	0.0000	0.0001	0.0004
	g = .1	0.0000	0.0000	0.0000	0.0001	0.0004
Yaw [deg]	g = 0	0.0000	0.0000	0.0002	0.0013	0.0035
	g = .05	0.0000	0.0000	0.0002	0.0013	0.0035
	g = .1	0.0000	0.0000	0.0002	0.0013	0.0035

12.4.2 Discussion

Again, viscous damping affects the response as expected, by lowering the response at every frequency. This decreased response, however, has little effect on the standard deviation of system motion due to the location of the natural frequencies. Because the natural frequencies of the system are below the frequencies where the peaks of the sea state spectra occur, standard deviations of system motion are mitigated only slightly by increased viscous damping.

12.5 Comparison of MIT/NREL TLP Surface and MIT/NREL TLP Submerged

The submersion of the MIT/NREL TLP Submerged results in reduced added mass terms, reduced damping, and reduced exciting forces. These properties have the net effect of reduced system responses at all frequencies, and reduced standard deviations of system motions for the base case.

The reduction of hydrodynamic properties also has the effect of increasing the significance of the properties of the wind turbine. Therefore, the submerged system is affected to a greater extend by wind speed effects than the surface system. This is apparent in the RAOs as well as the standard deviations of system motions due to wind speed effects.

Water depth affects the systems in a similar manner, by lowering the system's natural frequency with increased water depth. The standard deviations of system motions for the two systems display similar trends, as they decrease with increasing water depth.

13. NREL TLP Tower Draft = 10, Reserve Buoyancy = 2

13.1 Base Case – Coupled Effects

13.1.1 Results

Table 48. Steady-State Offsets, NREL TLP RB2, Base Case

Wind Speed	9	m/s
Thrust	800000	N
Water Depth	200	m
Surge	7.03	m
Sway	0	m
Heave	0	m
Roll	0	deg
Pitch	0	deg
Yaw	0	deg

Table 49. Natural Frequencies, NREL TLP RB2, Base Case

Mode	Natural Frequency	
Surge	0.1847	[rad/s]
Sway	0.1847	[rad/s]
Yaw	0.4985	[rad/s]

Table 50. Standard Deviations of System Motions, NREL TLP RB2, Base Case

Sea State		1	2	3	4	5
Hs	[m]	0.09	0.67	2.44	5.49	10
Tm	[s]	2	4.8	8.1	11.3	13.6
Surge	[m]	0.000	0.056	0.524	1.787	4.196
Sway	[m]	0.00000	0.00000	0.00011	0.00052	0.00156
Yaw	[deg]	0.00000	0.00004	0.00073	0.00244	0.00476

Table 51. Dynamic Tether Tensions, NREL TLP RB2, Base Case

Max	8.18E+06	N
Min	2.68E+06	N

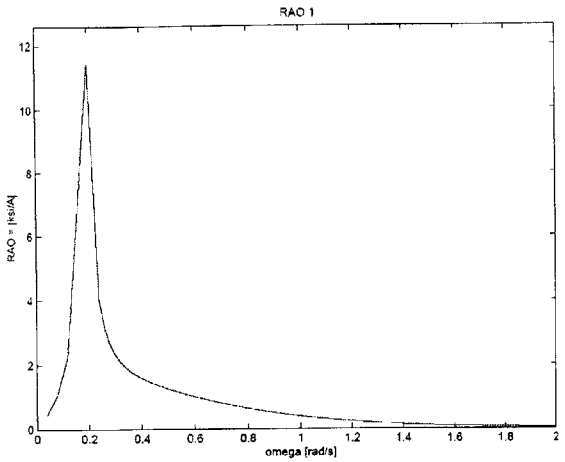

(a) RAO 1

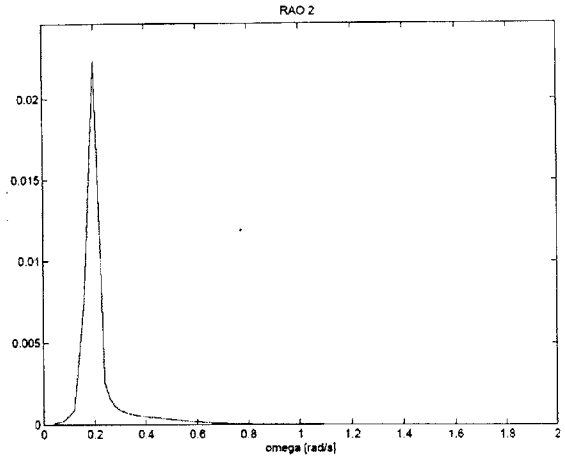

(b) RAO 2

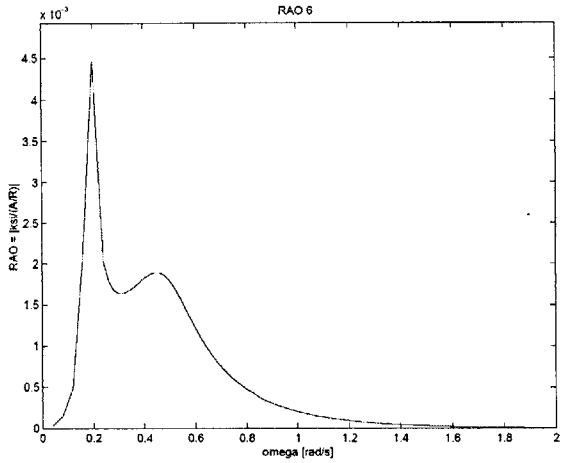

(c) RAO 6

Figure 29. RAOs, NREL TLP RB2, Base Case

13.1.2 Discussion

The NREL TLP TD10 RB2 (Tower Draft = 10 m, Reserve Buoyancy = roughly 2) demonstrates favorably small motions, with RAOs comparable to the MIT/NREL TLP Submerged.

The RAOs also show indications of cross coupling. This can be seen in RAO 2 and RAO 6. Although these modes of motion are not directly excited by wind or waves, the system

demonstrates a response in these modes, indicating cross coupling between those modes and the mode of surge. In addition, the system natural frequency in yaw is about .5 rad/s. However, the RAO in yaw shows a stronger response at the frequency of .18 rad/s, which is the natural frequency of the system in sway and surge.

13.2 Wind Speed Effects

13.2.1 Results

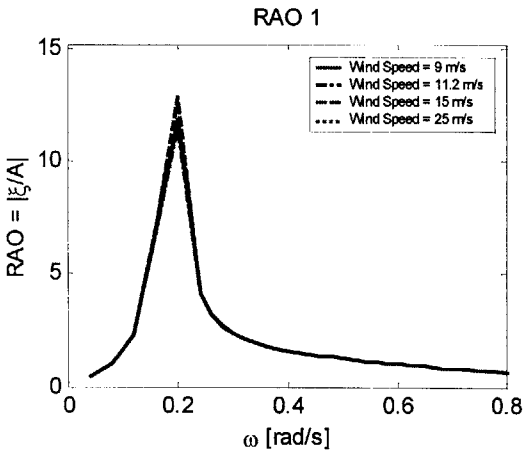

(a) RAO 1

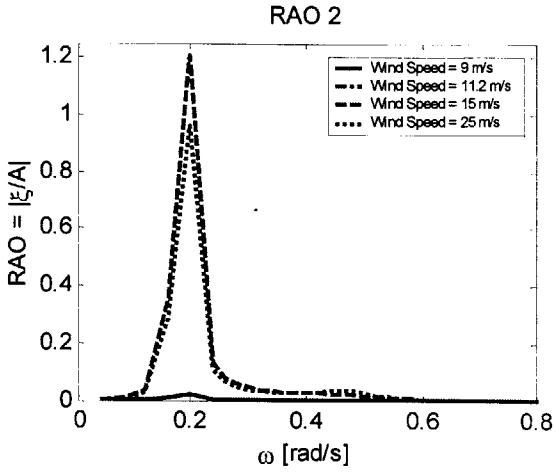

(b) RAO 2

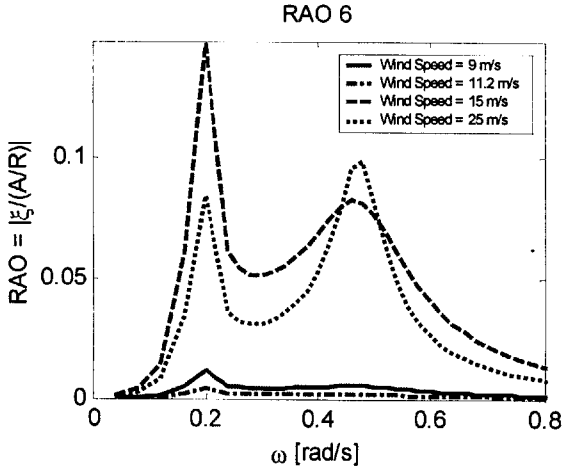

(c) RAO 6

Figure 30. RAOs, NREL TLP RB2, Wind Speed Effects

Table 52. Steady-State Offsets, NREL TLP RB2, Wind Speed Effects

Water Depth [m]		200
Wind Speed [m/s]	Thrust [N]	Surge [m]
9	600	5.27
11.2	800	7.03
15	500	4.39
25	400	3.51

Table 53. Natural Frequencies, NREL TLP RB2, Wind Speed Effects

Wind Speed	[m/s]	9	11.2	15	25
Surge	[rad/s]	0.185	0.185	0.185	0.185
Sway	[rad/s]	0.185	0.185	0.185	0.185
Yaw	[rad/s]	0.491	0.499	0.484	0.478

Table 54. Standard Deviations of System Motions, NREL TLP RB2, Wind Speed Effects

Sea States	Hs [m]	0.09	0.67	2.44	5.49	10
	Tm [s]	2	4.8	8.1	11.3	13.6
Surge [m]	9 m/s	0.0003	0.0561	0.5240	1.7880	4.1998
	11.2 m/s	0.0003	0.0561	0.5238	1.7872	4.1956
	15 m/s	0.0003	0.0561	0.5242	1.7906	4.2120
	25 m/s	0.0003	0.0561	0.5241	1.7901	4.2092
Sway [m]	9 m/s	0.0000	0.0000	0.0002	0.0008	0.0021
	11.2 m/s	0.0000	0.0000	0.0001	0.0005	0.0016
	15 m/s	0.0000	0.0001	0.0051	0.0277	0.0803
	25 m/s	0.0000	0.0001	0.0067	0.0319	0.0765
Yaw [deg]	9 m/s	0.0000	0.0001	0.0020	0.0067	0.0129
	11.2 m/s	0.0000	0.0000	0.0007	0.0024	0.0048
	15 m/s	0.0000	0.0012	0.0274	0.0953	0.1767
	25 m/s	0.0000	0.0007	0.0247	0.0891	0.1536

Table 55. Dynamic Tether Tensions, NREL TLP RB2, Wind Speed Effects

Wind Speed	Max [N]	Min [N]
9 m/s	7.62E+06	3.23E+06
11.2 m/s	8.18E+06	2.68E+06
15 m/s	7.34E+06	3.51E+06
25 m/s	7.07E+06	3.79E+06

13.2.2 Discussion

As observed for the other structures, wind speed affects the structure's steady-state offsets by affecting the wind turbine's thrust, and it affects the structure's coupled dynamic response by affecting the turbine's dynamic properties.

Also similar to the effects observed for other systems, the wind speed has a minor effect on the RAO in surge, and a more significant effect on the RAOs in sway and yaw. As a consequence, the standard deviations of system motions are affected accordingly.

Again, it is observed that the wind speeds of 15 and 25 m/s elicit the highest responses, with the wind speed of 15 m/s resulting in only a slightly higher response of the two. The jump in responses between wind speeds of Region 2 and Region 3 of the power curve can be explained by the level of wind turbine damping in these areas. While wind turbine damping is increasing throughout Region 2 of the power curve, it drastically drops off in Region 3, as the blades are feathered to allow wind to pass by.

13.3 Water Depth Effects

13.3.1 Results

Table 56. Steady-State Offsets, NREL TLP RB2, Water Depth Effects

	Wind Speed [m/s]	11.2
	Thrust [N]	800000
Water Depth [m]	Restoring [N]	Surge [m]
62.5	473664.069	1.69
100	254375.148	3.14
200	113836.392	7.03
300	73325.2207	10.91

Table 57. Natural Frequencies, NREL TLP RB2, Water Depth Effects

Water Depth	[m]	62.5	100	200	300
Surge	[rad/s]	0.452	0.280	0.185	0.148
Sway	[rad/s]	0.452	0.280	0.185	0.148
Yaw	[rad/s]	1.154	0.728	0.499	0.413

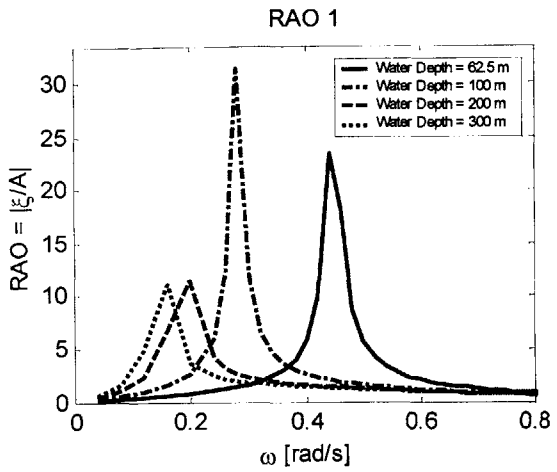

(a) RAO 1

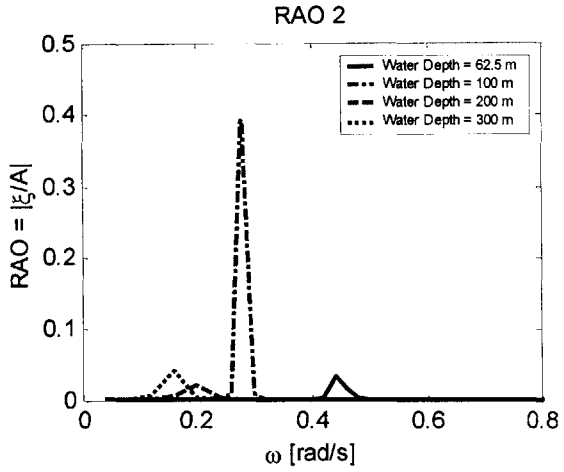

(b) RAO 2

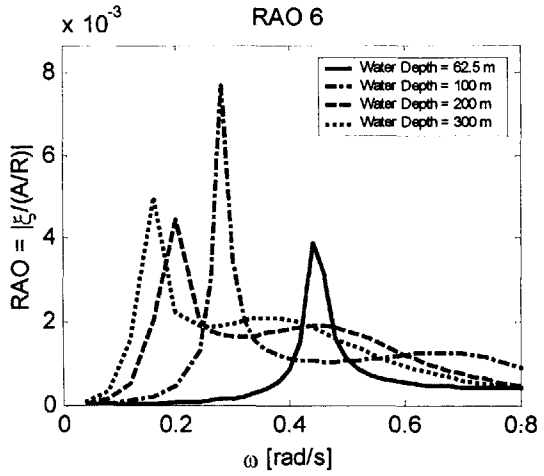

(c) RAO 6

Figure 31. RAOs, NREL TLP RB2, Water Depth Effects

Table 58. Standard Deviations of System Motions, NREL TLP RB2, Water Depth Effects

Sea States	Hs [m]	0.09	0.67	2.44	5.49	10
	Tm [s]	2	4.8	8.1	11.3	13.6
Surge [m]	62.5 m	0.0003	0.0726	2.6103	12.0387	20.2552
	100 m	0.0003	0.0594	0.6271	3.8429	18.3624
	200 m	0.0003	0.0561	0.5238	1.7872	4.1956
	300 m	0.0003	0.0552	0.5032	1.6359	3.5679
Sway [m]	62.5 m	0.0000	0.0000	0.0026	0.0135	0.0225
	100 m	0.0000	0.0000	0.0001	0.0246	0.1855
	200 m	0.0000	0.0000	0.0001	0.0005	0.0016
	300 m	0.0000	0.0000	0.0001	0.0006	0.0016
Yaw [deg]	62.5 m	0.0000	0.0001	0.0006	0.0024	0.0039
	100 m	0.0000	0.0001	0.0007	0.0019	0.0060
	200 m	0.0000	0.0000	0.0007	0.0024	0.0048
	300 m	0.0000	0.0000	0.0006	0.0024	0.0051

Table 59. Dynamic Tether Tensions, NREL TLP RB2, Water Depth Effects

Water Depth	Max [N]	Min [N]
62.5	8.18E+06	2.68E+06
100	8.18E+06	2.68E+06
200	8.18E+06	2.68E+06
300	8.18E+06	2.68E+06

13.3.2 Discussion

The major effects of water depth are again the effects on the restoring coefficient in surge and sway. These effects are evident in the RAOs, as the natural frequencies shift to lower values with increasing depth. These effects then reverberate through the system via cross-coupling mechanisms, and shift the RAOs to lower frequencies.

Shifting the natural frequencies of the system to lower values shifts the entire system's RAOs to lower frequencies, reducing the overlap with the sea state spectra. This results in lower standard deviation of system motions for increasing water depth.

13.4 Viscous Damping Effects

13.4.1 Results

Steady-state offsets, natural frequencies, dynamic tether tensions are unaffected by viscous damping, and are summarized in the base case results section.

Table 60. Standard Deviations of System Motions, NREL TLP RB2, Viscous Damping Effects

Sea States	Hs [m]	0.09	0.67	2.44	5.49	10
	Tm [s]	2	4.8	8.1	11.3	13.6
Surge [m]	g = 0	0.0003	0.0561	0.5238	1.7872	4.1956
	g = .05	0.0003	0.0559	0.5223	1.7782	4.1495
	g = .1	0.0003	0.0557	0.5201	1.7636	4.0784
Sway [m]	g = 0	0.0000	0.0000	0.0001	0.0005	0.0016
	g = .05	0.0000	0.0000	0.0001	0.0005	0.0015
	g = .1	0.0000	0.0000	0.0001	0.0005	0.0015
Yaw [deg]	g = 0	0.0000	0.0000	0.0007	0.0024	0.0048
	g = .05	0.0000	0.0000	0.0007	0.0024	0.0047
	g = .1	0.0000	0.0000	0.0007	0.0024	0.0047

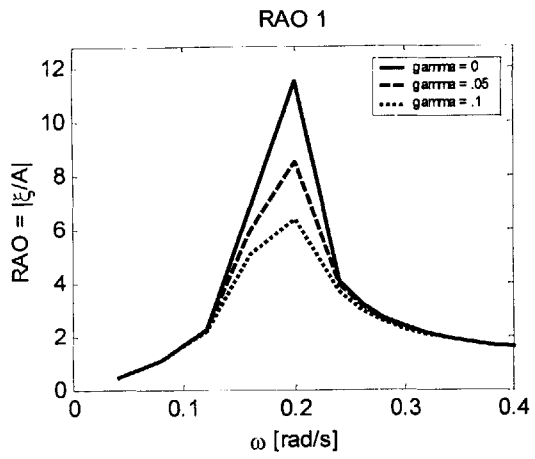

(a) RAO 1

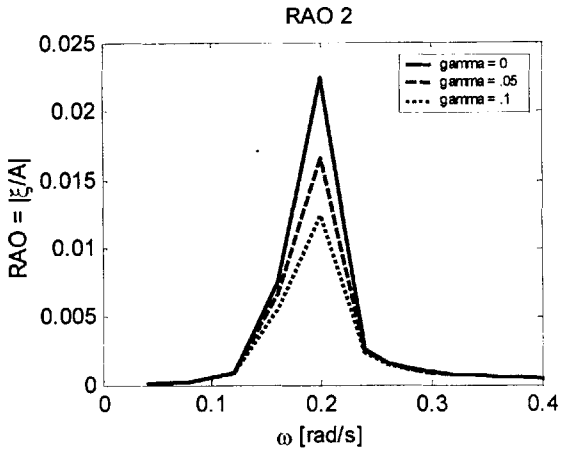

(b) RAO 2

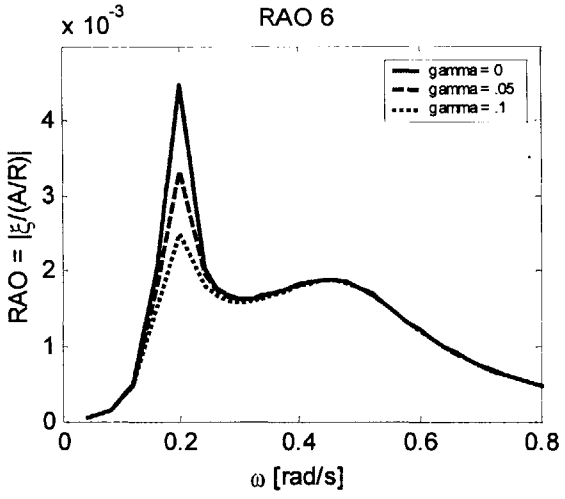

(c) RAO 6

Figure 32. RAOs, NREL TLP RB2, Viscous Damping Effects

13.4.2 Discussion

Reasonable levels of viscous damping considered here decrease the system's RAOs at every frequency. This results in decreasing standard deviation of system motion with increasing levels of viscous damping. The effects of viscous damping, however, have a

less significant impact on reducing the standard deviations of system motion than the effects of decreased restoring properties.

13.5 Comparison of NREL TLP TD10 RB2 with MIT/NREL TLP Submerged

Due to the smaller size of the structure, the NREL TLP TD10 RB2 has much lower values of added mass, damping, and exciting forces. This, however, results in comparable system responses, as seen by the RAOs. The RAOs of the NREL TLP, however, have a slightly higher natural frequency. This results in notably higher standard deviations of system motions.

The NREL TLP's reduced values of damping leads to an increased effect of wind turbine damping on the system response. As a result, the NREL TLP is more sensitive than the more massive MIT/NREL TLP to the change in damping properties due to changes in wind speed.

Finally, the water depth and viscous damping levels effect both structures similarly, as increasing water depth results in decreasing natural frequency, and as increasing viscous damping results in decreasing response at every frequency.

The comparison of these structures indicates that similar responses may be achieved by submerged structures of different size. The main drawback of a smaller, less massive structure is its sensitivity to different wind speeds.

14. NREL TLP Tower Draft = 10, Reserve Buoyancy = 6

14.1 Base Case – Coupled Effects

14.1.1 Results

Table 61. Steady-State Offsets, NREL TLP RB6, Base Case

Wind Speed	9	m/s
Thrust	800000	N
Water Depth	200	m
Surge	2.19	m
Sway	0	m
Heave	0	m
Roll	0	deg
Pitch	0	deg
Yaw	0	deg

Table 62. Natural Frequencies, NREL TLP RB2, Base Case

Mode	Natural Frequency	
Surge	0.2460	[rad/s]
Sway	0.2460	[rad/s]
Yaw	0.8460	[rad/s]

Table 63. Standard Deviations of System Motions, NREL TLP RB6, Base Case

Sea State		1	2	3	4	5
Hs	[m]	0.09	0.67	2.44	5.49	10
Tm	[s]	2	4.8	8.1	11.3	13.6
Surge	[m]	0.000	0.053	0.624	2.682	12.367
Sway	[m]	0	0.000002	0.000015	0.000451	0.013181
Yaw	[deg]	0	0.000065	0.000379	0.00077	0.001817

Table 64. Dynamic Tether Tensions, NREL TLP RB6, Base Case

Max	2.41E+07	N
Min	1.82E+07	N

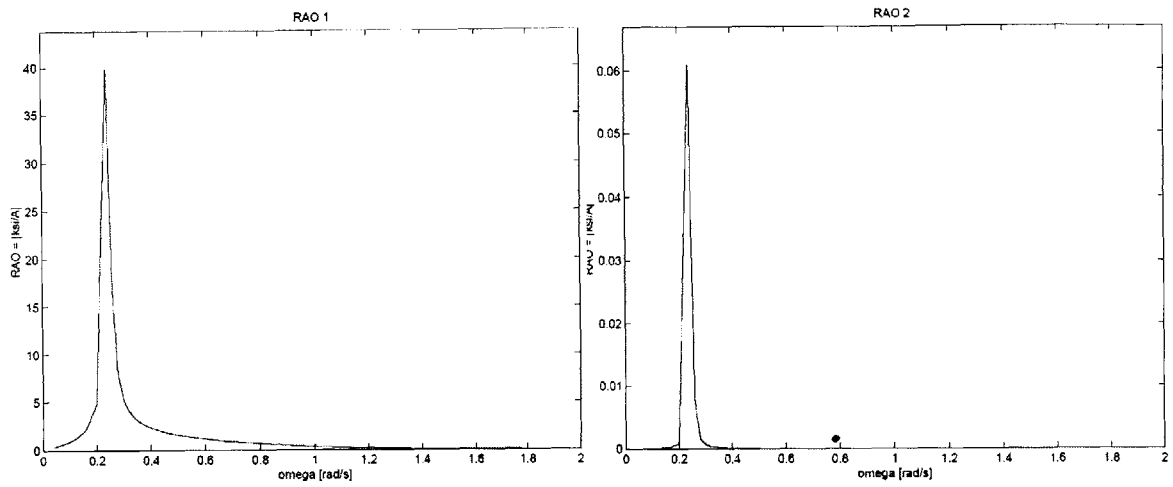

(a) RAO 1 **(b) RAO 2**

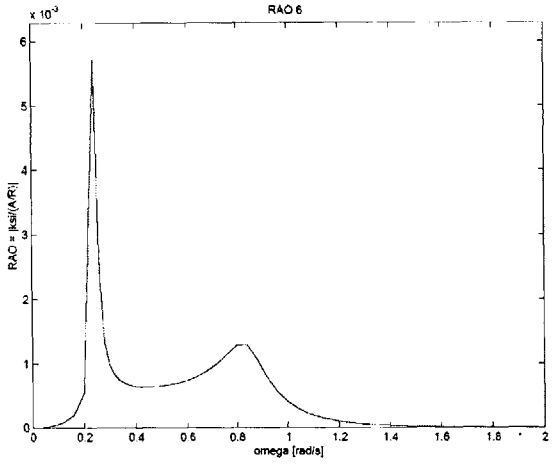

(c) RAO 6

Figure 33. RAOs, NREL TLP RB2, Base Case

14.1.2 Discussion

The high level of reserve buoyancy results in two general system properties; (1) the tether tension is relatively high, and (2) the size of the platform required to provide the tension to the tethers is relatively large. These properties in turn result in two main effects; (1) the restoring in surge, and thus the natural frequency of the system, is relatively high, and (2) the magnitudes of the system's hydrodynamic properties are relatively high, including added mass, damping, and exciting forces.

These characteristics combine to make the structure the best performing structure in the steady-state, but the poorest performing structure dynamically. The high levels of restoring result in low steady-state offsets. However, the RAOs demonstrate high response, and a very high concentration of response about the natural frequency. In addition, the natural frequencies of these responses are closer to the peaks of the sea state spectra. As a result, the standard deviations of motions are much higher than any other system.

14.2 Wind Speed Effects

14.2.1 Results

Table 65. Steady-State Offset, NREL TLP RB6, Wind Speed Effects

Water Depth [m]		200
Wind Speed [m/s]	Thrust [N]	Surge [m]
9	600000	1.64
11.2	800000	2.19
15	500000	1.37
25	400000	1.09

Table 66. Natural Frequencies, NREL TLP RB6, Wind Speed Effects

Wind Speed	[m/s]	9	11.2	15	25
Surge	[rad/s]	0.246	0.246	0.246	0.246
Sway	[rad/s]	0.246	0.246	0.246	0.246
Yaw	[rad/s]	0.843	0.846	0.841	0.839

Table 67. Dynamic Tether Tensions, NREL TLP RB6, Wind Speed Effects

Wind Speed	Max [N]	Min [N]
9 m/s	2.37E+07	1.86E+07
11.2 m/s	2.41E+07	1.82E+07
15 m/s	2.34E+07	1.89E+07
25 m/s	2.32E+07	1.91E+07

Table 68. Standard Deviations of System Motions, NREL TLP RB6, Wind Speed Effects

Sea States	Hs [m]	0.09	0.67	2.44	5.49	10
	Tm [s]	2	4.8	8.1	11.3	13.6
Surge [m]	9 m/s	0.0001	0.0526	0.6239	2.6850	12.7775
	11.2 m/s	0.0001	0.0526	0.6238	2.6819	12.3667
	15 m/s	0.0001	0.0526	0.6244	2.6934	13.9382
	25 m/s	0.0001	0.0526	0.6243	2.6915	13.6799
Sway [m]	9 m/s	0.0000	0.0000	0.0000	0.0012	0.0338
	11.2 m/s	0.0000	0.0000	0.0000	0.0005	0.0132
	15 m/s	0.0000	0.0001	0.0005	0.0066	0.1901
	25 m/s	0.0000	0.0001	0.0006	0.0063	0.1802
Yaw [deg]	9 m/s	0.0000	0.0002	0.0010	0.0019	0.0044
	11.2 m/s	0.0000	0.0001	0.0004	0.0008	0.0018
	15 m/s	0.0000	0.0024	0.0125	0.0229	0.0532
	25 m/s	0.0000	0.0022	0.0100	0.0158	0.0318

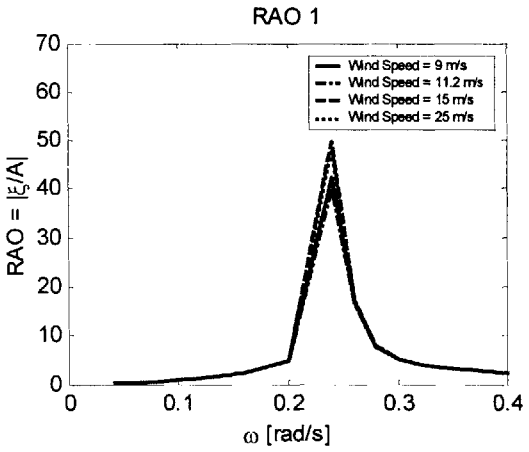

(a) RAO 1

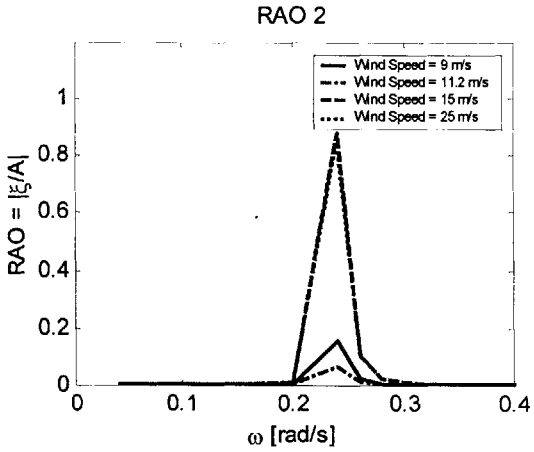

(b) RAO 2

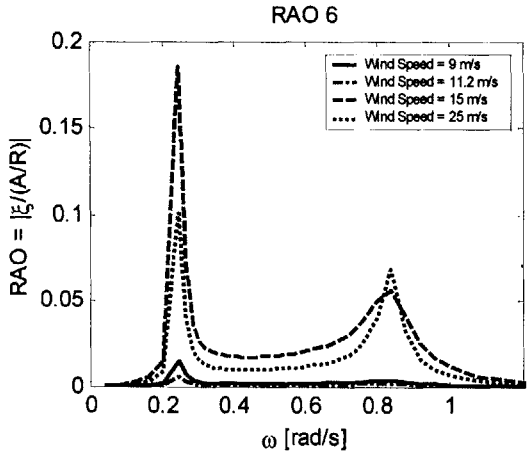

(c) RAO 6

Figure 34. RAOs, NREL TLP RB6, Wind Speed Effects

14.2.2 Discussion

The NREL TLP TD10 RB6 is affected by wind speed in a similar manner as the other structures, with a highest response and standard deviation of system motions demonstrated in wind speeds of 15 m/s.

14.3 Water Depth Effects

14.3.1 Results

Table 69. Steady-State Offsets, NREL TLP RB6, Water Depth Effects

	Wind Speed [m/s]	11.2
	Thrust [N]	800000
Water Depth [m]	Restoring [N]	Surge [m]
62.5	1912302.43	0.42
100	887854.7	0.90
200	365587.23	2.19
300	230184.552	3.48

Table 70. Natural Frequencies, NREL TLP RB6, Water Depth Effects

Water Depth	[m]	62.5	100	200	300
Surge	[rad/s]	0.561	0.383	0.246	0.195234
Sway	[rad/s]	0.561	0.383	0.246	0.195232
Yaw	[rad/s]	1.914	1.308	0.846	0.676497

Table 71. Dynamic Tether Tensions, NREL TLP RB6, Water Depth Effects

Water Depth [	Max [N]	Min [N]
62.5	2.42E+07	1.82E+07
100	2.41E+07	1.82E+07
200	2.41E+07	1.82E+07
300	2.41E+07	1.82E+07

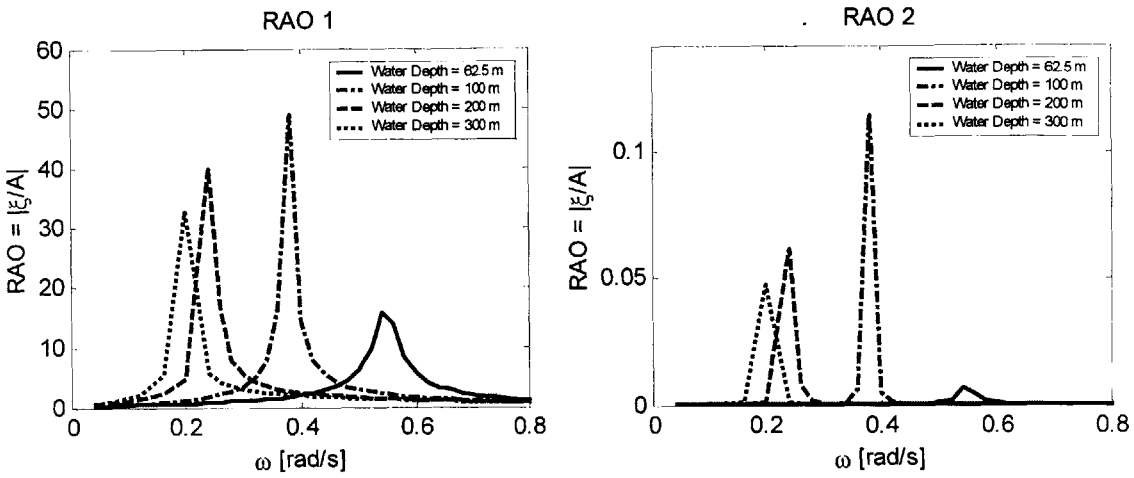

(a) RAO 1

(b) RAO 2

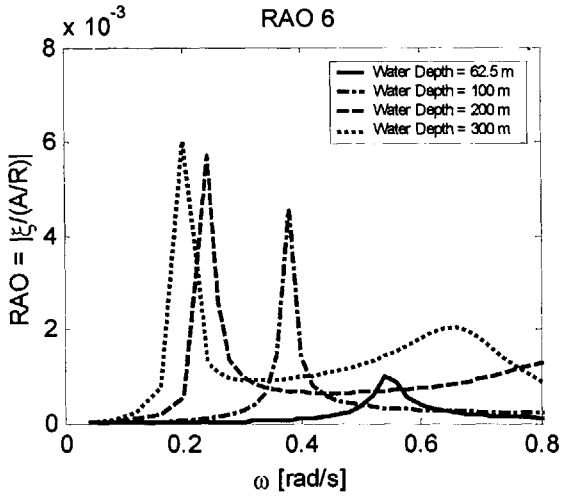

(c) RAO 6

Figure 35. RAOs, NREL TLP RB6, Water Depth Effects

Table 72. Standard Deviations of System Motions, NREL TLP RB6, Water Depth Effects

Sea States	Hs [m]	0.09	0.67	2.44	5.49	10
	Tm [s]	2	4.8	8.1	11.3	13.6
Surge [m]	62.5 m	0.0001	0.0887	3.4309	7.8744	11.5397
	100 m	0.0001	0.0604	1.3991	17.9236	38.2879
	200 m	0.0001	0.0526	0.6238	2.6819	12.3667
	300 m	0.0001	0.0509	0.5737	2.1105	5.1746
Sway [m]	62.5 m	0.0000	0.0000	0.0011	0.0025	0.0035
	100 m	0.0000	0.0000	0.0019	0.0374	0.0798
	200 m	0.0000	0.0000	0.0000	0.0005	0.0132
	300 m	0.0000	0.0000	0.0000	0.0001	0.0008
Yaw [deg]	62.5 m	0.0000	0.0000	0.0002	0.0004	0.0005
	100 m	0.0000	0.0000	0.0001	0.0013	0.0027
	200 m	0.0000	0.0001	0.0004	0.0008	0.0018
	300 m	0.0000	0.0000	0.0006	0.0013	0.0022

14.3.2 Discussion

The effects of water depth are somewhat unique to this structure. For sea states 4 and 5, the water depth of 100 meters results in the largest standard deviation of system motions, while for sea states 3 and below, the standard deviations decrease with increasing water depth. Although the outcomes of increasing water depth are different, the same mechanism is responsible for these effects. Again, as water depth increases, natural frequency decreases.

For sea states 4 and 5, the natural frequencies of the system are actually higher than the frequency of the peak of the sea state spectra for water depths of 62.5 m. At a water depth of 100 m, the peak of the RAO and the peak of the sea state spectrum almost align, resulting in a large value for the standard deviations of motions. At water depths beyond 100 m, the natural frequencies continue to decrease as the frequency of the peak of the sea state remains at its original value. This results in decreasing standard deviations with water depth from 100 to 300 m.

For sea states 1 through 3, the frequencies of the peak of the sea state spectra are all greater than the natural frequencies of the system at the shallowest water depth. Therefore as the depth increases, the natural frequency only moves away from the peak of the sea state spectra, resulting in decreasing standard deviations of system motions.

14.4 Viscous Damping Effects

14.4.1 Results

Steady-state offset, natural frequencies, and dynamic tether tension are unaffected by viscous damping, and are summarized in the base case results sections.

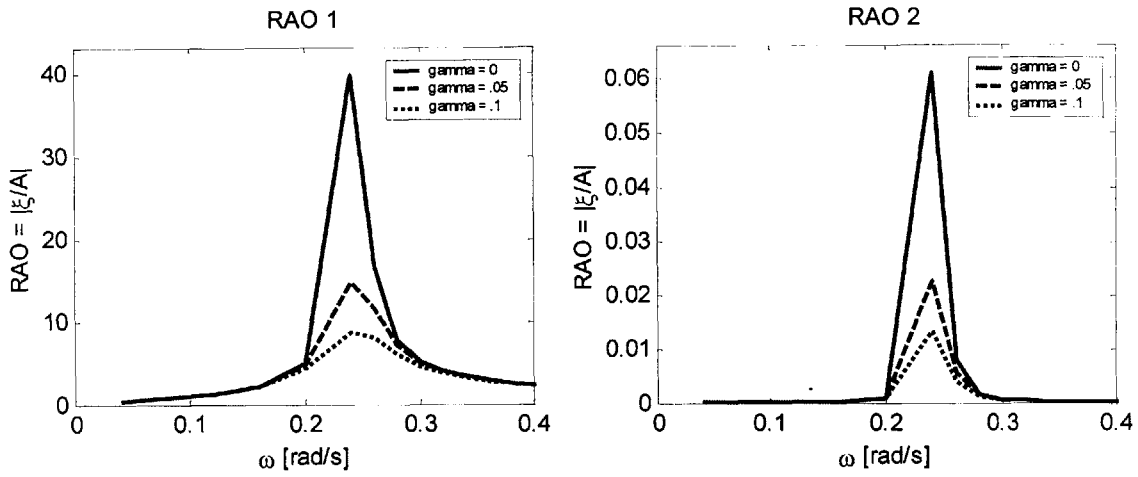

(a) RAO 1 **(b) RAO 2**

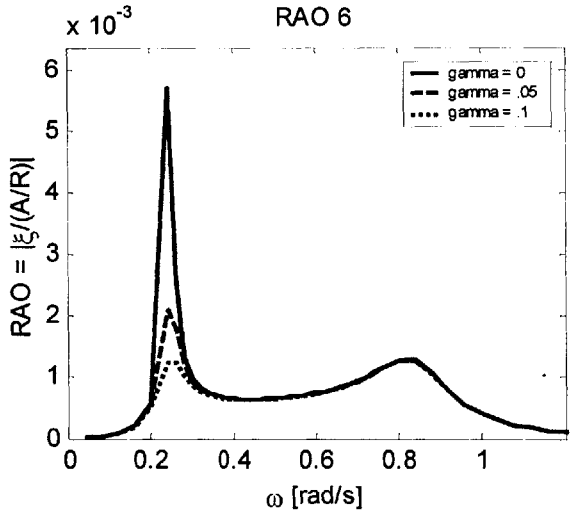

(c) RAO 6

Figure 36. RAOs, NREL TLP RB6, Viscous Damping Effects

Table 73. Standard Deviations of System Motions, NREL TLP RB6, Viscous Damping Effects

Sea States	Hs [m]	0.09	0.67	2.44	5.49	10
	Tm [s]	2	4.8	8.1	11.3	13.6
Surge [m]	g = 0	0.0001	0.0526	0.6238	2.6819	12.3667
	g = .05	0.0001	0.0523	0.6197	2.6153	8.5260
	g = .1	0.0001	0.0519	0.6139	2.5331	7.2498
Sway [m]	g = 0	0.0000	0.0000	0.0000	0.0005	0.0132
	g = .05	0.0000	0.0000	0.0000	0.0003	0.0052
	g = .1	0.0000	0.0000	0.0000	0.0002	0.0031
Yaw [deg]	g = 0	0.0000	0.0001	0.0004	0.0008	0.0018
	g = .05	0.0000	0.0001	0.0004	0.0008	0.0015
	g = .1	0.0000	0.0001	0.0004	0.0008	0.0014

14.4.2 Discussion

As expected, increasing viscous damping reduces the system's response at ever frequency. This effect results in a very mild mitigation of system response in sea states 1 through 4, and a dramatic mitigation at sea state 5. Standard deviations of system motions are mitigated only slightly in sea states 1 through 4 because the peaks of the RAOs for those sea states at a water depth of 200 m fall outside of the peaks of the sea state spectra in sea states 1 through 4. In sea state 5, the peaks of the RAOs of this system fall within the peak of the sea state spectra. Because increasing levels of viscous damping decreases the RAOs most drastically around the natural frequency, and the natural frequency falls within the peak of the sea state spectrum, the standard deviations of system motions are reduced dramatically.

14.5 Comparison of the NREL TLP RB2 and the NREL TLP RB6

The MIT NREL TLP RB2 shows a lower response than the RB6 in all conditions. Two reasons contribute to this occurrence. The first reason is that the RB6 TLP requires a larger structure to create a larger buoyant force to provide additional tension to the mooring lines. This results in higher hydrodynamic forces on the body. The second reason is that the larger restoring matrix resulting from the higher tension in the mooring lines causes the RAOs to have a higher natural frequency that is closer to the frequencies of the peaks of the sea state spectra, and a stronger response about that natural frequency.

15. Conclusions

The RAOs and the standard deviations of system motions for each structure in its base case are reproduced for comparison below.

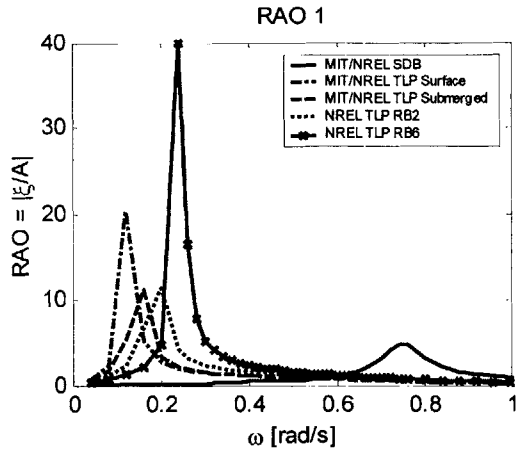

(a) RAO 1

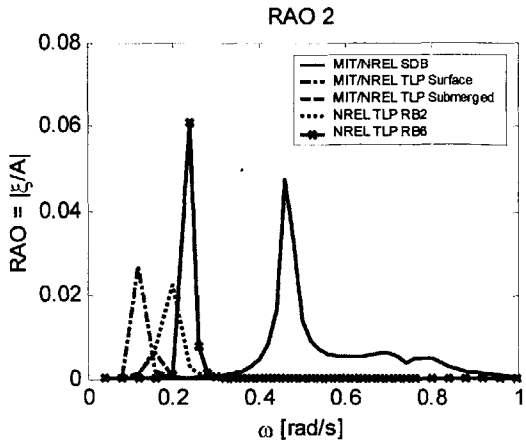

(b) RAO 2

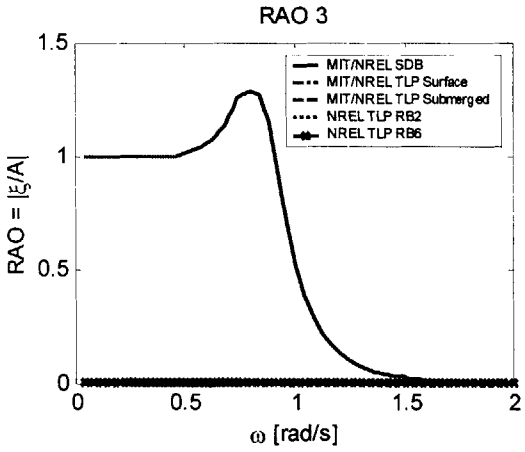

(c) RAO 3

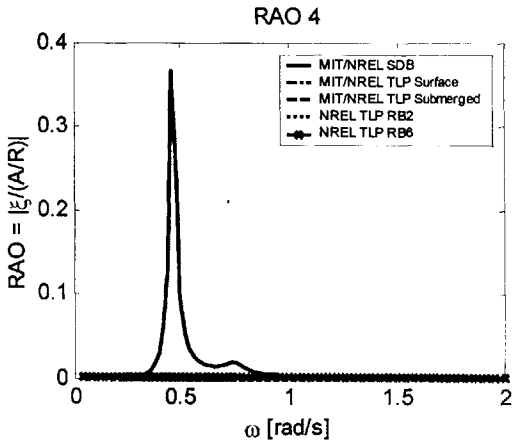

(d) RAO 4

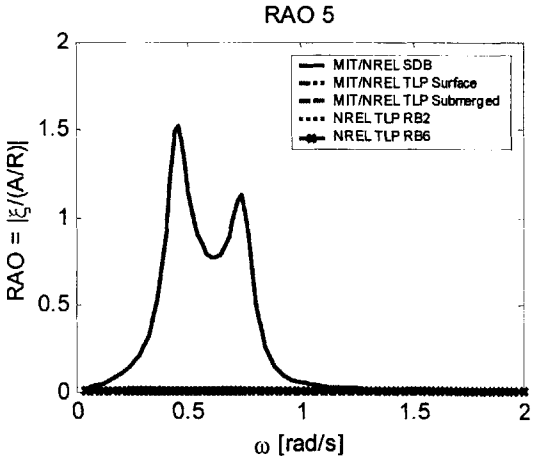

(e) RAO 5

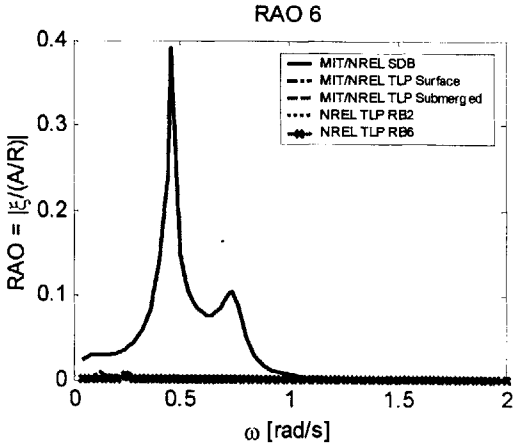

(f) RAO 6

Figure 37. RAOs for all Structures in the Base Case

Table 74. Standard Deviations of System Motions for all Systems in the Base Case

	SDB	M/N TLP Surface	M/N TLP Submerged	NREL TLP RB 2	NREL TLP RB 6
Surge	2.598	2.912	2.798	4.196	12.367
Sway	0.035	0.00035	0.00036	0.00156	0.01318
Heave	2.532	0	0	0	0
Roll	0.109	0	0	0	0
Pitch	0.927	0	0	0	0
Yaw	0.156	0.00334	0.00355	0.00476	0.00182

These responses, and the responses of the individual systems in different conditions, lead to the following conclusions.

- **RAOs and the standard deviations of system motions of the MIT/NREL SDB are relatively low**. This is due to the location of the natural frequency. The natural frequency of this system falls in a region with high hydrodynamic damping, and therefore high total damping. This leads to a lower and less narrow-banded response than those demonstrated by the other structures. The shape of the RAO then leads to a low standard deviation of system motion compared to the other structures.
- **RAOs of the TLP structures are narrow-banded and demonstrate relatively high response around the natural frequency**. These characteristics of the RAOs again are attributable to the location of the natural frequencies of the systems. The natural frequencies of the TLP systems all fall where little hydrodynamic damping exists. This leads to the high response at these frequencies, as shown by the RAOs.
- **Except for the NREL TLP RB6, the standard deviations of system motions for the TLPs remain fairly low**, despite the systems' high response around the natural frequencies. The values of the standard deviations of system motions can again be attributed to the location of the natural frequencies. For all structures except the NREL TLP RB6, the natural frequencies fall below the frequencies of the peaks of the sea state spectra. This results in little overlap between these systems' RAOs and the spectra, which results in low standard deviations of system motions. The NREL TLP RB6, however, has the highest natural frequency of the TLPs, and its closer proximity to the frequency of the peak of the

sea state spectra coupled with its high response about the natural frequency results in a high standard deviation of system motions.

- **All structures are affected similarly by wind speed**, and demonstrate the highest response at wind speeds of 15 m/s, and only a slightly lower response at 25 m/s. The elevated responses at 15 and 25 m/s are due to the decreased damping from the wind turbine in Region 3 of the wind turbine power curve.
- The standard deviations of system motions of the SDB decrease with water depth for all modes of motion. This occurs because the RAOs in surge and roll become more narrow-banded without significantly increasing in magnitude, while the RAO in pitch decreases in magnitude with depth, and while the others show little change. These changes in shape of the RAOs lead to reduced standard deviations of system motions with water depth.
- **The TLPs are all affected similarly by water depth, and demonstrate lower natural frequencies with increasing water depth**. This results in lower standard deviations of system motions with water depth for all structures except the NREL TLP 6. The NREL TLP 6 has higher natural frequencies than the other structures that coincide with the frequencies of the peaks of the sea state spectra. As the natural frequency reduces from a water depth of 62.5 to 100 m, the natural frequency passes through the frequency of the peak of the most severe sea state spectrum. As a result the standard deviations of system motions at 100 m are much higher than the system's response at any other depth. The natural frequencies of the other structures lie below the peak frequencies at all water depths. Therefore, as water depth increases and natural frequencies decrease, the standard deviations of system motions only decrease.
- **All structures' responses are mitigated by reasonable levels of viscous damping**. The result of viscous damping is reduced RAOs at all frequencies, but especially at frequencies around the natural frequency. The result of the reduced RAOs depends on where the structure's natural frequency is located relative to the peaks of the sea state spectra. The NREL TLP RB 6 demonstrates a higher degree of mitigation of the standard deviations of system motions because the natural frequency occurs close to the frequency of the peak of the sea state spectra. This

results in a higher degree of reduction of the standard deviations of system motions due to viscous damping.

These observations then lead to a set of more general conclusions

- Coupled modes of excitation are important to consider in compliant systems, and not as important in stiff systems.
- The system response can be largely tuned by designing the system for a particular natural frequency. Ideally, to avoid large spikes in the RAOs, the natural frequency would be located at a frequency where hydrodynamic damping occurs, and to achieve low standard deviations of system motions, the natural frequency would be located at a frequency that does not coincide with the peak frequency of the sea state spectra of the likely sea state at the installation site.

16. Cost of Energy Assessment

A Cost of Energy (COE) assessment was carried out to determine the cost per kWh that could be attributed to the floating foundation of floating wind turbine systems. To accomplish this, estimates of the total cost of the platforms were made first, following the same procedure and making the same assumption as described in **Section 7**. The structures resulting from the dynamic analysis phase are estimated to have installed costs between $1.5M and $4.5M. The total cost estimates are summarized in **Figure 38** through **Figure 41** below.

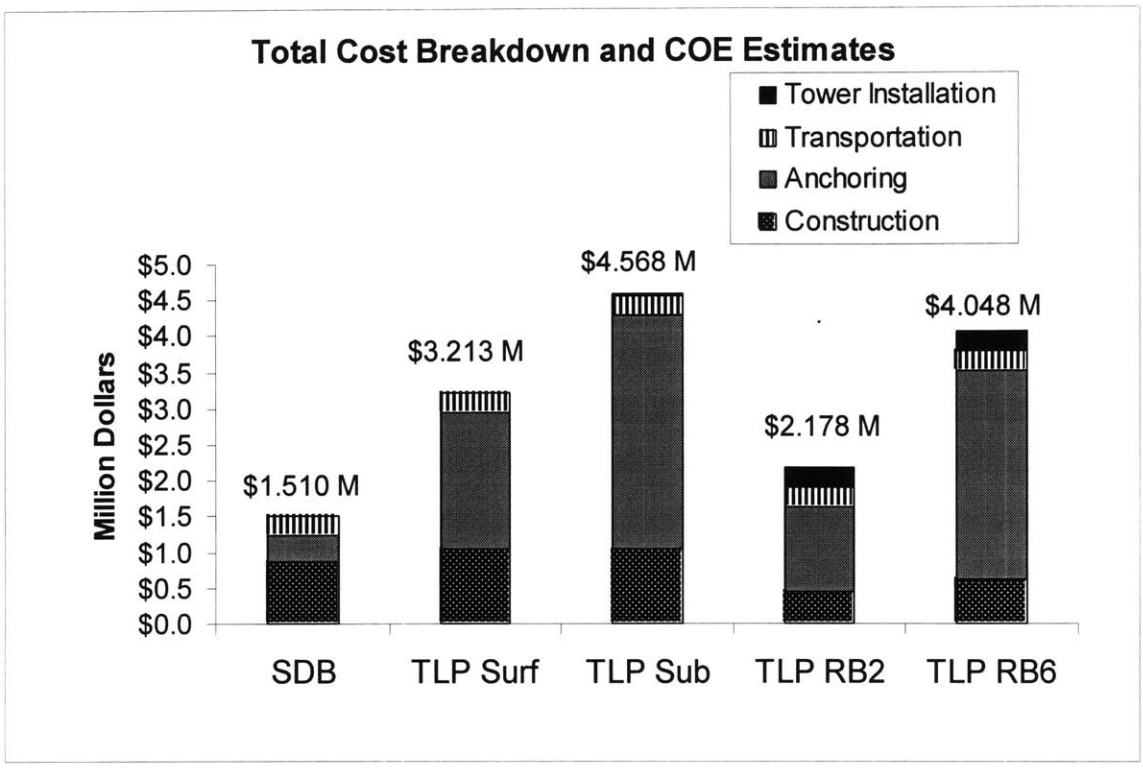

Figure 38. Total Cost Breakdown of Final Structures

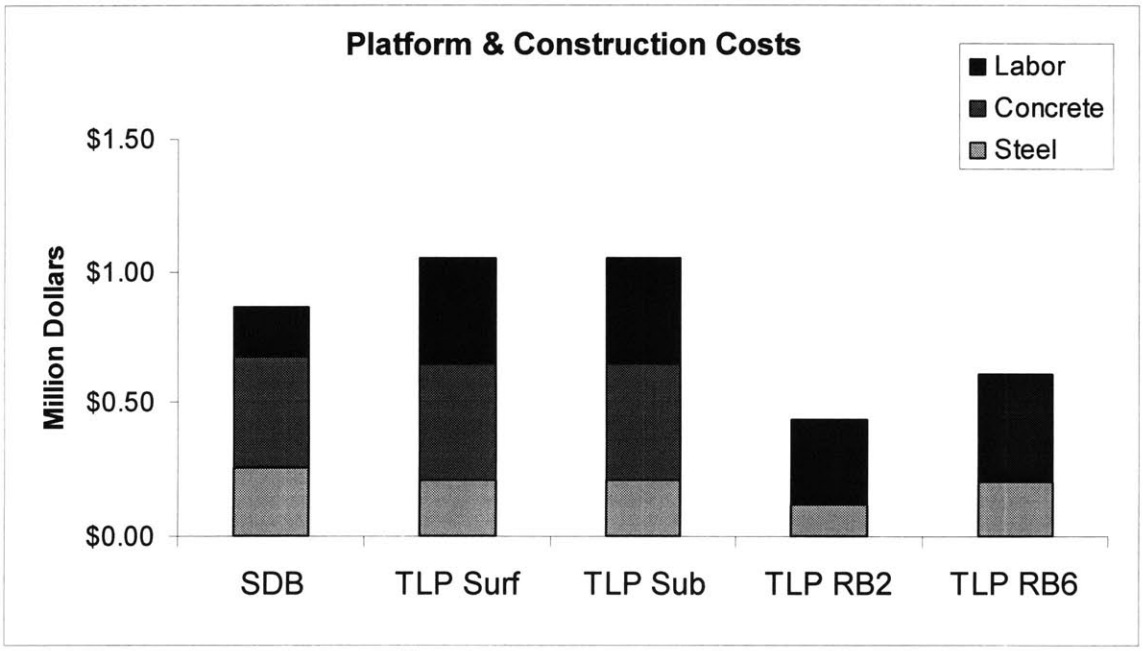

Figure 39. Cost of Construction of Final Structures

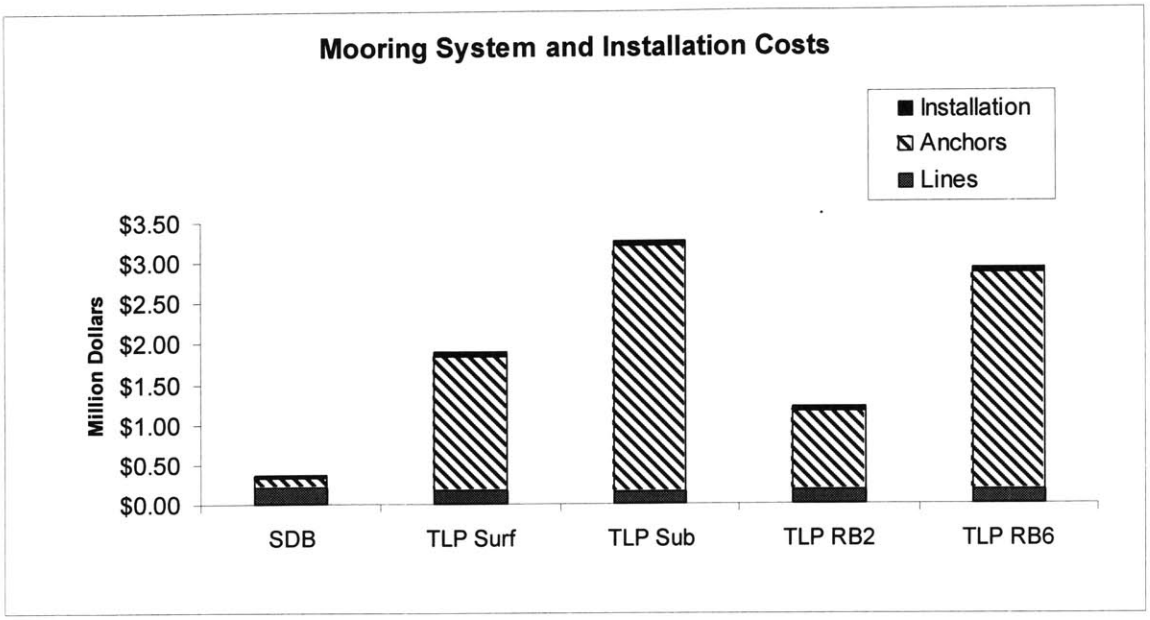

Figure 40. Cost of the Mooring Systems and Mooring system Installation for the Final Structures

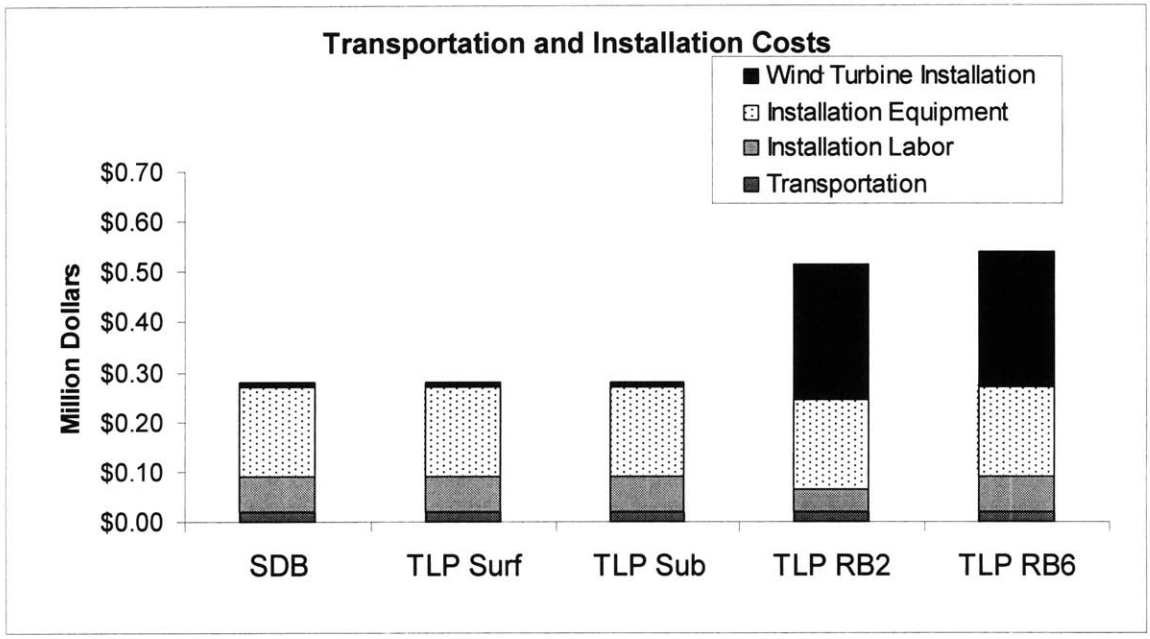

Figure 41. Cost of Transportation and Installation for the Final Structures

The costs of some of the final structures are much higher than the costs of the initial structures. This is mostly attributable to the mooring system. The evolution of all parts of the structure resulted in the requirement of a more robust mooring system than initially estimated. The mooring system was designed with anchors and lines that are capable of

withstanding the maximum forces experienced due to wind and wave loading, with a safety factor of 2. The anchors required for these mooring systems drove the mooring system cost up significantly, which resulted in a significant increase in total system cost. More details pertaining to the cost estimates are provided in Appendix B.

The total installed costs summarized above were then used to perform the COE analysis. This analysis was carried out to adhere to NREL's COE procedures, and is given by the equation below.

$$COE = R\frac{ICC}{AEP} + \frac{(LRC + O\&M + Land)}{AEP}$$

In this equation, R stands for the Fixed Charge Rate, *ICC,* Initial Capital Cost, *AEP*, Annual Energy Production, *LRC*, Levelized Replacement Cost, *O&M*, Operation and Maintenance, and *Land*, the fee charged to the wind farm operator to occupy the land. This study only considers the *ICC*, and the equation is reduced to the following.

$$COE = R\frac{ICC}{AEP}$$

AEP is also approximated following NREL's standard procedure, and is calculated for two mean wind speeds; 5.8 and 8 m/s. This calculation is performed by considering the turbine's power curve and the Weibull distribution of wind speeds with a specified mean wind speed to determined the number of MWh expected to be produced by one wind turbine.

AEP values of 15257.41 and 22057.48 MWh/y were estimated for wind speeds of 5.8 and 8 m/s respectively. These values were used with the fixed charge rate, R, given by NREL as 11.85% to calculate the COE due to the platform and platform installation for each structure. These figures are reported on **Figure 42** below.

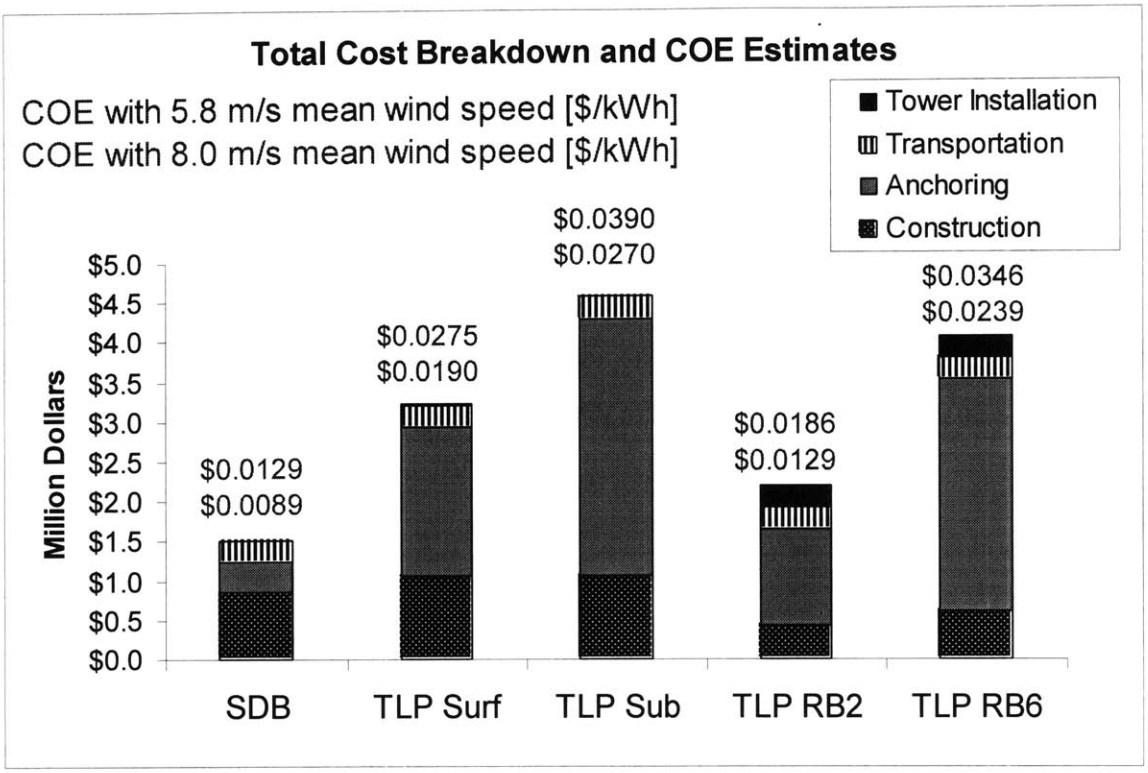

Figure 42. Total Cost Breakdown and COE Estimates for the Final Structures

It is important to note that these costs do not include operation and maintenance costs or levelized replacement costs. These costs in an offshore setting are highly uncertain, and could be high relative to comparable onshore projects.

17. Suggested Future Work

- Development of a fully integrated time domain analysis and modeling tool
- Detailed design, cost analysis, structural analysis
- Turbine control for motion mitigation
- Active or passive inertial control of the platform for motion mitigation
- Careful consideration of the design of a wind turbine suitable for offshore deployment

Appendix A: Hydrodynamic Quantities

This appendix contains plots of the added mass, and damping matrices, and the exciting forces of each system. The symbols in these figures are defined below.

A(i,j)	=	The (i,j) entry of the added mass matrix over all frequencies
B(I,j)	=	The (i,j) entry of the damping matrix over all frequencies
P	=	Platform damping only
P+WT	=	Platform plus wind turbine damping
P+WT+V	=	Platform plus wind turbine plus viscous damping
X(i)	=	The i^{th} component of the exciting force over all frequencies

A.1 MIT/NREL SDB

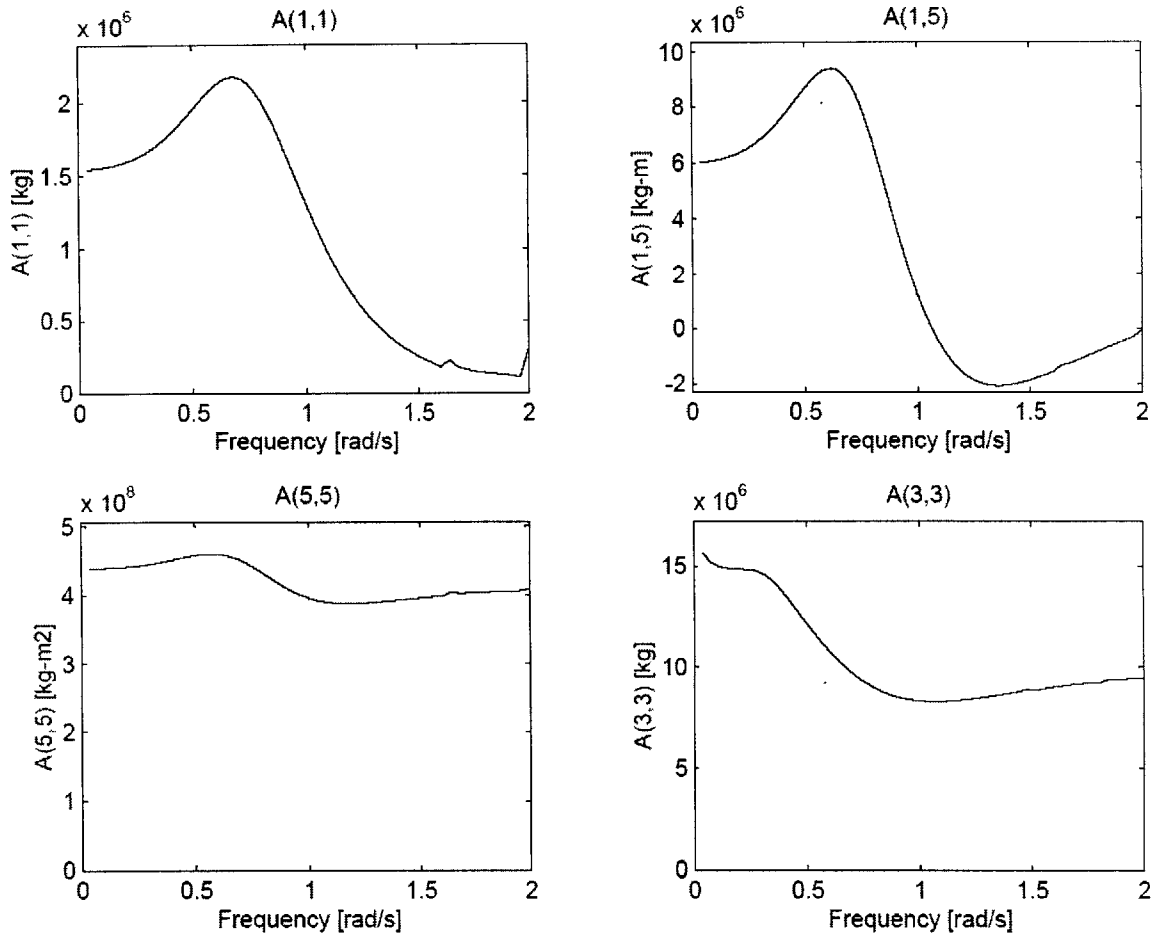

Figure A.43. Added Mass, MIT/NREL SDB, Base Case

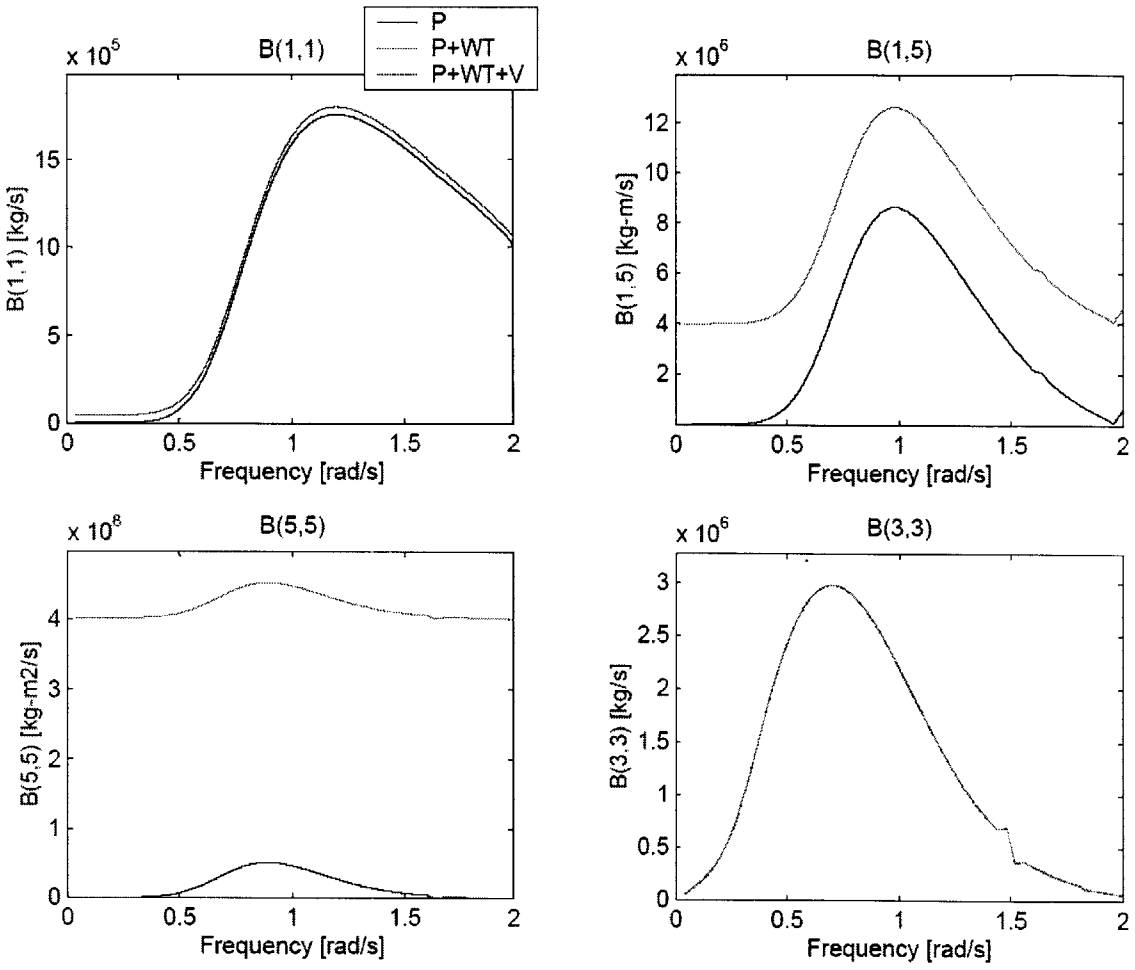

Figure A.44. Damping, MIT/NREL SDB, Base Case

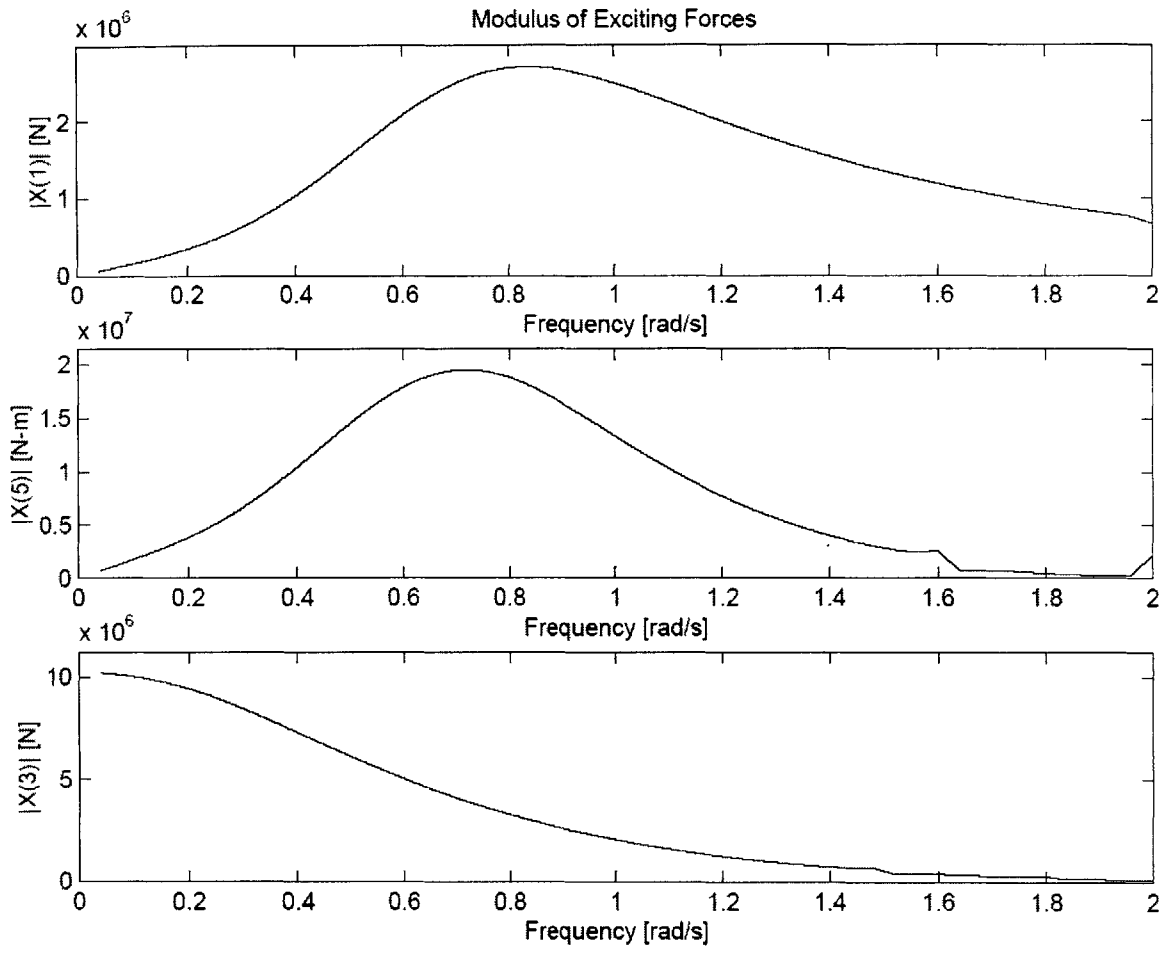

Figure A.45. Exciting Forces, MIT/NREL SDB, Base Case

A.2 MIT/NREL TLP Surface

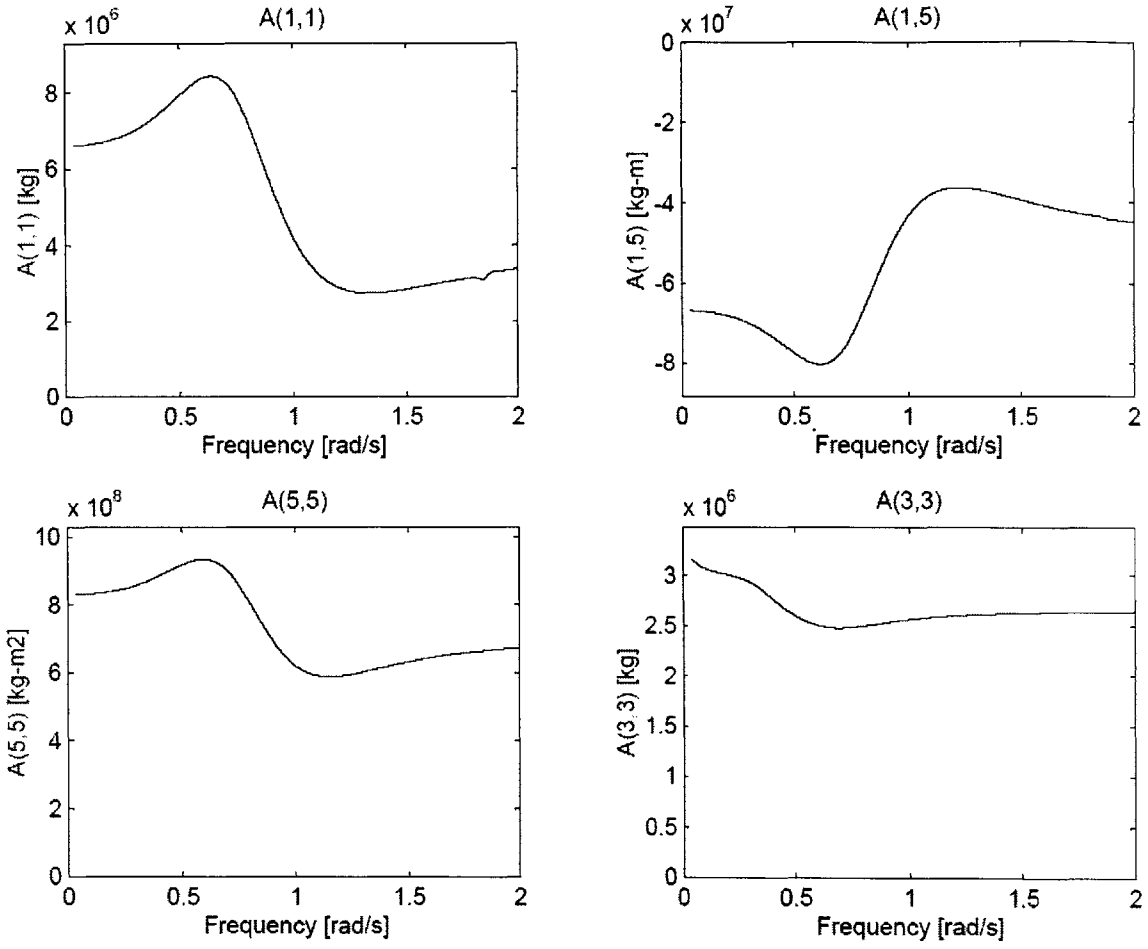

Figure A.46. Added Mass Matrices, MIT/NREL TLP Surface, Base Case

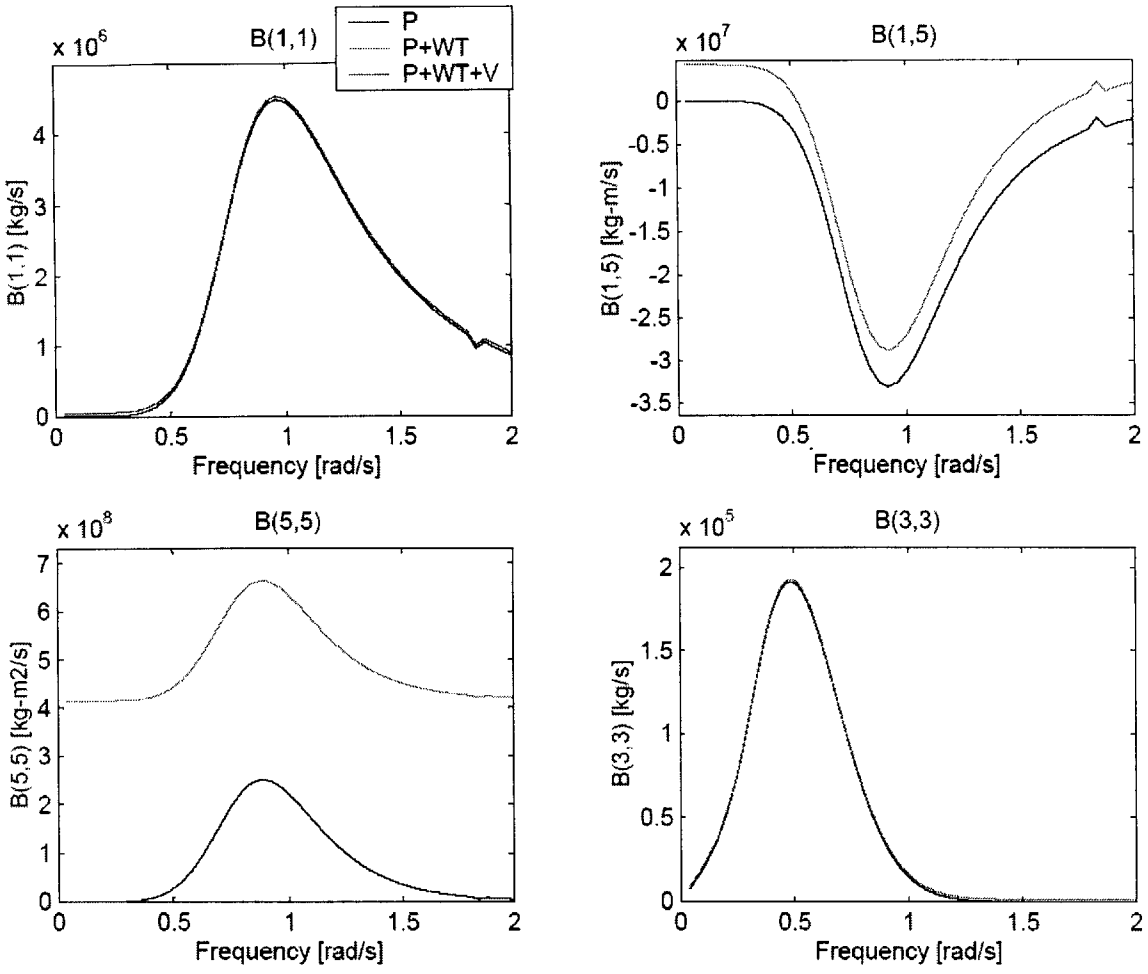

Figure A.47. Damping Matrices, MIT/NREL TLP Surface, Base Case

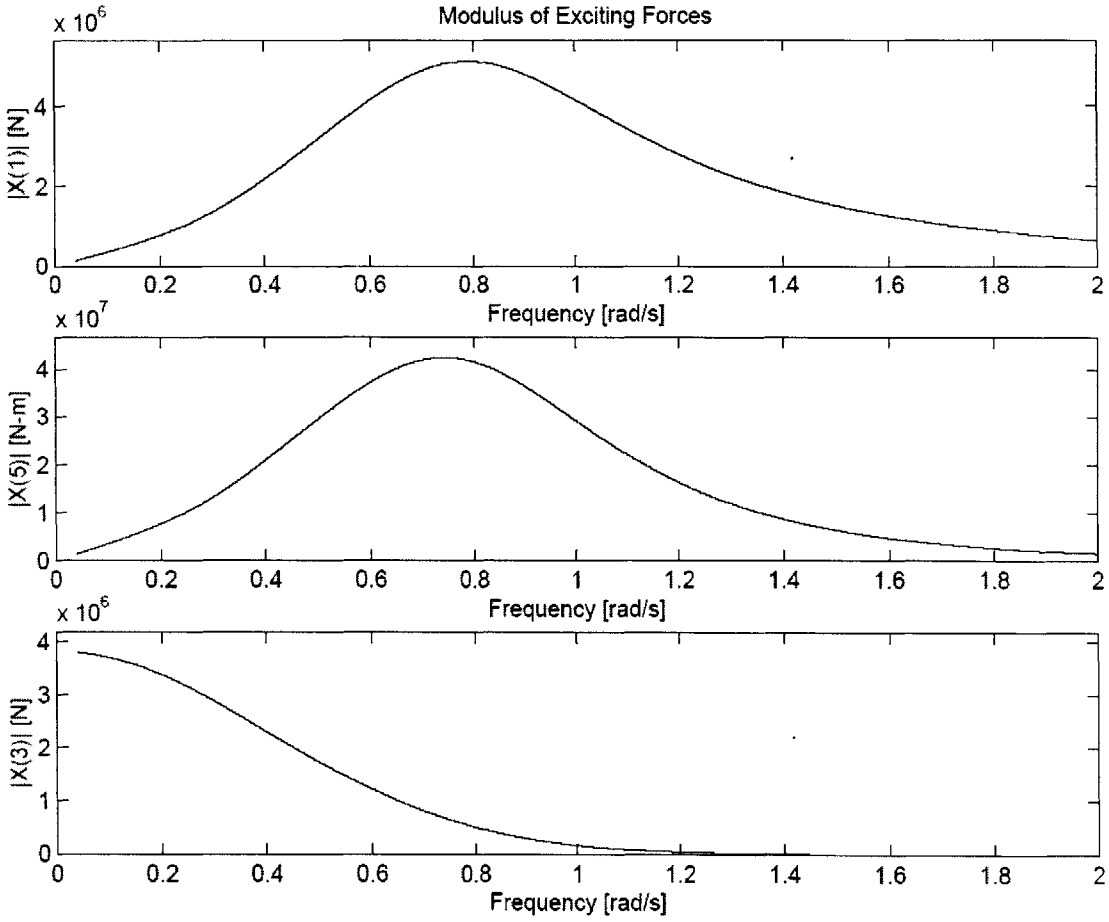

Figure A.48. Exciting Forces, MIT/NREL TLP Surface, Base Case

A.3 MIT/NREL TLP Submerged

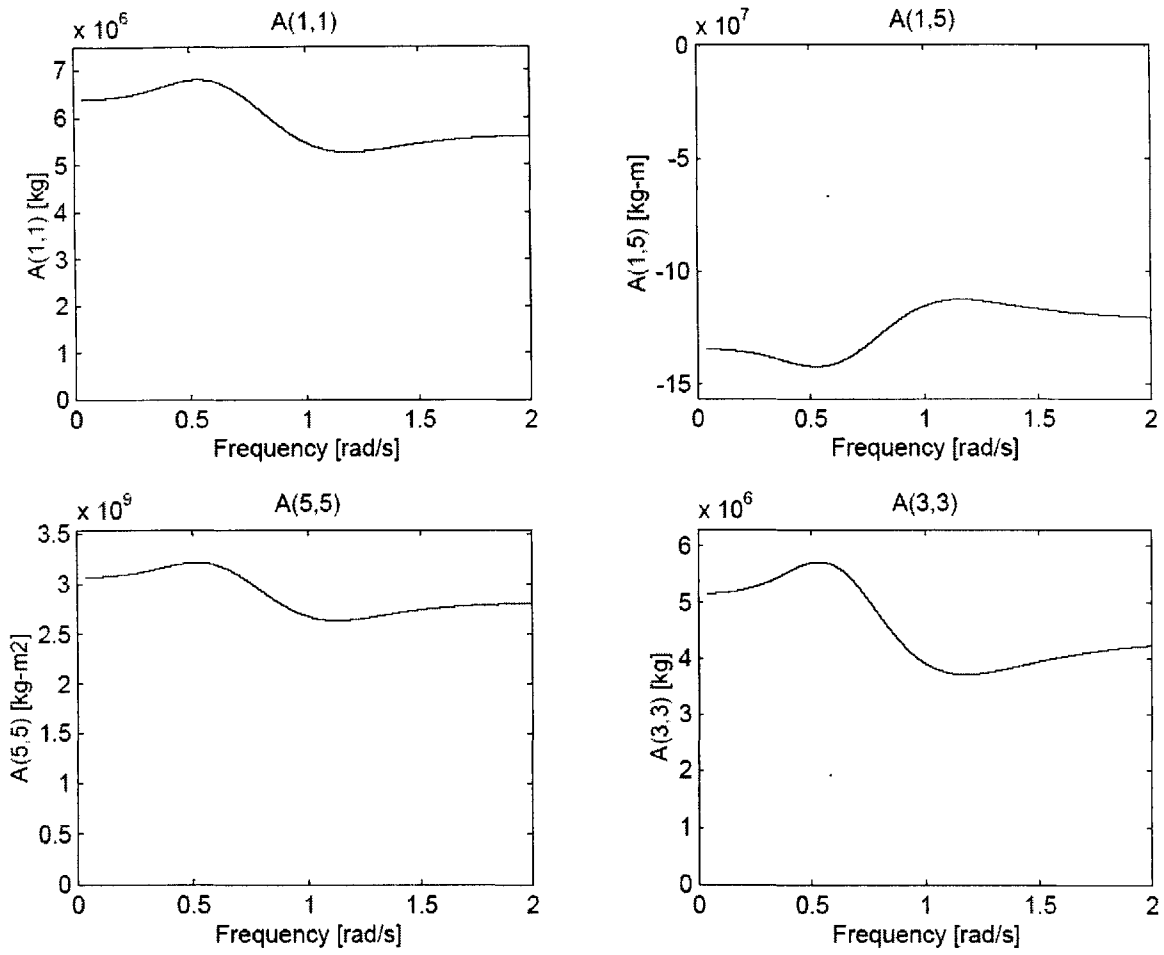

Figure A.49. Added Mass Matrices, MIT/NREL TLP Submerged, Base Case

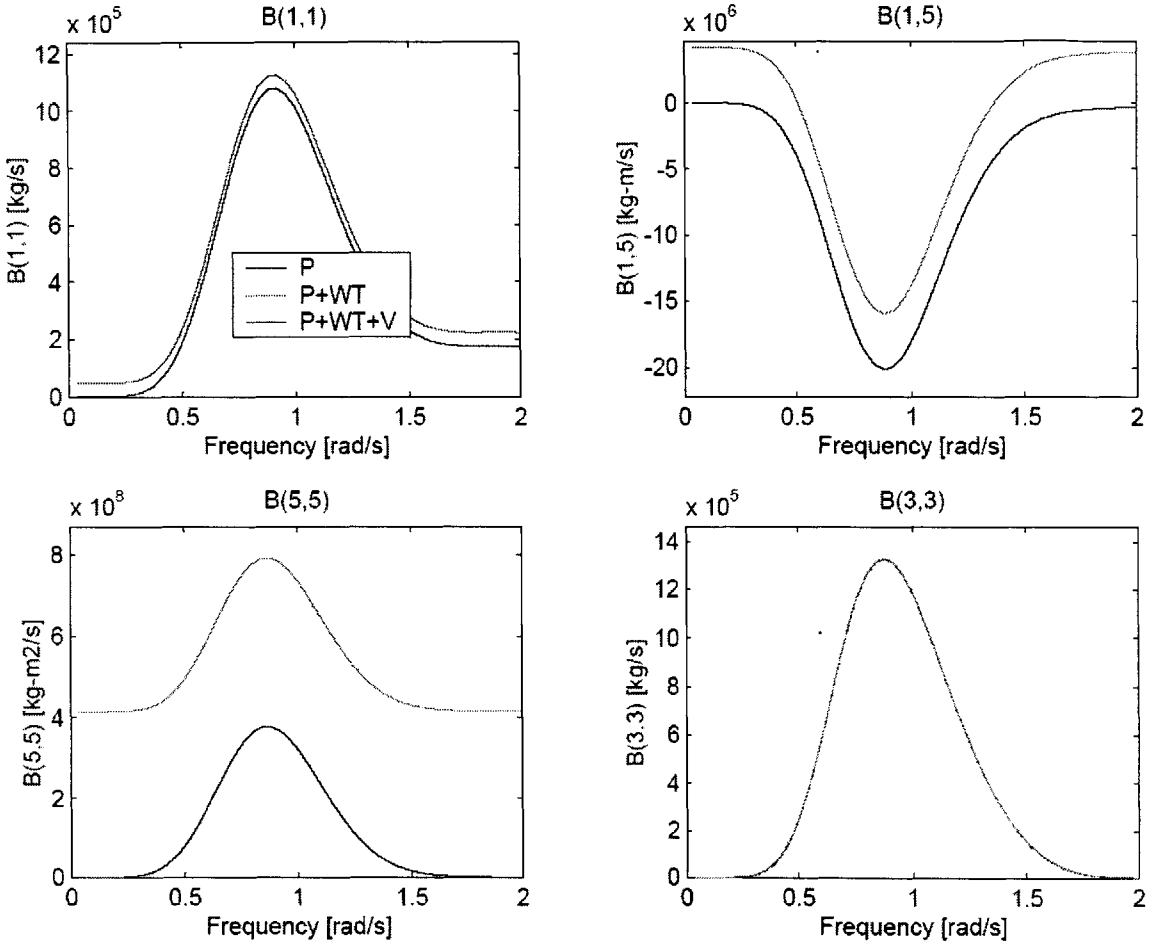

Figure A.50. Damping Matrices, MIT/NREL TLP Submerged, Base Case

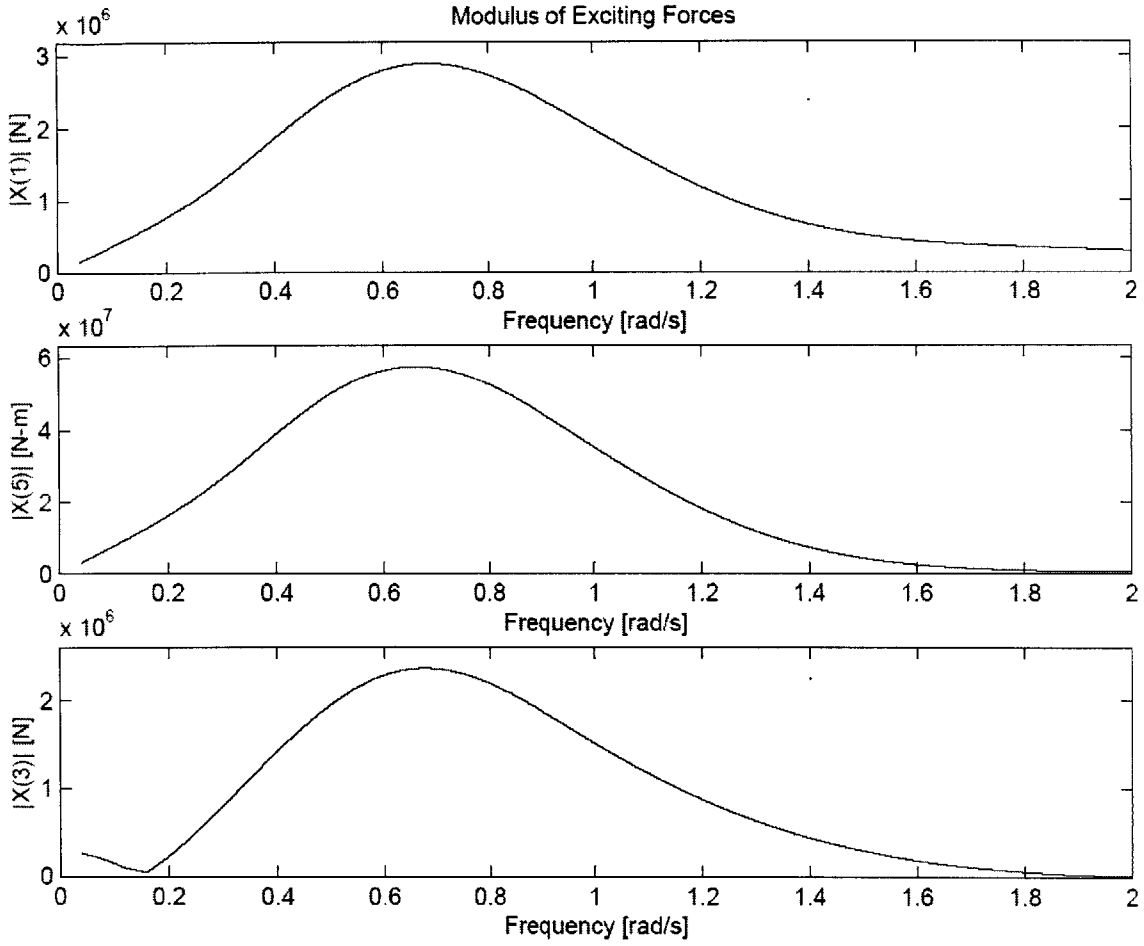

Figure A.51. Exciting Forces, MIT/NREL TLP Submerged, Base Case

A.4 NREL TLP RB=2

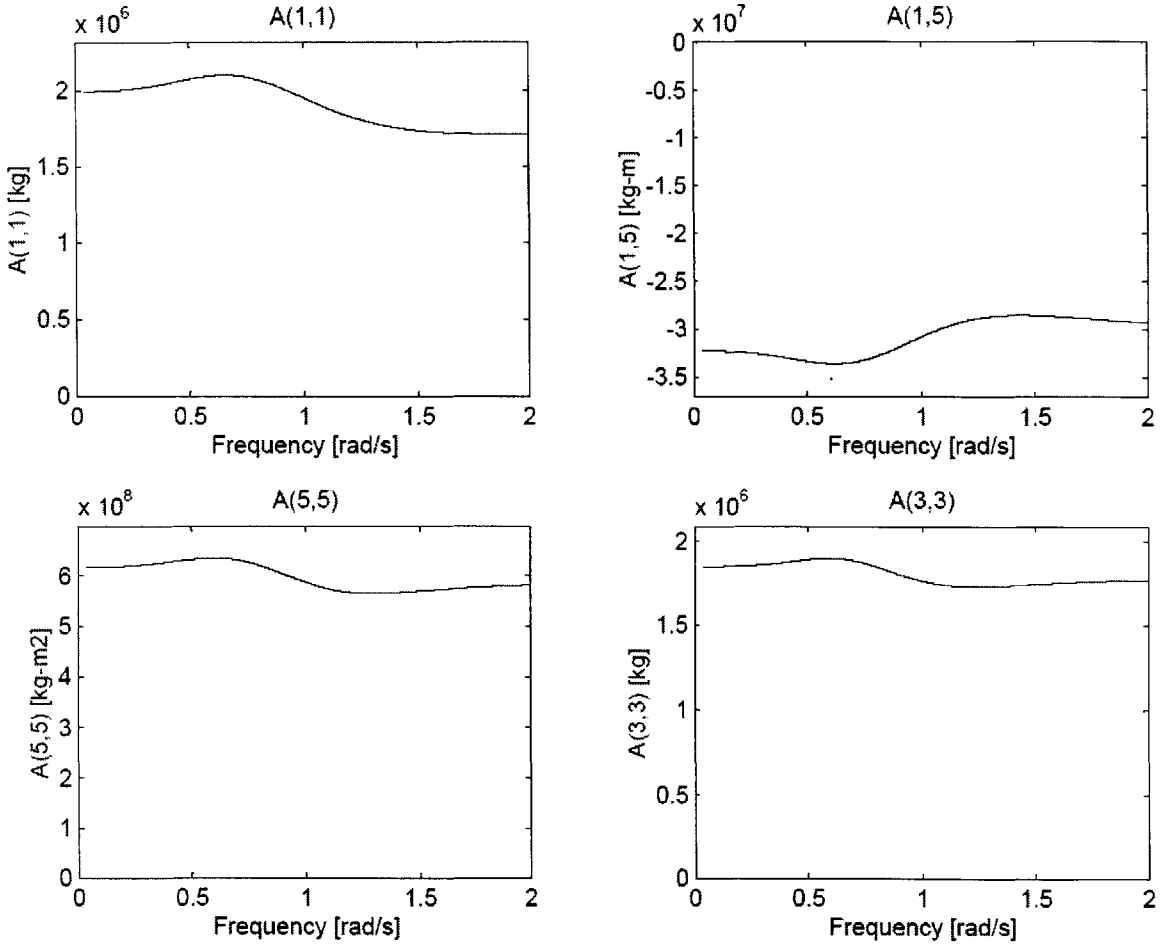

Figure A.52. Added Mass Matrices, NREL TLP RB2, Base Case

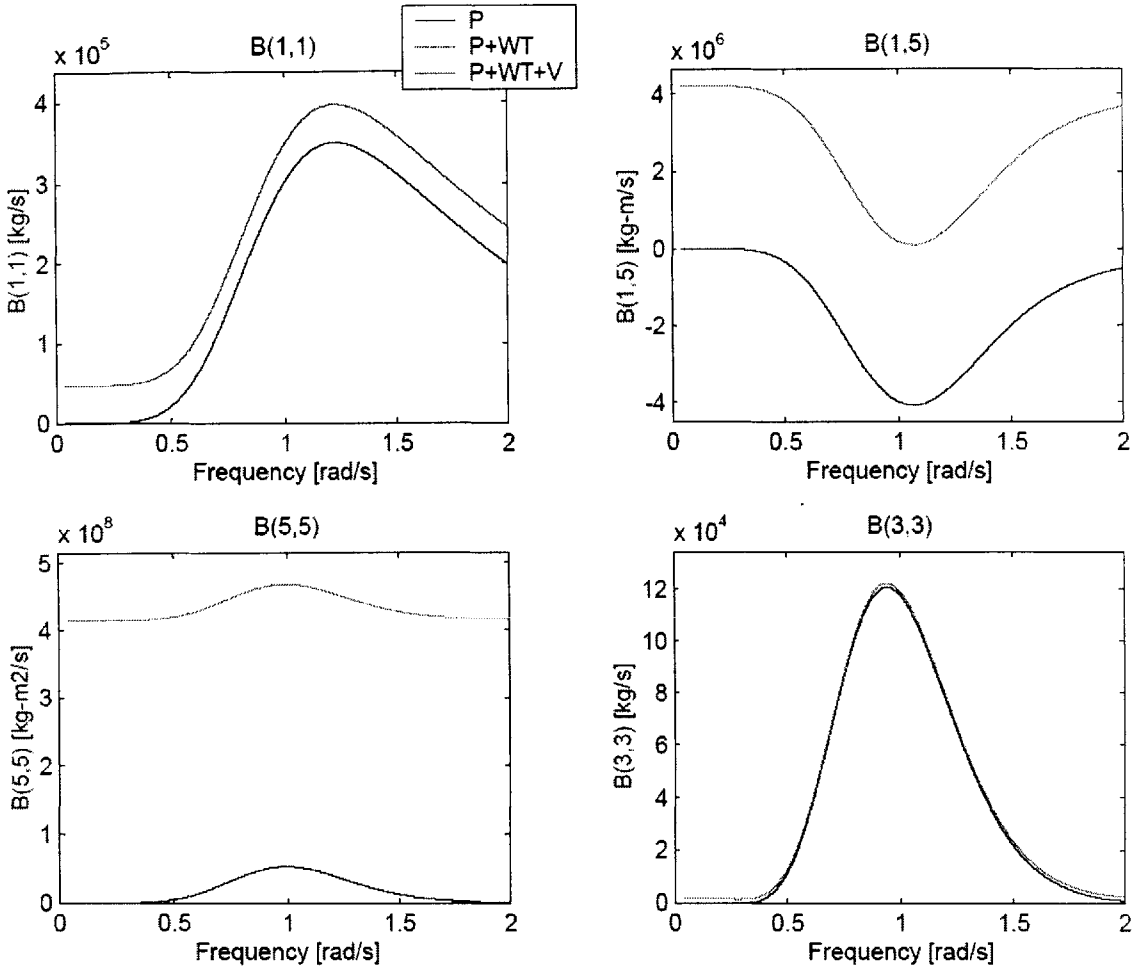

Figure A.53. Damping Matrices, NREL TLP RB2, Base Case

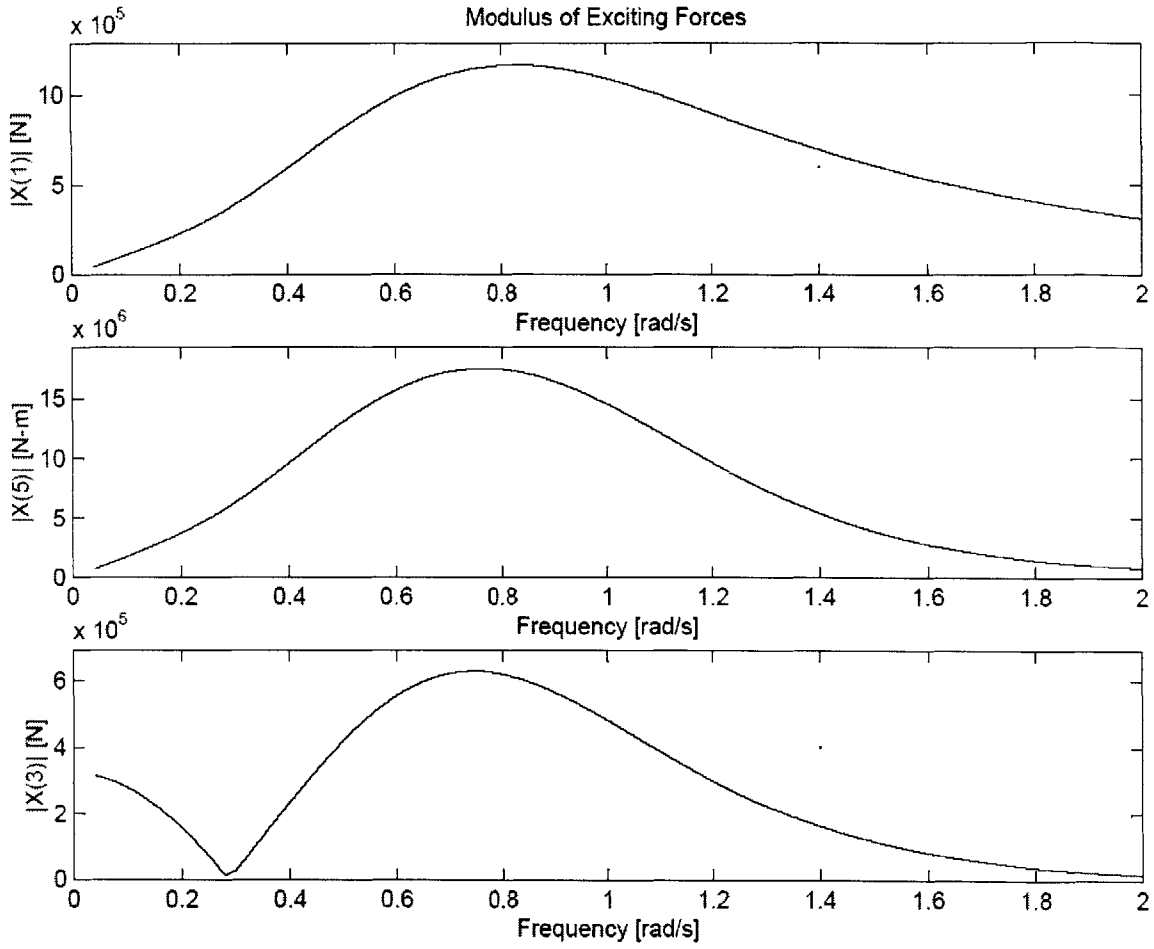

Figure A.54. Exciting Forces, NREL TLP RB2, Base Case

A.5 NREL TLP RB = 6

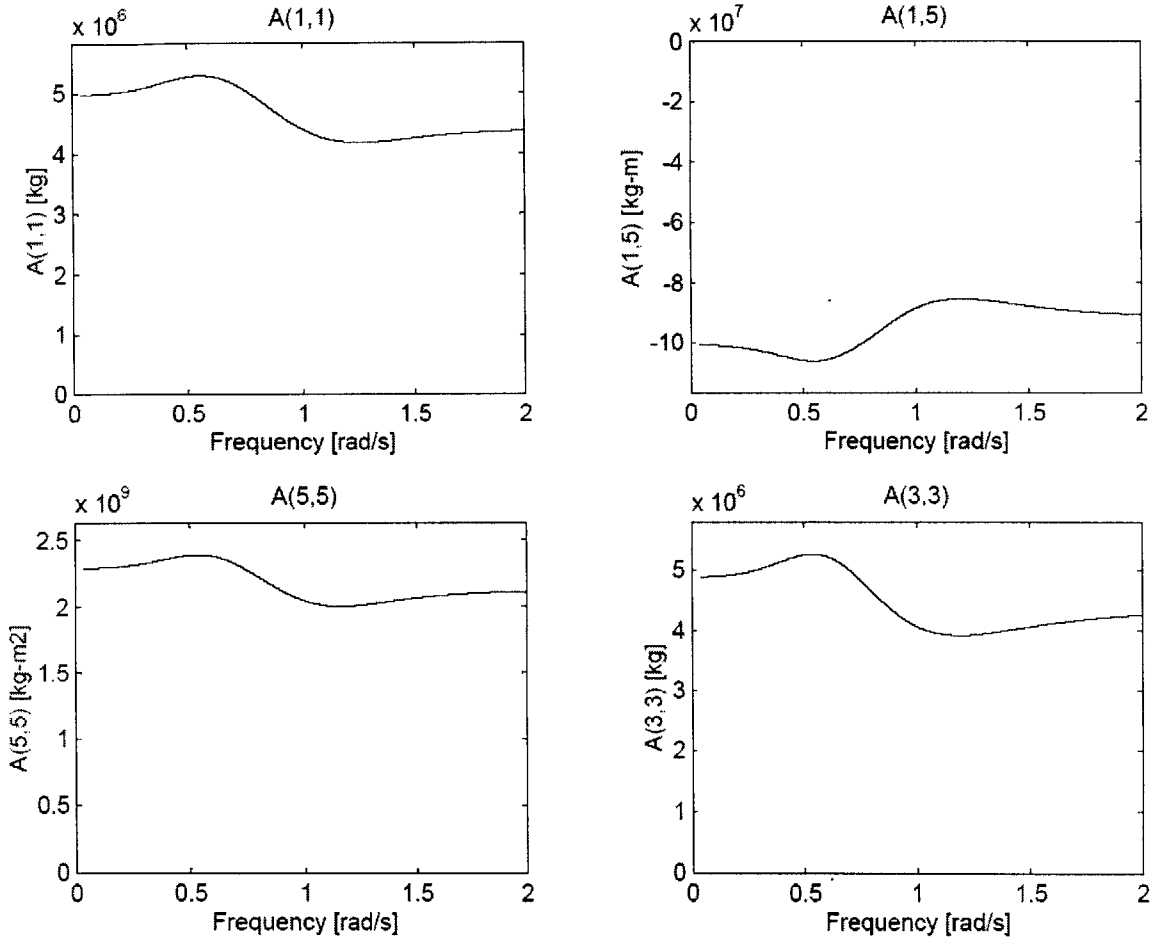

Figure A.55. Added Mass Matrices, NREL TLP RB6, Base Case

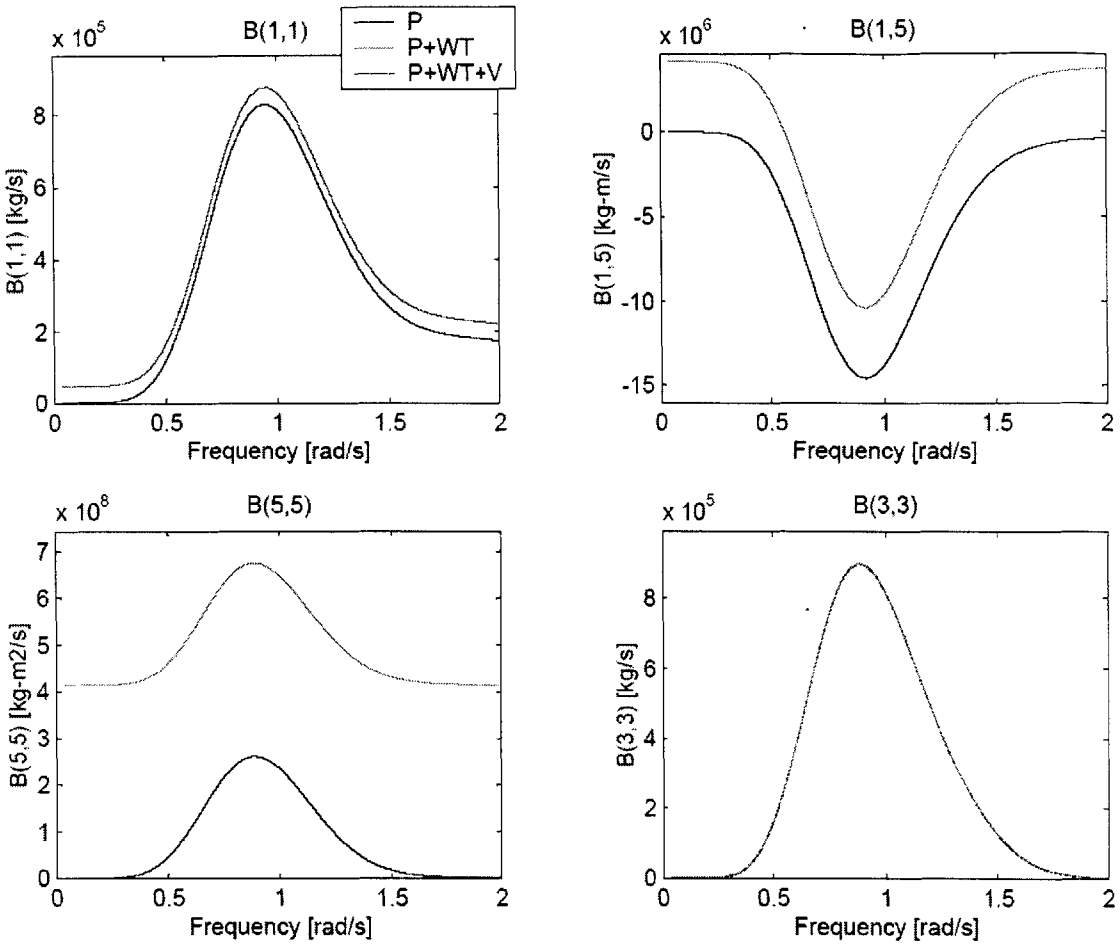

Figure A.56. Damping Matrices, NREL TLP RB2, Base Case

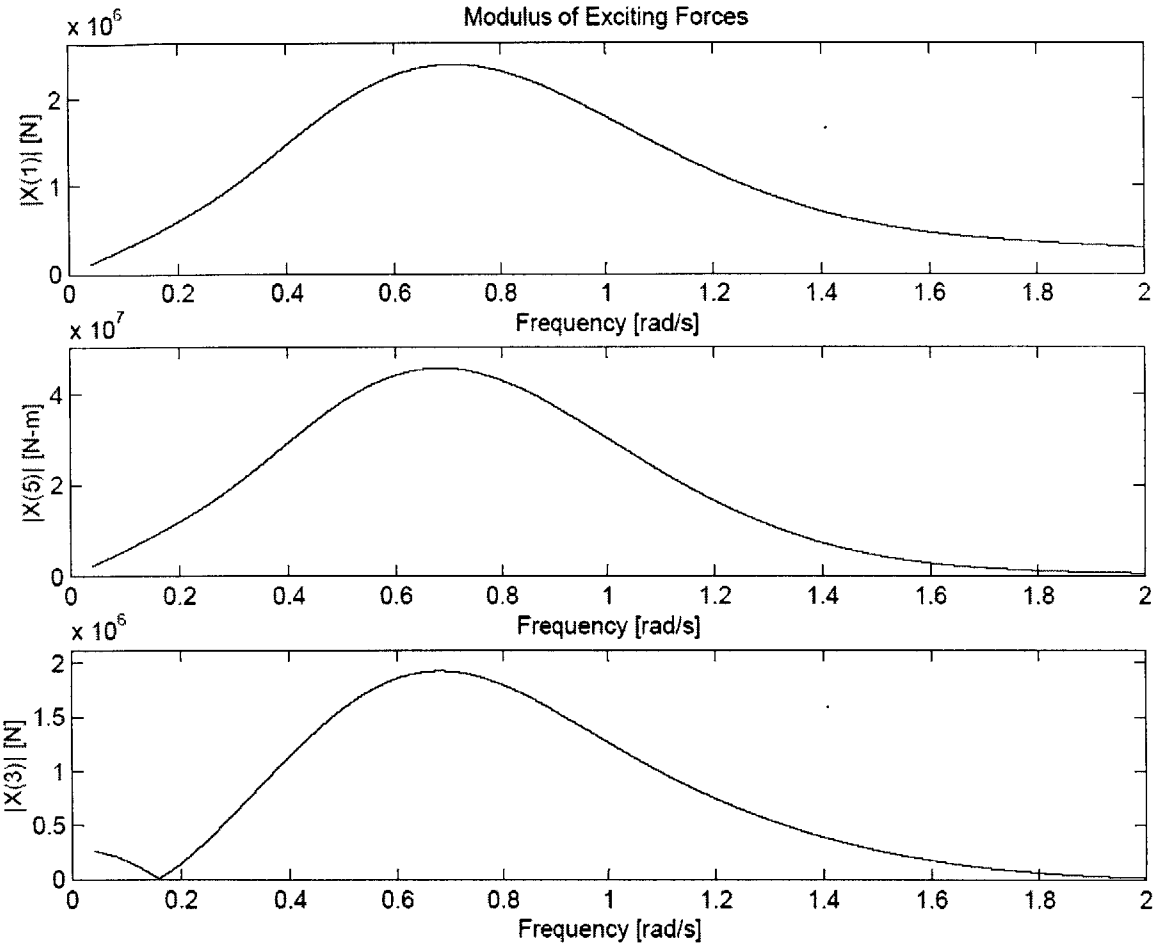

Figure A.57. Exciting Forces, NREL TLP RB2, Base Case

Appendix B: Cost Calculations

B.1 MIT/NREL SDB

			Unit Cost	Unit	Cost
1) Construction and Materials					
Steel	366.22	Ton Steel	$700	$/Metric Ton	$256,356.32
Concrete	4153.32	Ton Concrete	$100	$/Metric Ton	$415,331.93
Construction l	4800	Labor Hours	$40	$/hour	$192,000.00
		Total Construction Cost per Platfrom			**$863,688.25**
2) Anchors, Mooring Lines, and Anchor Installation					
Lines					
Number of Lir	8	Lines	---	---	---
Max Tension	2.17E+06	Newtons	---	---	---
Max Line Stre	1.20E+09	Pa	---	---	---
Diameter Req	0.05		---	---	---
Length of Line	212.00	meters/line	---	---	---
Length of Cha	508.80	meters	$270	$/meter	$137,376.00
Length of Wir	1187.2	meters	$60	$/meter	$71,232
Anchors					
Heave Forcep	1.91E+06	Newtons	---	---	---
Anchor Type	DEA	---	---	---	---
Cost Per Verti	---	---	$15	$/kNewton	
Number of An	4	Anchors	$28,674	$/anchor	$114,696.05
Installation					
Number of An	4	Anchors	$11,285.71	hours	$45,142.86
		Total Anchor, Line, and Installation Cost per Platform			**$368,446.91**
3) Platform Transportation and Installation					
Miles Travele	100	miles	$200	$/mile	$20,000
T&I Days	3	days	---	---	---
Tug	2	tugs	$30,000	$/day	$180,000
Crew per Plat	14	Crew Members	---	---	---
T&I Labor	1008	Hours	$70	$/hour	$70,560
			T&I Cost per Platform		**$270,560**
2) Tower Installation on Shore					
Hours per Inst	6	Hours			
Crane	1	Cranes	$6,250	$/Turbine	$6,250
Tower Installa	30	Hours	$40	$/hour	$1,200
		Tower Installation Cost per Platform			$7,450
				Total System Cost	**$1,510,145.16**

B.2 MIT/NREL TLP Surface

			Unit Cost	Unit	Cost
1) Construction and Materials					
Steel	301.12	Ton Steel	$700	$/Metric Ton	$210,781.86
Concrete	4371.46	Ton Concrete	$100	$/Metric Ton	$437,145.87
Construction Labor	10000	Labor Hours	$40		$400,000.00
		Total Construction Cost per Platfrom			**$1,047,927.73**
2) Tower Installation on Shore					
Hours per Installation	6	Hours	---	---	---
Crane	1	Cranes	$6,250	$/Turbine	$6,250
Tower Installation Labor	30	Hours	$40	$/hour	$1,200
		Tower Installation Cost per Platform			**$7,450**
3) Anchors, Mooring Lines, and Anchor Installation					
Lines					
Max Force experienced at fairlead x SF	2.78E+07	Newtons	---	---	---
Number of Lines	8	Lines	---	---	---
Max Tension per line	13900000	Newtons	---	---	---
Max Line Stress allowed	1.20E+09	Pa	---	---	---
Diameter required	0.12	meters	---	---	---
Length of Lines	177.25	meters/line	---	---	---
Length of Chain	425.39	meters	$270	$/meter	$114,854.82
Length of Wire Rope	992.57	meters	$60	$/meter	$59,554.35
Anchors					
Heave Forceper Anchor x SF	2.78E+07	Newtons	---	---	---
Anchor Type	Suction Pile	---	---	---	---
Number of Anchors	4	Anchors	$417,000	$/anchor	$1,668,000.00
Installation					
Number of Anchors	4	Anchors	$11,285.71	$/Anchor	$45,142.86
		Total Anchor, Line, and Installation Cost per Platform			**$1,887,552.03**
4) Platform Transportation and Installation					
Miles Traveled	100	miles	$200	$/mile	$20,000
T&I Days	3	days	---	---	---
Tug	2	tug	$30,000	$/day	$180,000
Crew per Platform	14	Crew Members	---	---	---
T&I Labor	1008	Hours	$70	$/hour	$70,560
			T&I Cost per Platform		**$270,560**
			Total System Cost		**$3,213,489.76**

B.3 MIT/NREL TLP Submerged

1) Construction and Materials			Unit Cost	Unit	Cost
Steel	301.12	Ton Steel	$700	$/Metric Ton	$210,781.86
Concrete	4371.46	Ton Concrete	$100	$/Metric Ton	$437,145.87
Construction Labor	10000	Labor Hours	$40	$/hour	$400,000.00
		Total Construction Cost per Platfrom			**$1,047,927.73**

2) Tower Installation on Shore					
Hours per Installation	6	Hours	---	---	---
Crane	1	Cranes	$6,250	$/Turbine	$6,250
Tower Installation Labor	30	Hours	$40	$/hour	$1,200
		Tower Installation Cost per Platform			**$7,450**

3) Anchors, Mooring Lines, and Anchor Installation					
Lines					
Max Forcce experienced at Fairlead x SF	5.06E+07	Newtons	---	---	---
Number of Lines	8	Lines	---	---	---
Max Tension Experienced in each line x SF	2.53E+07	Newtons	---	---	---
Max Line Stress	1.20E+09	Pa	---	---	---
Diameter Required	0.16	meters	---	---	---
Total Chain Length	3.94E+02	meters	$270	$/meter	$106,272.00
Total Wire Rope Length	918.40	meters	$60	$/meter	$55,104.00
Anchors					
Heave Forceper Anchor	5.06E+07	Newtons	---	---	---
Anchor Type	Suction Pile	---	---	---	---
Number of Anchors	4	Anchors	$759,000	$/anchor	$3,036,000.00
Installation					
Number of Anchors	4	Anchors	$11,285.71	$/Anchor	$45,142.86
		Total Anchor, Line, and Installation Cost per Platform			**$3,242,519**

4) Platform Transportation and Installation					
Miles Traveled	100	miles	$200	$/mile	$20,000
T&I Days	3	days	---	---	---
Tug	2	tug	$30,000	$/day	$180,000
Crew per Platform	14	Crew Members	---	---	---
T&I Labor	1008	Hours	$70	$/hour	$70,560
			T&I Cost per Platform		**$270,560**

Total System Cost **$4,568,456.59**

B.4 NREL TLP RB=2

			Unit Cost	Unit	Cost
1) Construction and Materials					
Steel	169.14	Ton Steel	$700	$/Metric Ton	$118,394.75
Concrete	0.00	Ton Concrete	$100	$/Metric Ton	$0.00
Construction Labor	8000	Labor Hours	$40	$/hour	$320,000.00
		Total Construction Cost per Platfrom			**$438,394.75**
4) Tower Installation at Sea					
Hours per Installation	12	Hours	---	---	---
Crane	1	Cranes	$500,000	$/24H	$250,000
Barge	1	Barges	$10,000	$/24H	$2,500
Tug	1	Tugs	$30,000	$/24H	$7,500
Tower Installation Labor	120	Hours	$70	$/hour	$8,400
		Tower Installation Cost per Platform			**$268,400**
3) Anchors, Mooring Lines, and Anchor Installation					
Lines					
Max Force experienced at Fairlead x SF	1.64E+07	Newtons	---	---	---
Number of Lines	8	Lines	---	---	---
Max Tension per line x SF	8.18E+06	Newtons	---	---	---
Max Line Stress	1.20E+09	Pa	---	---	---
Diameter Required	0.09	meters	---	---	---
Length of Lines	177.00	meters/line	---	---	---
Total Chain Length	4.25E+02	meters	$270	$/meter	$114,696.00
Total Wire Rope Length	991.20	meters	$60	$/meter	$59,472.00
Anchors					
Heave Forceper Anchor	1.64E+07	Newtons	---	---	---
Anchor Type	Suction Pile	---	---	---	---
Number of Anchors	4	Anchors	$245,400	$/anchor	$981,600.00
Installation					
Number of Anchors	4	Anchors	$11,285.71	$/Anchor	$45,143
		Total Anchor, Line, and Installation Cost per Platform			**$1,200,910.86**
4) Platform Transportation and Installation					
Miles Traveled	100	miles	$200	$/mile	$20,000
T&I Days	3	days	---	---	---
Tug	2	tug	$30,000	$/day	$180,000
Crew per Platform	14	Crew Members	---	---	---
T&I Labor	1008	Hours	$70	$/hour	$70,560
				T&I Cost per Platform	**$270,560**
				Total Platform Cost	**$2,178,265.61**

B.5 NREL TLP RB=6

1) Construction and Materials			Unit Cost	Unit	Cost
Steel	297.31	Ton Steel	$700	$/Metric Ton	$208,119.46
Concrete	0.00	Ton Concrete	$100	$/Metric Ton	$0.00
Construction Labor	8000	Labor Hours	$50		$400,000.00
		Total Construction Cost per Platfrom			**$608,119.46**
4) Tower Installation at Sea					
Hours per Installation	12	Hours	---	---	---
Crane	1	Cranes	$500,000	$/24H	$250,000
Barge	1	Barges	$10,000	$/24H	$2,500
Tug	1	Tugs	$30,000	$/24H	$7,500
Tower Installation Labor	120	Hours	$70	$/hour	$8,400
		Tower Installation Cost per Platform			**$268,400**
3) Anchors, Mooring Lines, and Anchor Installation					
Lines					
Max Force experienced at each Fairlead x SF	4.48E+07	Newtons	---	---	---
Number of Lines	8	Lines	---	---	---
Max Tension per line	2.24E+07	Newtons	---	---	---
Max Line Stress	1.20E+09	Pa	---	---	---
Diameter Required	0.15	meters	---	---	---
Max Stress Allowed	3.69E+08	Pa	---	---	---
Length of Lines	170.00	meters/line	---	---	---
Total Chain Length	4.08E+02	meters	$270	$/meter	$110,160.00
Total Wire Rope Length	952.00	meters	$60	$/meter	$57,120.00
Anchors					
Heave Forceper Anchor	4.48E+07	Newtons	---	---	---
Anchor Type	Suction Pile	---	---	---	---
Number of Anchors	4	Anchors	$672,000	$/anchor	$2,688,000.00
Installation					
Number of Ancors	4	Anchors	$11,285.71	$/Anchor	$45,143
		Total Anchor, Line, and Installation Cost per Platform			**$2,900,423**
4) Platform Transportation and Installation					
Miles Traveled	100	miles	$200	$/mile	$20,000
T&I Days	3	days	---	---	---
Tug	2	tug	$30,000	$/day	$180,000
Crew per Platform	14	Crew Members	---	---	---
T&I Labor	1008	Hours	$70	$/hour	$70,560
			T&I Cost per Platform		**$270,560**
				Total Cost	**$4,047,502**

References

1 Butterfield, S., Musial, W., Jonkman, J., Sclavounos, P., Wayman, E., "Engineering Challenges for Floating Offshore Wind Turbines," *Copenhagen Offshore Wind 2005 Conference and Expedition Proceedings, 25-28 October 2005, Copenhagen, Denmark* (to be published).

2 Eltaher, A., Rajapaksa, Y., Chang, K. "Industry Trends for Design of Anchoring Systems for Deepwater Offshore Structures," *Offshore Technology Conference*, 2003.

3 Faltinsen, O. M. *Sea Loads on Ships and Offshore Structures*, Cambridge, UK: Cambridge University Press, 1999.

4 Global Wind Energy Council, "Record Year for Wind Energy", Press Release, Brussels, Belgium, February 17 2006.

5 Jonkman, J. M., Buhl, M. L., *FAST User Guide*, Golden, CO: National Renewable Energy Laboratory, 2005.

6 Jonkman, J, Butterfield, S., Musial, W., and Scott, G., "Definition of a 5-MW Reference Wind Turbine for Offshore System Development," NREL/TP-500-38060, Golden, CO: National Renewable Energy Laboratory, January 2006 (to be published).

7 Jonkman, J. M., Sclavounos, P. D., "Development of Fully Coupled Aeroelastic and Hydrodynamic Models for Offshore Wind Turbines," *Proceedings of the 44th AIAA Aerospace Sciences Meeting and Exhibit, 9-12 January 2006, Reno, NV,* Washington D.C.: American Institute of Aeronautics and Astronautics, January 2006; NREL/CP-500-39066.

8 Kim, S., Sclavounos, P. D., "Fully Coupled Response Simulations of Theme Offshore Structures in Water Depths of up to 10,000 Feet," *Proceedings of the Eleventh International Offshore and Polar Engineering Conference*, 2001.

9 Lee, K. H., *Responses of Floating Wind Turbines to Wind and Wave Excitation,* Master of Science Thesis, Massachusetts Institute of Technology, 2004.

10 Lee, K. H., Sclavounos, P. D., Wayman, E. N., "Floating Wind Turbines," Workshop on Water Waves and Floating Bodies, May 29, 2005.

11 Lewis, E.V. Principles of Naval Architecture, Second Revision, Volume III Motions in Waves and Controllability, Jersey City, New Jersey: The Society of Naval Architects and Marine Engineers, 1989.

12 Musial, W., Butterfield, S., Boone, A., "Feasibility of Floating Platform Systems for Wind Turbines," *23rd SSME Wind Energy Symposium,* 2004.

13 Newman, J. N., *Marine Hydrodynamics,* Cambridge, MA: The MIT Press, 1977.

14 Sclavounos, P. D. 13.022 Surface Waves and their Interaction with Floating Bodies, Lecture Notes, Cambridge, MA: Massachusetts Institute of Technology.

15 Sclavounos, P.D. *SML Papers, LINES User Manual*, Cambridge MA: Massachusetts Institute of Technology, 2004.

16 Studie narr halldaarheid van en randvoorwaarden voor drijvende offshore windturbines. Ecn, MARIN, Lagerwey the Windmaster, TNO, TUD, MSC, December 2002.

17 Tong, K.C., "Technical and Economic Aspects of a Floating Offshore Wind Farm," *Journal of Wind Engineering and Industrial Aerodynamics,* 1998.

18 Vryhof Anchor Manual, Vryhof Systems, 2000.

19 *WAMIT® User Guide*, Cambridge, MA: WAMIT, Inc. and MIT, 1998.

20 Wind Energy Weekly, "Wind Power Cost Depend on Ownership, Financing", Wind Energy Weekly #709, August 12, 1996

21 Withee, J. E., *Fully Coupled Dynamic Analysis of a Floating Wind Turbine System*, Doctoral Thesis, Massachusetts Institute of Technology, 2004.

22 NREL Study on wind resource